Title
Neuromechanics of Maneuverability: Sensory-Neural and Mechanical Processing for the Control of High-Speed Locomotion

Author
Mongeau, Jean-Michel

Publication Date
2013

Peer reviewed|Thesis/dissertation

Neuromechanics of Maneuverability: Sensory-Neural and Mechanical Processing for the Control of High-Speed Locomotion

By

Jean-Michel Mongeau

A dissertation submitted in partial satisfaction of the

requirements for the degree of

Doctor of Philosophy

in

Biophysics

in the

Graduate Division

of the

University of California, Berkeley

Committee in charge:

Professor Robert J. Full, Chair

Professor Noah J. Cowan

Professor Ronald S. Fearing

Professor Frederic E. Theunissen

Spring 2013

Neuromechanics of Maneuverability: Sensory-Neural and Mechanical Processing for the Control of High-Speed Locomotion

by Jean-Michel Mongeau

Abstract

Neuromechanics of Maneuverability: Sensory-Neural and Mechanical Processing for the Control of High-Speed Locomotion

by

Jean-Michel Mongeau

Doctor of Philosophy in Biophysics

University of California, Berkeley

Professor Robert J. Full, Chair

Maneuverability in animals is unparalleled when compared to the most maneuverable human-engineered mobile robot. Maneuverability arises in part from animals' ability to integrate multimodal sensory information with an ongoing motor program while interacting within a spatiotemporally complex world. Complicating this integration, actions from the nervous system must operate through the mechanics of the body. Since sensors and muscles are fused to a mechanical frame, mechanical processing occurs at both at the sensory (input) and motor (output) levels. To reveal the basic organization of the neural and mechanical parts of organisms during locomotion, I studied high-speed sensorimotor tasks in a remarkably maneuverable insect, the cockroach, which integrates sensory information to navigate through irregular, unpredictable environments.

Animals can expend energy to acquire information by emitting signals or moving sensory structures. However, it is not clear if the energy from locomotion, itself, could permit a different form of sensing, in which animals transfer energy from movement to reconfigure a passive sensor. In the first chapter, I demonstrate that cockroaches can transfer the self-generated energy from locomotion to actively control the state of the antenna via passive mechanical elements, with important effects on body control. This chapter advances our current understanding of sensorimotor integration during rapid running by showing how the whole body, not just the sensor, can participate in sensory acquisition.

Information flow from individual sensory units operating on locomotion-driven appendages to the generation of motor patterns is not well understood. The nervous system must rapidly integrate sensory information from noisy channels while constrained by neural conduction delays. When executing high-speed wall following using their antennae, cockroaches presumably integrate information between self and obstacles to generate appropriate turns, preventing collisions. Previous work on modeling high-speed wall following within a control theoretic framework predicted that a sensory controller for antenna tactile sensing of wall position (P) and the derivative of position (D) was sufficient for control of the body. I hypothesized that individual mechanoreceptive units along the antenna were tuned to enable stable running. Extracellular multi-unit recordings revealed P and D sensitivity and variable-latency responses, suggesting the antenna may function as a delay line. In the second chapter, I show how

individual sensor units distributed on the antenna precondition neural signals for the control of high-speed turning.

Since sensors of animals are embedded within the body, they must function through the mechanics of the body. In Chapter 3, I studied mechanical properties of the primary tactile sensors of cockroaches, the antennae, using experimental and engineering approaches. I revealed how both the static and dynamic properties of the antenna may influence sensory acquisition during quasi-static and dynamic sensorimotor tasks. Further elucidation of antennal mechanical tuning will lead to new hypotheses, integrating distributed mechanosensory inputs from a dynamic sensory appendage operating on a moving body.

During rapid escape from predators, the neuromechanical system of animals is pushed to operate closer to its limits. When operating at such extremes, small animals are true escape artists benefiting from enhanced maneuverability, in part due to scaling. In Chapter 4, I show a novel neuromechanical strategy used by the cockroach *P. americana* and the gecko *H. platyrus* which may facilitate their escape when encountering a gap. Both species ran rapidly at 12–15 body lengths-per-second toward a ledge without braking, dove off the ledge, attached their feet by claws like a grappling hook, and used a pendulum-like motion that can exceed one meter-per-second to swing around to an inverted position under the ledge, out of sight. In cockroaches, I show that the behavior is mediated by a rapid claw-engagement reflex initiated during the fall. Finally, I show how the novel behavior has inspired the design of a small, hexapedal robot that can assist rescuers during natural and human-made disasters.

Table of Contents

[1] Reprinted from the original publication: Mongeau J-M, McRae B, Jusufi A, Birkmeyer P, Hoover AM, et al. (2012) Rapid Inversion: Running Animals and Robots Swing like a Pendulum under Ledges. *PLoS ONE* 7(6): e38003. doi:10.1371/journal.pone.0038003. This is an open-access article distributed under the terms of the Creative Commons Attribution License. Please include this citation when referencing the work from Chapter 4.

List of Figures

List of Tables

Acknowledgements

I am truly indebted to all who have contributed to my journey towards a doctorate. It has been quite an adventure. I consider my dissertation the result of teamwork, in the broadest of sense of the word. Countless individuals have directly or indirectly contributed to this work and to those I am sincerely and heartily grateful. I could not have done it without them.

Reaching the end of the marathon journey would have not been possible without the love and caring support I received from my father, Claude, my mother, Céline, and my sisters, Ariane and Marie-Ève. The strong foundation I acquired from my family prepared me well for the difficult road ahead. Their encouragement and wisdom got me through challenging periods of grad school and kept me grounded. Merci beaucoup. Margaret's love brightened my days during these last few years and made my life much more fun and interesting! I thank her for her patience during these last few challenging months.

I am very grateful for the inspiring, big-picture mentoring provided by my advisor, Robert Full. Bob's thoughtful guidance and coaching aroused in me the desire to perform at a level that I didn't think I was capable of attaining. I am very thankful for the world-class resources – including access to the Center for Interdisciplinary Bio-inspiration in Education and Research (CiBER) – and a fertile environment that he provided during more than five productive years.

Interdisciplinary research is possible only through fruitful collaborations. I am particularly thankful for my collaboration with Noah Cowan and Alican Demir at Johns Hopkins who made important contributions to Chapter 1, allowing us to test biological hypotheses with an elegant physical model. Early experiments by Jusuk Lee sowed the seeds, which led to the development of the ideas and further experiments in this chapter. My collaboration and friendship with fellow graduate student Simon Sponberg gave an early jumpstart to my graduate research. His extensive training and continued, exceptional mentoring set the stage for the development of Chapter 2. In Chapter 3, fellow graduate student Kaushik Jayaram helped develop the beam model while visiting student Chris Dallmann worked tirelessly to help collect and analyze data. Finally, Chapter 4 benefited from a truly diverse team effort. Undergraduate Brian McRae helped to develop and carry out the first set of experiments while fellow graduate student Ardian Jusufi provided surprising field results from the rainforests of Singapore. Engineers Paul Birkmeyer and Aaron Hoover, under the supervision of Ron Fearing, added a new behavior to the repertoire of the DASH robot inspired from our experimental work.

I thank undergraduates Brian McRae, Anil Mahavadi, Talia Moore, Avantika Pathak and Andy Mohapatra and Biophysics rotation students Vladislav Belyy and Albert Kao for their laboratory assistance and contagious enthusiasm for doing research. I will miss my collaboration with Kaushik Jayaram, with whom I had many crazy and fun discussions about science. Tom Libby's knowledge of lab equipment and wisdom for experimental biology saved me a lot of time and headaches. Pauline Jennings was very helpful in assisting with administrative hurdles and creation of scientific media. In addition, my work benefited from enlightening discussions with other fellow graduate students including Sam Burden, Shai Revzen, Daniel Cohen, and Evan Chang-Siu.

I would like to thank Simon Sponberg for his kindness and generosity, including an invitation to go up to Seattle to work at the University of Washington in 2010. I thank Tom Daniel for hosting me and Armin Hinterwirth for being so kind and providing laboratory assistance during my stay. While few, if any, experiments were successful, I very much appreciated having the opportunity to learn and try a new technique while getting out of Berkeley to experience a different lab.

I thank qualifying exam committee members Robert Dudley, Damian Elias, Frederic Theunissen and Jose Carmena for taking time out of their busy schedules to help me reach an important milestone. My thesis committee members Robert Full, Noah Cowan, Ron Fearing and Frederic Theunissen gave me valuable feedback over the last few years to improve the conceptual breath and technical depth of my dissertation.

I would like to extend my thanks to Berkeley Biophysics for providing a flexible graduate program that opened my eyes to the diversity of work at the interface of biology and physics. I am particularly grateful for the assistance of Kate Chase who was both kind and caring during my time in the program. I valued my friendships and support from members of the biophysics community. I very much appreciated the thoughtful feedback I received while participating in the IB Biomechanics Seminar. Special thanks to Robert Dudley and Mimi Koehl and their graduate students for giving me in-depth critique. I thank the talented students of the 2009 IB135L class for their patience and support during my first teaching assistantship. While stressful at times, I cherished my time in CiBER, whether it was to do preps for the day's experiments, debugging equipment, or discussing concepts of sensorimotor integration with students.

I wish to acknowledge the support and inspiration from early mentors and teachers, particularly Mrs. Gabet and Dr. Hartmann.

I wish to thank members of the biophysics house for sharing their time with me and the Hillegass/Parker coop house for providing a welcoming, enriching, and interesting environment. My social education at the house will remain with me as well as all the memories forged and friendships made while living with such a diverse community of students.

Finally, I would like to offer my special thanks to Margaret for taking time off her busy schedule to proofread the final version of my dissertation.

This work was made possible through the generous support of a NSF Graduate Research Fellowship and a NSF IGERT traineeship. I would also like to acknowledge financial support from the Society of Integrative and Comparative Biology and International Society for Neuroethology.

Chapter 1

Locomotion and mechanics mediated tactile sensing: antenna reconfiguration simplifies control during high-speed navigation in cockroaches

Summary

Animals can expend energy to acquire sensory information by emitting signals and/or moving sensory structures. We propose that the energy from locomotion, itself, could permit control of the sensor whereby animals use the energy from movement to reconfigure a passive sensor. We investigated high-speed, antenna-mediated tactile navigation in the cockroach *Periplaneta americana*. We discovered that the passive antennal flagellum can assume two principal mechanical states: the tip is either projecting backward or forward. Using a combination of behavioral and robotic experiments, we demonstrate that a switch in the antenna's state is mediated via the passive interactions between the sensor and its environment, and this switch strongly influences wall tracking control. When the tip of the antenna is projected backward, the animals maintain greater body-to-wall distance, with fewer body collisions and less leg wall contact than when the tip is projecting forward. We hypothesized that distally pointing mechanosensory hairs at the tip of the antenna mediate the switch in state by interlocking with asperities in the wall surface. To test this hypothesis, we performed laser ablation of chemo-mechanosensory hairs and added artificial hairs to a robotic antenna. In both the natural and artificial systems, the presence of hairs categorically increased an antenna's probability to switch state. Antennal hairs, once thought to only play a role in sensing, are sufficient for mechanically reconfiguring the state of the entire antenna when coupled with forward motion. We show that the synergy between antennal mechanics, locomotion and the environment simplifies tactile sensing.

Introduction

Animals can directly control the acquisition of sensory information by using self-generated energy via muscle action to control their sensor, a process termed "active sensing" (Bajcsy, 1988; Nelson and Maciver, 2006). Active sensing systems are characterized as information-seeking (Prescott et al., 2011). From these definitions arises a common theme: the control of a sensor to suit the task. The energy source of active sensing may come from muscles directly controlling the sensor, the body, or both. Research in active tactile sensing that has focused on slow, exploratory tasks such as sniffing in lobsters (Koehl et al., 2001), whisking in rats (Hartmann, 2001), and antenna-mediated exploration in invertebrates (Staudacher et al., 2005; Okada and Toh, 2004) has shown the importance of integrating knowledge of the sensor, body and environment to understand how animals can exert active control over their sensor to tune the gain, phase, and spatial direction of the signal for acquiring information. During slow, exploratory tasks animals rely predominantly on distributed neural feedback from sensors in order to execute effective control actions, via the direct regulation of motor activity and subsequent actuation of sensor and/or body (Chiel et al., 2009).

When animals are involved in extremely rapid control tasks – such as predatory escape, where the neuromechanical system is pushed near its operating limit due to neural conduction delays (More et al., 2010) – sensorimotor control bandwidth constraints impose fundamental limits on the gains that can be achieved for stable closed-loop control (Cowan et al., 2006; Elzinga et al., 2012). In such cases, animals require a well-tuned control system to compensate for the delays and locomotor dynamics, thus relying on shared processing between the neural and mechanical system (Cowan et al., 2006; Holmes et al., 2006). Sharing processing loads further, biomechanical sensory structures, themselves, can mechanically process sensory information prior to neural transduction (Sane and McHenry, 2009). In some cases, these properties can simplify downstream neural computations by performing mechanical computations on the incoming stimulus before sensory transduction. For example, in echolocation in bats, the mechanics of the pinnae and tragi acts as a filter allowing bats to determine elevation angle of prey (Wotton et al., 1995). In flies, the geometry and wiring of photoreceptors in the eye simplify optical flow computations (Egelhaaf et al., 2002). In barn owls, asymmetries in the arrangement of the facial ruff play a critical role in sound localization (Coles and Guppy, 1988).

Here we examine if animals use the self-generated energy from locomotion to control the state of their sensor when their neuromechanical system is pushed near its limit during escape. Animals under these conditions could benefit from having tuned passive mechanical sensory structures adapted to their natural environment to simplify control by reconfiguring the sensor's state parameters according to the sensing strategy (Bajcsy, 1988; Fig. 1A). We abstract this reconfiguration by showing distinct mechanical states x_1 and x_2, that are "switched" by an interaction between three systems: locomotion as the self-generated energy source, a mechanically tuned passive sensor and the environment. In turn, these states can affect the information $I(x_n)$ available to the neural controller that generates movement.

To explore the interaction between locomotion, passive sensors and the environment, we studied thigmotaxis in cockroaches, *Periplaneta americana*, during blinded high-speed wall following where they employ their antennae. During wall following, cockroaches use their antennae to sense obstacles such as walls and control their body by executing rapid turns (Camhi and Johnson, 1999). While the natural habitat of *P. americana* is uncertain, these artificial walls represent extended obstacles that may be relevant to the natural ecological context of the genus *Periplaneta* in the form of caves and/or large rocks (Bell et al., 2007). Its hypothesized cave-like native environment is likely one reason this species predominantly adopts present day, human-made structures such as dwellings (Seelinger, 1984), It has been hypothesized that to avoid collisions with extended obstacles such as walls, these animals can control or track their relative distance to the wall effectively, even at very high speeds (Cowan et al., 2006). For task-level control of this behavior, cockroaches use information obtained predominantly from the flagellum, the long (up to 1.3 times body length), unactuated part of the antenna. Cockroaches can initiate a turn in response to a wall projection in less than 30 ms, leaving little time available for processing by the nervous system (Camhi and Johnson, 1999). This sensorimotor delay is within the range of rapid turns in other insects, such as 90° turns in fruit flies (50 ms; Dickinson, 2005) and turns in prey pursuit in dragonflies (33-50 ms; Olberg et al., 2000). Moreover, it appears that cockroaches hold the angle of their antennae relative to their body midline relatively constant during high-speed wall following (Camhi and Johnson, 1999; Cowan et al., 2006), and thus whole-body motions dominate sensory movements. This contrasts with low-speed

exploration tasks in which local joint activity dominates sensory motion (Chiel et al., 2009). Distributed along cockroach flagella is a vast array of mechanosensors that include hair sensillae and campaniform sensillae. The antennal nerve relays information from over 270,000 sensors, forming a vast network of extero- and interoceptive sensors (Shafer and Sanchez, 1973; Schaller, 1978). It has been shown that a Proportional-Derivative (PD) controller operating on a whole body or template model is sufficient to reliably predict wall-following behavior (Cowan et al., 2006). Furthermore, this controller is sufficient for task-level control when integrated into a more dynamically representative model of running (Lee et al., 2008).

Here we demonstrate that during wall following in cockroaches, an antenna's mechanical state can be switched between two states based on wall roughness (Fig. 1B). First, we show evidence that the change in mechanical state of the antenna – which we characterize as projecting "forward" or "backward" – is mediated passively via the interactions between the antenna and the environment. We compare the frequency of states for cases when the surface is smoother versus rougher, effectively pushing the mechanical performance of the antenna. Secondly, we show that this change in state affects control and performance. Specifically, the mechanical state of the antenna affects the body-to-wall distance – the proposed state variable for control – which in turn has implications on performance and control strategy. Therefore, a dynamic change in the state of the sensor results in changes in tracking. Thirdly, we show that passive mechanical hair sensillae on the antenna are sufficient for mediating a change in the overall mechanical state of the antenna, that is, from its resting position to projecting "backward". This conclusion is reached through a set of experiments in which the hairs are ablated with a high-precision laser system and corroborated independently by testing the role of artificial antennal hairs added to a tunable physical model inspired by arthropod antennae. We show that large mechanosensory hairs play a critical mechanical role in mediating sensor reconfiguration. We thereby propose a novel function for these structures, previously described as having an exclusively sensory function.

Materials and Methods

Animal husbandry

Adult male American cockroaches, *Periplaneta americana*, were acquired from a commercial vendor (Carolina Biological Supply Company, Burlington, NC, USA) and housed in plastic cages maintained at a temperature of 27°C. Cockroaches were exposed to a L:D cycle of 12h:12h and given fruits, dog chow and water *ad libitum*.

Arena for turn perturbation

We built a rectangular arena as described in Cowan et al. (2006; Fig. 2A). Within the rectangular arena of dimensions 85 cm × 45 cm × 15 cm (length × width × height), we placed acrylic (smoother) and wood (rougher) blocks cut at angles of 30°, 45°, and 60° to induce turning in wall-following cockroaches. To capture the high-speed escape behavior, two high-speed video cameras (Kodak Ekta Pro 1000, Eastman Kodak Company, Rochester, NY, USA) were

positioned at 1.5 m above the area. Adjacent camera views overlapped to enable calibration and provide continuity of data for each trial sequence. Video sequences were synchronously captured at 500 frames s^{-1} with an average resolution of 0.8 mm per pixel. To enhance contrast and tracking of cockroach body and legs, we used retroreflective sheets (3M, St Paul, MN, USA) as the running substrate and placed retroreflective markers on the cockroach body.

Animal preparation

Prior to running experiments, we prepared each cockroach using the protocol described in Cowan et al. (2006). While cockroaches were anesthetized we taped two small round retroreflective dots dorsally aligned with the body fore-aft axis. The dots were placed directly over the wings but did not restrict their motions. These two dots allowed us to estimate the cockroach position and heading vector from the high-speed videos. To prevent visual cues from influencing wall-following behavior, we covered the compound eyes and ocelli with a white nail polish while carefully avoiding the head/scape joint. Following the preparation we allowed cockroaches at least 24 h for recovery at room temperature prior to conducting experiments.

Kinematics

We used the camera calibration procedure described in Cowan et al. (2006) for digitization. For each frame, we digitized the two markers on the cockroach body to extract the point of rotation (POR) and body angle (Fig. 2B). The procedure for determining the POR is described in Cowan et al. (2006) and involves performing a least-square fit using the velocity and angular velocity for two consecutive frames, assuming cockroaches run like an ideal no-slip planar unicycle. Here we use the POR metric solely as a body reference to estimate body-to-wall distances of cockroaches. We filtered the position data using a zero-phase low-pass Butterworth filter with a cut-off frequency of 62.5 Hz, which corresponds to a frequency nearly three times the fastest turning rates described in cockroach wall following (Camhi and Johnson, 1999). We accepted all trials when the animals rapidly followed the wall and executed a turning response when contacting the angled wall, but excluded trials when animals tried to climb the wall or stopped. Trials were rejected when the distance of the POR to the wall exceeded 2.5 cm while running along the angled wall.

Wall properties

To determine the relationship between wall roughness and antenna configuration, we manually tracked videos of running cockroaches encountering a turn perturbation with smoother acrylic walls and rougher wood walls. We recorded the initiation of a stride by manually determining onset of stance initiation of the hind leg contralateral to the wall perturbation. We rejected strides when the antenna position could not be clearly determined to be either projecting forward or backward for the entire stride (4% of strides). We also rejected strides when the antenna was not in contact with the wall for at least 80% of the stride (35% of strides) to ensure sufficient

interaction between the antenna and the wall. In these rejected strides, the animals would often steer away from the wall that would then cause the ipsilateral antenna to momentarily lose contact with the wall. We defined an antenna "flip" as when an antenna moved from a forward-projecting to a backward-projecting position and vice versa on a stride-by-stride basis. Only animals (n = 8 animals total) with at least 15 accepted strides were included in the final analysis. Another parameter which could possibly affect the distribution of antenna states is the antennal joint angles. While previous studies suggest little variation in antenna angles and little-to-no contribution from basal segments during wall following (Camhi and Johnson, 1999), we measured whether animals could actively modulate antennal joint angles as a control. We randomly sampled trials within our dataset for smoother and rougher walls. We sampled 98 strides following the turn perturbation (6 animals total: 3 on rough, 3 on smooth; 12 trials total: 6 on rough walls, 6 on smooth) and found no statistically significant changes in per-stride body-antenna (ipsilateral) angles (t test, p=0.99) and inter-antennal angles (t test, p=0.74) between smoother and rougher walls. These changes remained insignificant even after correcting for the possible effect of individual animals (mixed effect model, F test, body-antenna angles: p=0.95, inter-antenna angles: p=0.67). Therefore, we did not include this parameter in explaining the variation in antenna state.

Wall contact

To determine the effect of the antenna state on body-to-wall distance, we ran a separate set of animals using the same track. We selected trials before the turn perturbation with clearly identifiable antenna positions (either projecting forward or backward) and computed the shortest distance between the POR and the wall using custom scripts (Matlab, The MathWorks, Inc., Natick, MA, USA). We categorized the effect of body-to-wall distance on wall-following performance by manually tracking the videos of running cockroaches on a stride-to-stride basis. As before, we determined the initiation of a stride by manually determining the onset of stance initiation of the hind leg contralateral to the wall perturbation. We rejected strides when (1) the antenna position could not be clearly determined to be either projecting forward or backward for the entire stride (8% of all strides), (2) the antenna was not in contact with the wall for at least 80% of the stride (29% of all strides), and (3) the antenna flipped (either forward or backward; 17% of all strides). For each stride, we manually recorded evidence of leg contact by the tibia and femur joints (excluding contact of the tarsal segment) as well as evidence of body (head, thorax, and/or abdomen) contact with the wall.

Tracking control

We quantified the effects of backward-to-forward antenna flips on wall-following control by manually identifying flips within our dataset *after* cockroaches encountered the turn perturbation. We recorded the frame at the onset of the flip for each instance. We rejected all events when the antenna flip was initiated by the cockroach turning; that is, when the body angle was greater or equal to $\pm 15^{\circ}$ from the wall within the stride when the flip occurred. This occurred in 5% of flips (1/19). We estimated the stride time ($\approx$ 80 ms) by taking the reciprocal of the median stride

frequency (11.9 strides s^{-1}). For each flip, we normalized the body angle of the animals by their respective averages approximately 1 stride prior to the flip (80 ms). Body angles were computed by taking the arctangent between the vector formed by the two dots on the animal's body and the reference wall vector (Fig. 2B). We then analyzed the normalized body angles approximately 3 strides (240 ms, one stride ~ 80 ms) after the onset of the flip. To determine any significant effect of these "flip" events on wall-following control, we compared these kinematic variables to control sequences with no antenna flips by randomly selecting trials 240 ms after turning (average timing of flip occurrences after turn) within a 100 ms window downstream of the turn. The same body angle normalization procedure was applied to the control dataset. To determine statistical significance between the two groups, we applied a statistical mixed effect model of the form *abs(angle) = time + animal + group + animal * time + group*time* where *abs* is the absolute value, *angle* is the angle measurement at each *time* point (2 ms interval), *animal* is a random factor, and *group* is a fixed effect (flip vs. control). To determine if the statistical result was sensitive to the possible effect of a small sample size and a non-normal distribution, we calculated 95% confidence intervals on bootstrapped means for both groups using 1,000 replications. We compared the bootstrapped means from an original sample of 18 flip events and 30 control events.

Passive antenna reconfiguration – biological experiments

We measured the effect of passive hairs on the antenna state by developing a technique using a diode-pumped Q-switched micromachining laser (Matrix 355, Coherent, Santa Clara, CA, USA) to ablate hair arrays on each antennal annulus. High-precision laser ablation has been successfully used on arthropods in the past, for example, to ablate genital hairs in *Drosophila bipectinata* (Polak and Rashed, 2010). Hairs on individual annuli were ablated by pulsing the laser at a frequency of 20 KHz while drawing a rectangle the size of each annulus at 10 μm spacing at a speed of 250 mm s^{-1}. For each annulus, coordinates were manually defined at a 1 μm resolution to avoid hitting the intersegmental membranes. We ablated hairs of the first ten distal annuli in head and antenna-fixed animals in both the dorsal and ventral directions. We found that orienting the antenna with dorsal and ventral side up was sufficient to ablate hairs circumferentially. We acquired high-magnification (25-50X) images of individual annuli under a microscope in both the dorsal and ventral directions to determine the quality of the ablation process. After ablation, under a high-magnification microscope, we observed that the treated portion of the antenna retained hemolymph flow and that the cockroach responded to touch on the treated antenna. To demonstrate the effect of antenna hairs, we compared the performance of ablated and non-ablated antennae when sliding along a surface (Fig. 3A). After cold-anesthetizing the animals by placing them in glass beakers on ice for 30 minutes (thus avoiding direct contact with the ice), we used staple pins to mount the animal on a gel plate and fixed the head and base of the antenna with dental silicone (President light body, Coltène, Altstätten, Switzerland). We fixed the base of the antenna at an angle of 30° relative to the body long axis which is similar to the angle observed in wall following (Camhi and Johnson, 1999). The candidate antenna was allowed to rest freely against a paraffin plate. The paraffin plate was made by melting paraffin on a glass plate placed on a hot plate. Because of surface tension, the paraffin melted and created a thin coat of wax. The plate was attached to a linear micro-translation stage

(M112.1DG, Physik Instrumente, Palmbach, Germany). After carefully allowing the antenna to come into contact with the wall under a microscope with the antenna in a "forward" projecting position, we drove the wall towards, but parallel to, the cockroach at a speed of 2 mm s^{-1} over a distance of 2.5 cm (Fig. 3B). To control for the possible effect of antennal contact area biasing our results, we varied the initial conditions such that the antenna was initially mounted with 1 to 10 annuli in contact with the wall. To control for surface irregularities on the wall, we randomized the initial position of the antenna against the wall for all annulus numbers. We observed and noted whether or not the antenna flipped and measured the frequency for each condition from high-resolution video recordings of each trial under a microscope. After a trial, we measured the antenna length from the scape to the last annulus of the flagellum.

Passive antenna reconfiguration – physical model of antenna

We tested the sufficiency of passive hairs in changing the antenna state by adding artificial hairs to a highly tunable and modular physical model inspired by arthropod antennae (Demir et al., 2010). To approximate the stiffness distribution of insect antennae (Staudacher et al., 2005), we designed an eight-segment model with tunable joint stiffness. We ran our eight-segment (8 × 40 mm) robotic antenna with a constant base velocity v_{base} of 15 mm s^{-1} against a wall (Fig. 4A). In the middle of each segment, we placed an 18 mm long anisotropic "hair" protruding at 45° towards the distal end of the antenna (Fig. 4B). The hairs were anisotropic which is a known bio-mechanical feature of the thick-wall chemo/mechanosensory sensilla (Chaetica B) of the cockroach, *P. americana* (Shafer and Sanchez, 1973). Here, anisotropy refers to the direction that a hair can collapse.

We performed a total of seven experiments each with 10 trials (total of 70 trials). For each trial the base angle θ was set to 30° and the distance to the wall, d, from the antenna base was kept at 135 mm. As an initial condition, the robotic antenna posture was always projecting towards the direction of motion (forward). The forward velocity of the base was determined such that the antenna was at a quasi-static state in motion, in order to minimize inertial effects. The linear actuator was a belt-driven Velmex BiSlide (Velmex inc., Bloomfield, NY, USA) with a resolution of 25 μm and a travel distance of 1 meter. Each antenna segment data was sampled via a common I2C bus facilitated by a 600 MHz Gumstix Verdex Pro base computer (Gumstix Inc., Portola Valley, CA, USA). Both the linear actuator and the base computer were controlled asynchronously by custom-designed client software. We recorded each segment joint angle with a resolution of 0.35° at a rate of 120 Hz.

Figure 4C is a CAD rendering of the antenna segment, showing the hair design. Two hairs (Fig. 4C-2) – one at each side – were placed per segment; each hair was placed on one of the two available cylindrical extrusions, about which it was free to rotate (Fig. 4C-5). We designed two different hair types: a distally-projecting and a proximally-projecting hair. These two types mirrored each other about the segment's sagittal plane and thus determined the direction in which they were free to collapse. Both hair types could be, at most, 45° from the segment, after which a mechanical hard stop is encountered (Fig. 4C-3). Each hair was also spring-loaded to swing open (to 45°) by a 0.1 mm diameter Nitinol wire. This wire simultaneously acted as the

pointy hair tip that anchored into the wall surface (Fig. 4C-1). The hair was placed so that in the event of a collapse, it triggered the contact sensor shown in Fig. 4C-6.

During a trial, when a distally oriented hair was anchored to asperities in the wall, the entire antenna went into a transition phase. This transition could result in a "flip", where the antenna switched to a backwards-projecting configuration. We defined a "flip" as a successful transition in which the most distal segment angle exceeded 90° with respect to the wall. Figure 7C illustrates the antenna's transition phase (left to right) during a successful flip.

Statistical analysis

We performed all statistical analysis of our data using the statistics toolbox in Matlab (Matlab, The MathWorks, Inc., Natick, MA, USA) and Minitab (Minitab Inc, State College, PA, USA). Bootstrapping was applied by randomly resampling with replacement.

Results

Wall properties change state of antenna

To determine the interactions between the ipsilateral antenna and the environment (wall surface) during high-speed wall following, we ran male cockroaches along both smoother (acrylic) and rougher (wood) wall surfaces in an arena with a turn perturbation (Fig. 2A). We accepted a total of 259 strides from 39 trials with $n = 3$ animals running along smoother walls (body length = 3.57 ± 0.2 cm s^{-1}; ipsilateral antenna length = 4.10 ± 0.4 cm s^{-1}, mean ± std unless otherwise noted). We accepted a total of 354 strides from 40 trials with $n = 5$ animals running along rougher walls (body length = 3.60 ± 0.2 cm s^{-1}; ipsilateral antenna length = 4.42 ± 0.4 cm s^{-1}). The combined group of animals ran with a mean speed of 37.8 cm s^{-1} ranging from 34.8 to 41.1 cm s^{-1}. Speeds were not statistically different between the two groups (*t*-test, p=0.15). During these experiments, we observed antennae using a 2D dorsal projection and determined the antenna tip's flipped state between being forward and backward projecting and vice versa as the antenna interacted with the wall (Fig. 5A). We found the "backward" and "forward" states to be the dominant antenna configurations, persisting for many strides. In the backward projecting configuration, most of the flagellum was typically out in front of the animal, but the tip was projecting rearward, so the flagellum assumed an inverted-J shape. When comparing wall following performance for both groups, we found that animals encountering rougher walls had their antennae projecting backward more often than animals running along smoother acrylic walls (smoother: 51%, rougher: 85%; Fig. 5B). Similarly, for animals following smoother walls, the ipsilateral antennae assumed a forward position more often than animals running along rougher walls (smoother: 26%, rougher: 1%). Antennae "flipped" (either forward to backward or backward to forward) at similar frequencies for both wall surfaces (smoother: 11%, rougher: 14%). When comparing the proportion of forward versus backward antennal positions during a stride (excluding strides when the antenna flipped), we found that four of five individuals never had a forward projecting antennae on the rougher surface (0/34, 0/48, 0/17, 0/102), and only one individual showed five instances in 102 strides. By contrast, all individuals following smoother

walls showed a large proportion of strides with forward-projecting antennae (16/83, 40/95, 15/23). We found a significant association between wall properties and the state of the antenna (Pearson χ^2 test, $p<0.001$). To investigate antenna flips further, we calculated transition probabilities within and between states by treating antenna positions as a two-state discrete Markov chain (Fig. 5C). We found that if the antenna was in a forward state on smoother walls, the probability that it remained in that state in the next stride was 93%, whereas if it was forward on rougher walls, it never remained in the forward state in the next stride. Given these observations suggesting that wall properties categorically influence the antenna configuration, we investigated whether the antenna's state affected task-level control.

Body-to-wall distance depends on state of antenna

To test the effect of the antenna's mechanical state on wall-following control, we ran a separate set of male cockroaches (n = 12 animals; body length = 3.29 ± 0.18 cm; ipsilateral antenna length = 3.96 ± 0.37 cm) on both smoother and rougher wall surfaces. Animals ran with a mean speed of 46.2 cm s^{-1} that ranged from 37.7 to 53.1 cm s^{-1}. We analyzed 80 trials after a turn perturbation and divided the data into two groups based on the position or state of the antenna and measured the body-to-wall distance for both groups (Fig. 2B), the putative control variable for wall following (Cowan et al., 2006). We found that animals with an antenna projecting forward following a turn perturbation ran significantly closer to the wall (12.0 ± 1.72 mm, n = 18 trials; t-test $p<0.001$) than those running with an antenna projecting backward (19.9 ± 4.86 mm, n = 62 trials). This effect persisted even after including the effect of individuals (random factor) and running speed (covariate) using a mixed effect model (F-test, $p<0.001$; Fig. 6A,B). This change in body-to-wall distance corresponds to approximately the body width of *P. americana*. We found that the variance between the two groups were significantly different (F-test for equivariance, p=0.002). Since running speed has been shown to be correlated to body-to-wall distance (Camhi and Johnson, 1999), we tested for the effect of speed. We found no significant difference in running speeds (antenna backward: 44.8 ± 8.22 cm s^{-1}, antenna forward: 41.0 ± 7.35 cm s^{-1}) between the two groups (t-test, p=0.728) even after correcting for the possible effect of individuals (F-test, p=0.792).

Tracking performance depends on state of antenna

To determine possible effects of body-to-wall distance on running performance, we tracked individual strides of wall-following cockroaches running alongside rougher and smoother walls using the same dataset to measure body-to-wall distances as presented earlier. We accepted a total of 129 strides with the ipsilateral antenna projecting forward and 231 strides with the antenna projecting backward. When comparing wall-following performance for cockroaches before and after a turn perturbation, we found that animals running with an antenna projecting forward had a significant increase in frequency of leg (tibia and/or femur) and body contact with the adjacent wall (Fig. 6C). The state of the antenna had a statistically significant association with leg contacts and body contacts (Pearson χ^2 test, $p<0.001$ for both leg and body contacts). This association remained significant even after correcting for the possible effect of individuals

(Cochran-Mantel-Haenszel test, $p<0.001$ for both leg and body contacts). For strides where the body contacted the wall (35 strides total), these collisions often led to a decrease in speed, likely due to the impact. We found the median change in velocity to be -7.48 ± 6.84 cm s^{-1} when comparing approximately 2 strides before and after contact. We estimated the stride time (70.0 ms) by taking the reciprocal of the median stride frequency for all trials (14.3 strides s^{-1}). Thus, animals slowed down after body contact on average. This change in speed following body contact is consistent with observations by Baba and Tsukada (2010).

Change in antenna state affects tracking control

From behavioral observations, we hypothesized that a dynamic switch in the state of the antenna affects control as evidenced by a change in body angle. We quantified one state change, a "flip", when the antenna moved from a backward to forward position. To test the effect of antenna flips on wall-following control, we ran male cockroaches on rougher (wood) surfaces (n = 11 male cockroaches, body length: 3.70 ± 0.17 cm, mass = 0.77 ± 0.11 g, ipsilateral antenna length: 4.36 ± 0.41 cm). Animals ran at a mean speed of 46.2 ± 8.4 cm s^{-1} ranging from 34.8 to 62.5 cm s^{-1}. We averaged body angles (Fig. 2B) for approximately 3 strides following a flip or non-flip control (Fig. 6D). We estimated the stride time (80.0 ms) by taking the reciprocal of the median stride frequency (11.9 strides s^{-1}). Here, our control was defined as any randomly chosen time point in our wall-following dataset after a turn perturbation that was not flagged as a flip (see Methods). Body angles greater than or equal to 15° suggest that a cockroach initiated a body turn (Camhi and Johnson, 1999). We found that flips occurred infrequently (18 strides with flips out of 676 strides). Using the mixed effect model described in the Methods, we found that flips had a significant effect on body angles. Specifically, we found that the term group (intercept) and group*time (slope) were both statistically significant in our model (F-test, $p<0.001$). This result remained significant after testing for a possible non-normal distribution of angles using a logarithmic transformation (F-test, $p<0.001$). When comparing bootstrapped 95% confidence intervals of the normalized mean angles (absolute value) for both groups, we found no overlap (flip = [6.91-9.69°]; control = [4.91-6.67°]; Fig. 6E). Applying the same test on angles without taking the absolute value did not change the statistical outcome.

Passive antenna reconfiguration - role of antenna hairs

We hypothesized that large chemo-mechanosensory hairs could allow the antenna to effectively stick to walls and mediate the transition from forward to backward bending. To determine the role of antenna hairs in mediating changes in antenna state, we developed a technique that allowed us to perform annulus-by-annulus hair ablation treatment on the first 10 annuli from the tip using a high-resolution micromachining laser (Fig. 3A). Results from one treatment are shown in Figure 3A. We compared the performance of control (n = 5 animals, 50 trials; mass = 0.81 ± 0.09 g; antenna length = 4.24 ± 0.43 cm) and experimental antennae (n = 5 animals, 50 trials; mass = 0.91 ± 0.06g; antenna length = 4.35 ± 0.33 cm) while sliding along a paraffin surface on head-fixed animals (Fig. 3B; Fig. 7A). During a flip, the hairs at the tip first engaged with the wall, causing the tip to stick. As the wall's motion progressed, the tip began to turn

backward by twisting (Fig. 7A). With ablated hairs, the flagellum would catch but fail to engage and subsequently slip back in a forward projecting state. We found a significant difference in flipping frequency between control and treated antennae (Pearson χ^2 test, $p<0.001$) (Fig. 7B). We found no effect of the number of annuli in contact with the wall on flipping frequency (Cochran-Mantel-Haenszel test, $p<0.001$). Interestingly, contact of a single annulus with the wall often was sufficient for interlocking and subsequent flipping.

Physical model tests biological hypotheses

To independently test the hypothesis that antenna hairs can mediate a change in state of the antenna when coupled with locomotion, we translated an eight-segment robotic antenna with a constant base velocity v_{base} of 15 mm s^{-1} against a wall (Fig. 4A). Across the six experiments, we varied the wall surface and the hair orientation using the following combinations: 1. Rough (felt-cloth) wall, distally pointing hairs; 2. Rough wall, three distal segments with no hairs; 3. Rough wall, proximally pointing hairs; 4. Smoother (glossy paper) wall, distally pointing hairs; 5. Smoother wall, three distal segments with no hairs; 6. Smoother wall, proximally pointing hairs. Proximally pointing hairs pointed towards the base, whereas distally pointed hairs pointed away from the base.

In experiment 1, we observed that the hair tips of the distal segments anchored to the asperities of the rough (felt) material almost immediately. Figure 7C illustrates data from one trial of experiment 1 where the antenna initiated a “flip" immediately after the smoother zone (glossy paper) of the wall. A similar response was observed for the remaining 9 trials. For experiment 2, we removed the three distal hairs analogous to the laser ablation experiments for the real cockroach flagellum. We did not observe a flip in any of the 10 trials. In 4 out of the 10 trials, we observed “catching” at the most distal segment, but these hair-substrate interactions were not enough to successfully flip the antenna. Figure 7D shows data from one trial of experiment 2 where such a failed transition is illustrated. For experiment 3, we reversed the orientation of the hairs to evaluate the effects of the hair orientation. This control would have been infeasible to test on a cockroach flagellum. In all 10 trials, the antenna did not flip. For all the other experiments (4-6) with the smoother wall, the antenna slid over the corresponding surface without initiating a flip. In some cases, the cockroach antenna changed state via torsion around the flagellum (Fig. 7A), but the robotic antenna could not flip via this mechanism (Fig. 7C-D); this degree of freedom was not available by design.

When a flip was completed with distally pointing hairs, the hairs pointed proximally and thus could not interlock with the asperities while forward motion progressed. We observed that the wall contact point initially moved with the same velocity as the base, remaining well ahead thus providing an effective preview distance. From this observation, we hypothesized that distally pointing hairs are critical in maintaining a wall contact point well ahead of the animal or robot on rough surfaces. For smoother surfaces, we would expect the coefficient of friction to become more important. To test the hypothesis that distally pointing hairs are critical to maintain an effective preview distance, we performed an additional experiment in which the side of the antenna ipsilateral to the wall had distally pointing hairs while the other side had proximally pointing hairs. When the antenna flipped, the proximally pointing hairs came into contact with

the wall, pointing toward the direction of movement. In all trials (10/10), the preview distance relative to the base became negative after the flip (Fig. 7E). These results demonstrate the importance of distally pointing hairs in maintaining an adequate preview distance following a flip on rough surfaces. Similarly, we would expect unidirectional friction to be an important property affecting preview distance on smoother surfaces.

Discussion

Locomotion-mediated tactile sensing

How animals integrate noisy sensory information with a dynamic body during rapid locomotor tasks, specifically where neural bandwidth limitations and conduction delays impose severe constraints on control, remains a challenge in neuromechanics. We discovered that during high-speed wall following, cockroaches' active antennal reconfiguration uses the energy from locomotion rather than energy generated by muscles directly associated with the sensor (Fig. 1A). Reconfiguration through running relies on the passive properties of the antenna to position the sensor in its most effective mechanical state: bent backward (Fig. 1B). A newly discovered mechanical function for antennal hairs, previously described exclusively as sensory structures (Shafer & Sanchez, 1973; Schaller, 1978), results from hairs interlocking with rough walls to produce the bent state. We abstract this reconfiguration by showing distinct mechanical states x_1 (forward) and x_2 (backward) that are "switched" by an interaction among locomotion as the self-generated energy source, a mechanically tuned passive sensor and the environment (Fig. 1B). These states can in turn affect the information $I(x_n)$ available to the neural controller that informs how the motor system modifies movement. We contend that during locomotor tasks where bandwidth limitations and neural conduction delays become significant, animals can shift control to the mechanics of their sensor for effective tactile sensing.

In contrast to previous studies on slow, exploratory active sensing with antennae in arthropods such as in cockroaches (Comer et al., 2003; Okada and Toh, 2004; Harley et al., 2009), crayfish (Basil & Sandeman, 2000) and stick insects (Dürr et al., 2001), here we show explicitly that body movement and sensor mechanics work synergistically in the sensing task and that the sensor is reconfigured as a result of this interaction. Previous studies during slow, exploratory active sensing tasks have shown the importance of integrating body, movement, and sensor (Chiel et al., 2009), but we are not aware of any studies demonstrating the case in Figure 1A, in which the energy from locomotion is transferred to the sensor, enabling it to reconfigure itself for the task of high-speed tactile navigation.

The effect of a tactile sensor's mechanical state and its interaction with the environment has also been studied in whisking in rats. It has recently been shown that a whisker can transmit different forces based on whether it hits the convex or concave side first, which could have important implications for sensory processing (Quist and Hartmann, 2012). Specifically Quist and Hartmann (2012) showed that when an applied force makes contact on the convex side of a whisker, the magnitude of the axial force generated at the base was higher when compared to the same force applied to the concave side. Trigeminal ganglion neurons are known to be very sensitive to axial forces; therefore, this biomechanical filtering, which depends on the force

direction, could have important implications for sensing and behavior (Quist and Hartmann, 2012). Although whiskers, unlike arthropod antennae, are nonsensate along their length, rich sensory information about spatial properties of object can be extracted such as surface texture, object size and shape by sensing at the base of the vibrissae (Diamond et al., 2008; Vincent, 1912; Carvell and Simons, 1990). Our results are related in that we observed a change in behavior depending on whether the ipsilateral antenna is concave or convex relative to the wall, where the applied force is a normal force generated from the wall surface. While these results from mechanical properties of whiskers have not yet been linked directly to behavior and control as we have done here in the cockroach, we suspect that similar principles may apply and may be an interesting avenue for investigation.

Antennal mechanical state affects control strategy

Our previous control theoretic model of antenna-mediated wall following predicted that control is more challenging as the velocity increases and simpler with a greater preview distance (i.e. a longer antenna; Cowan et al., 2006). In the present study, when wall-following cockroaches were presented with smoother and rougher walls, we found that the antenna could assume two states: projecting backward and forward (Fig. 5A). This result suggested that the transition between the observed antennal mechanical states was mediated by the mechanical properties of the environment coupled with locomotion. To understand how the environment affects antennal state, we compared the antennal posture of wall-following cockroaches running along smoother and rougher surfaces, and found significant differences in the proportions of forward and backward-projecting antennae (Fig. 5B). Furthermore, by comparing transition probabilities for a simple two-state Markov chain, we found that transition probabilities when the antenna occupied a forward state were significantly different between smoother and rougher walls (Fig. 5C). Using predictions from a control-theoretic model of wall following, we hypothesized that a forward state would give the cockroach a greater preview distance by geometry alone; thus, we predicted that wall following control would be easier according to the model developed by Cowan et al. (2006). By comparing body-to-wall distance, a putative state variable for control of wall following hypothesized by Cowan et al. (2006), we showed that animals running at similar speeds with an antenna projecting forward ran on average closer to the wall compared to those running with an antenna projecting backward (Fig. 6A,B). This change in body-to-wall distance corresponds to approximately a whole body width of *P. americana*. Interestingly, the body-to-wall distance for cockroaches running in the forward antenna state is similar to the one measured for cockroaches running with an ablated antennae ipsilateral to the wall (Camhi and Johnson, 1999), thus suggesting that the mechanical state is potentially affecting the encoding of information and the strategy that the animals are employing. Furthermore, we determined that dynamic changes in the state of the antenna were correlated with changes in wall-following tracking behavior, specifically initiation of body turns. Changes in mean body angles following a flip were statistically significant between the “flip” and control data (Fig. 6D,E).

To determine if this change in tracking strategy could have important consequences on wall following performance, we tracked the frequency of leg and body contact for both cases. Our results showed a significant difference in the proportion of leg and body contact associated with the antenna state (Fig. 6C). We observed that both leg and body contact, but especially body

contact, were linked with body-to-wall collisions, often leading to a decrease in speed due to body redirection. We found the median change in velocity to be -7.48 cm s^{-1} when comparing approximately 2 strides before and after contact. Our observations and measurement on wall collisions are in agreement with observations described in Baba and Tsukada (2010). They noted that cockroaches that ran sufficiently close to the wall "touched it with their body and this sometimes cause[d] them to fall" (Baba and Tsukada, 2010). In summary, for animals running with their antenna projecting forward, we observed marked changes in behavioral strategy including increased leg and body contact and wall collision leading to significant decreases in speed. This suggests that wall following behavior in cockroaches is robust. Our results raise the possibility that increased leg contact could allow a cockroach to sense the wall with its legs, thus relying on different sensory modalities (e.g. tarsus or leg hair contact) for thigmotaxis, as suggested by Camhi and Johnson (1999). Employing a strategy that relies on leg and body contact for sensing comes with a cost: the increased probability of body decelerations due to collisions with clear consequences when placed within the context of high-speed predator evasion. In conclusion, our results do not support the hypothesis that an increased preview distance afforded by a forward-projecting antenna leads to improved wall following. In fact, tracking performance and task-level control was superior with a backward-projecting antenna. However, it remains unclear if body-to-wall distance information can be sensed by the antenna when it is in a forward-projecting state. After demonstrating that the antenna state is critical for task-level control, we hypothesized that the mechanical tuning of the antenna – and in particular the mechanical role played by sensory hairs – may enable passive switching to the backward-projecting state.

Mechanical role of sensory hairs

We showed that passive antenna hairs coupled with forward motion are sufficient to allow an antenna to transition to a different mechanical state by selectively ablating mechanosensory hairs using a high-precision laser system (Fig. 3). By displacing a fixed animal with its antenna projecting forward against a wall surface, we showed that we could reproduce the forward to backward projecting sensor reconfiguration observed in the running animal. A repeat of the experiment with ablated hairs demonstrated that hairs play an important role in the reconfiguration (Fig. 7B). Effectively, we showed that a distributed hair array on a sensor is effective at allowing the sensory appendage to "stick" to a substrate by interlocking. Small, distributed hairs are especially effective as the ability of hairs to engage in asperities increases as the radius of the tip decreases (Asbeck et al., 2006).

The role of directionally tuned hair arrays has previously been studied during high-speed terrestrial locomotion in cockroaches, spiders and crabs (Spagna et al., 2007). Leg hairs or spines were shown to function as distributed contact points by increasing the probability of foot engagement when animals ran over terrain with sparse contacts. High-speed running cockroaches, spiders, and crabs attained increased mobility with collapsible spines without any detectable changes in neural feedback. Spagna et al. (2007) provided evidence for a novel mechanical function for these spines that were thought to only play a role in sensing. Similarly, in the present study we discovered that hairs on antennae, also once thought only to play a role in sensing, have a new function that is mechanical. Specifically, hairs can mechanically interlock

with surfaces and allow the antenna to adopt a different configuration when coupled with locomotion. The study on leg spines reinforced the importance of integrating passive mechanics to understand principles of stability and maneuverability in high-speed terrestrial locomotion when the neuromechanical system is pushed near its limits (Full and Koditschek, 1999). Analogously, we provide support that understanding the biomechanical processing of sensory appendages prior to neural transduction is critical to understanding sensorimotor integration during rapid behaviors (Sane and McHenry, 2009). While we found that the properties of the surface can influence the mechanical state of the antenna, it is important to note that another variable involved is the angle of attack of the antenna flagellum with respect to the wall as noted by Camhi and Johnson (1999). For low angles of attack, we would expect the hairs to play a more important role in influencing the antenna state, whereas for high angles of attack, hairs may not be necessary. Here, we found no evidence that animals employed high angles of attack to exploit this effect (median angle of attack relative to wall = 1.4°, n = 580 strides).

Finally, our biological results lead to a directly testable neurobiological hypothesis. Specifically, we hypothesize that the mechanical state of the antenna may affect sensory processing and subsequently affect the information available to the neural controller downstream. Recording directly from the antennal nerve in a virtual turning experiment as developed by Lee et al. (2008) within the control theoretic context developed by Cowan et al. (2006) could reveal how sensory processing is influenced by the interaction between the antenna and a wall projection.

Physical model of antenna provides insight on preview distance

To further explore biomechanical factors which may influence the process of antenna reconfiguration, we built a tunable physical model of an arthropod antenna inspired from the American cockroach (Fig. 4; Demir et al., 2010). This physical model allowed us to manipulate mechanical parameters that would otherwise be difficult or impossible to test in animals. In our experimental trials, we considered different initial conditions for wall roughness, hair geometry and orientation for a constant antenna length, antenna stiffness, base angle, base velocity and wall distance. We showed that the robotic antenna's flipping statistics were categorically affected by the existence of appropriately oriented hairs for a given wall roughness (Fig. 7C,D). Distally projecting hairs tended to anchor themselves immediately, and the shear forces at the surface easily overcame the inter-segmental joint stiffness along the antenna. As the base moved at a constant velocity, the joint angles changed continually either until the distal segments became perpendicular to the wall (flip) or until the shear forces between the distal segments and the wall overcame the hair-asperity contact strength (no flip). These results from the physical model confirm that distally pointing hairs increase the probability of engaging wall asperities, which constitutes the main physical interaction in mediating the flip on rough surfaces.

In addition, the physical model provided new biological insight. We showed that for rough surfaces, distally pointing hairs, following reconfiguration, are critical in maintaining an adequate preview distance such that the contact point can remain well ahead of the linear actuator base or “head” (Fig. 7E). We suspect that for rougher surfaces, hair-asperity engagement will dominate whereas for smoother surfaces the coefficient of friction will become more important. Thus, for smoother surfaces unidirectional friction will be an important factor

influencing preview distance. Preview distance is a critical parameter for stable high-speed tactile navigation, as rigorously demonstrated in a neuromechanical model of wall following using realistic cockroach running dynamics (Lee et al., 2008). We propose that distally pointing hairs for rough surfaces and unidirectional friction for smooth surfaces along with properly tuned mechanics (i.e. flexural stiffness profile) are important mechanical parameters that influence preview distance.

In future studies, it will be essential to further explore the design space for building an effective tactile sensor on a dynamic, mobile robot. For example, the backward-projecting "inverted-J" antenna shape may be more effective for following surfaces with asperities and/or obstacles. We hypothesize that this shape may significantly decrease the probability of the antenna to wedge into surface asperities, which may have important implications for sensing. Some of the advantages of this geometry have been successfully tested in a bio-inspired wall-following robot (Lee et al., 2008). We speculate that the bent-backward geometry can increase the effective preview sensory volume (Snyder et al., 2007) available to a surface-following robot by increasing the probability of contact ahead. However, there is an important design trade-off in the backward projecting geometry that will need to be explored further. Specifically, the potential advantages of this shape come at a cost of decreasing preview distance. Finally, it will be necessary to investigate the effect of the antennal stiffness profile during wall following and/or surface contour extraction tasks. Preliminary results from Demir et al. (2010) suggest that a more compliant tip – i.e. a decreasing stiffness profile – can help resolve finer details (higher spatial frequencies) during a contour extraction task. Studies on the biomechanics of arthropod antennae such as in crayfish (Sandeman, 1989) and stick insects (Dirks and Dürr, 2011) are consistent with a decreasing flexural stiffness from base to tip. While from geometry we expect similar mechanical properties in *P. americana* (Kapitskii, 1984), further mechanical testing will be necessary.

From an engineering point of view, we have shown that distally oriented hairs can facilitate a change of mechanical state of a physical model of an antenna when coupled with forward motion. On rough surfaces, distally pointing hairs allow the antenna to maintain an effective preview distance following reconfiguration. This is an important advance in bio-inspired antenna design for mobile robotic applications, as it provides a mechanism that relies on passive mechanics and locomotion without relying on actuated sensor control. Further studies will need to determine the effect of tactile sensor configuration on high-speed wall following performance and the feasibility of the flipping mechanism on mobile robots. This mechanism may afford a robust solution for mobile robots operating in challenging environments for search and rescue operations and exploration where sonar and vision-based sensors may be insufficient.

References

Asbeck, A. T., Kim, S., Cutkosky, M. R., Provancher, W. R., and Lanzetta, M. (2006). Scaling hard vertical surfaces with compliant microspine arrays. *Int. J. Rob. Res.* **25**, 1165–1179.

Baba, Y. and Tsukada, A. (2010). Collision avoidance by running insects: antennal guidance in cockroaches. *J. Exp. Biol.* **213**, 2294–2302.

Bajcsy, R. (1988). Active Perception. *Proc. IEEE*. **76,** 966-1005.

Basil, J., and Sandeman, D. (2000). Crayfish (*Cherax destructor*) use tactile cues to detect and learn topographical changes in their environment. *Ethology.* **106**, 247–259.

Bell, W., Roth, W.J., Louis, M. (2007). Cockroaches: Ecology, behavior, and natural history. p. 39. Johns Hopkins University Press.

Camhi, J. M. and Johnson, E. N. (1999). High-frequency steering maneuvers mediated by tactile cues: antennal wall-following in the cockroach. *J. Exp. Biol.* **643**, 631–643.

Carvell, G. E. and Simons, D. J. (1990). Biometric analyses of vibrissal tactile discrimination in the rat. *J. Neurosci.* **10**, 2638–2648.

Chiel, H. J., Ting, L. H., Ekeberg, O., and Hartmann, M. J. Z. (2009). The brain in its body: motor control and sensing in a biomechanical context. *J. Neurosci.* **29**, 12807–14.

Coles, R. B. and Guppy, A. (1988). Directional hearing in the barn owl (*Tyto alba*). *J. Comp. Phys. A.* **163**, 117–33.

Comer, C.M., Parks, L., Halvorsen, M.B., Breese-Terteling, A. (2003). The antennal system and cockroach evasive behavior II: stimulus identification and localization are separable antennal functions. *J. Comp. Phys. A*. **189**, 97-103.

Cowan, N. J., Lee, J., and Full, R. J. (2006). Task-level control of rapid wall following in the American cockroach. *J. Exp. Biol.* **209**, 1617–1629.

Demir, A., Samson, E., and Cowan, N. J. (2010). A tunable physical model of arthropod antennae. *IEEE Int. Conf. Robot. Autom*. 3793-3798.

Dickinson, M.H. (2005). The initiation and control of rapid flight maneuvers in fruit flies. *Integr. Comp. Biol.* **45**, 274-281.

Diamond, M. E., von Heimendahl, M., Knutsen, P. M., Kleinfeld, D., and Ahissar, E. (2008). "Where" and "what" in the whisker sensorimotor system. *Nat. Rev. Neurosci.* **9**, 601–12.

Dirks, J.H., Dürr, V. (2011). Biomechanics of the stick insect antenna: damping properties and structural correlates of the cuticle. *J. Mech. Behav. Biomed. Mater*. **4**, 2031-42.

Dürr, V., Konig, Y., Kittmann, R. (2001). The antennal motor system of the stick insect *Carausius morosus*: anatomy and antennal movements during walking. *J. Comp. Phys. A*. **187**, 131-144.

Egelhaaf, M., Kern, R., Krapp, H. G., Kretzberg, J., Kurtz, R., and Warzecha, A. K. (2002). Neural encoding of behaviourally relevant visual-motion information in the fly. *Trends Neurosci.* **25**, 96–102.

Elzinga, M.J., Dickson, W.B., Dickinson, M.H. (2012). The influence of sensory delay on the yaw dynamics of a flapping insect. *J. R. Soc, Interface*. **9**, 1685–1696.

Ghose, K. and Moss, C. F. (2006). Steering by hearing: a bat's acoustic gaze is linked to its flight motor output by a delayed, adaptive linear law. *J. Neurosci.* **26**, 1704–10.

Harley, C.M., English, B.A., Ritzmann, R.E. (2009). Characterization of obstacle negotiation behaviors in the cockroach, *Blaberus discoidalis*. *J. Exp. Biol.* **212**, 1463-1476.

Hartmann, M. (2001). Active sensing capabilities of the rat whisker system. *Auton. Robots.* **11**, 249–254.

Holmes, P., Full, R. J., Koditschek, D. E., and Guckenheimer, J. (2006). The dynamics of legged locomotion: models, analyses, and challenges. *SIAM Rev. Soc. Ind. Appl. Math.* **48**, 207-304.

Kapitskii, S.V. (1984). Morphology of the antenna of the male American cockroach *Periplaneta americana*. *J. Evol. Biochem. Physiol.* **20**, 55-66.

Koehl, M. A., Koseff, J. R., Crimaldi, J. P., McCay, M. G., Cooper, T., Wiley, M. B., and Moore, P. A. (2001). Lobster sniffing: antennule design and hydrodynamic filtering of information in an odor plume. *Science.* **294**, 1948–51.

Lee, J., Sponberg, S. N., Loh, O. Y., Lamperski, A. G., Full, R. J., and Cowan, N. J. (2008). Templates and anchors for antenna-based wall following in cockroaches and robots. *IEEE Trans. Robot.* **24**, 130–143.

More, H. L., Hutchinson, J. R., Collins, D. F., Weber, D. J., Aung, S. K. H., and Donelan, J. M. (2010). Scaling of sensorimotor control in terrestrial mammals. *Proc. R. Soc. Lond. B Biol. Sci.* **277**, 3563–3568.

Nelson, M. E. and MacIver, M. A. (2006). Sensory acquisition in active sensing systems. *J. Comp. Phys. A.* **192**, 573–586.

Okada, J. and Toh, Y. (2004). Antennal system in cockroaches: a biological model of active tactile sensing. *International Congress Series*. **1269**, 57–60.

Olberg, R.M., Worthington, A.H., Venator, K.R. (2000). Prey pursuit and interception in dragonflies. *J. Comp. Phys. A*. **186**, 155-162.

Polak, M. and Rashed, A. (2010). Microscale laser surgery reveals adaptive function of male intromittent genitalia. *Proc. R. Soc. Lond. B Biol. Sci.* **277**, 1371–1376.

Prescott, T.J., Diamond, M.E., Wing, A.M. (2011) Active touch sensing. *Phil. Trans. R. Soc. B.* **366**, 2989-2995.

Quist, B. W. and Hartmann, M. J. Z. (2012). Mechanical signals at the base of a rat vibrissa: The effect of intrinsic vibrissa curvature and implications for tactile exploration. *J. Neurophysiol.* **107**, 2298–2312.

Sandeman, D. (1989). Physical properties, sensory receptors and the tactile reflexes of the antenna of the Australian freshwater crayfish *Cherax destructor*. *J. Exp. Biol.* **141**, 197-217.

Sane, S. P. and McHenry, M. J. (2009). The biomechanics of sensory organs. *Integr. Comp. Biol.* **49**, 8–23.

Schaller, D. (1978). Antennal sensory system of *Periplaneta americana* L.: distribution and frequency of morphologic types of sensilla and their sex-specific changes during postembryonic development. *Cell Tissue Res.* **191**, 121–139.

Seelinger, G. (1984). Sex-specific activity patterns in *Periplaneta americana* and their relation to mate-finding. *Zeitschrift für Tierpsychologie*. **65**, 309-326.

Shafer, R. and Sanchez, T. V. (1973). Antennal sensory system of the cockroach, *Periplaneta americana*: postembryonic development and morphology of the sense organs. *J. Comp. Neurol.* **149**, 335–354.

Snyder, J. B., Nelson, M. E., Burdick, J. W., and Maciver, M. A. (2007). Omnidirectional sensory and motor volumes in electric fish. *PLoS Biol.* **5**, e301.

Spagna, J. C., Goldman, D. I., Lin, P.-C., Koditschek, D. E., and Full, R J (2007). Distributed mechanical feedback in arthropods and robots simplifies control of rapid running on challenging terrain. *Bioinspir. Biomim.* **2**, 9–18.

Staudacher, E., Gebhardt, M., and Durr, V. (2005). Antennal movements and mechanoreception: neurobiology of active tactile sensors. *Adv. In Insect Phys*. **32**, 49-205.

Vincent, S. B. (1912). The function of the vibrissae in the behavior of the white rat. *Behav. Monographs*. **1**, 1-82.

Wotton, J. M., Haresign, T., and Simmons, J. A. (1995). Spatially dependent acoustic cues generated by the external ear of the big brown bat, *Eptesicus fuscus*. *J. Acoust. Soc. Am*. **98**, 1423–1445.

Figure 1. Control diagram of locomotion-mediated tactile sensing with sensor reconfiguration via passive mechanics. (A) Abstraction of the interaction between an organism and its environment during the sensing task illustrated in (B). The interaction between locomotion (the self-generated energy source), a passive sensor (darker shaded box) and the environment (lighter shaded box) processed through the biomechanics of a sensor can change the mechanical state of a sensor. The resulting distinct mechanical states of the sensor expressed by state parameters x_1 and x_2 can influence the information $I(x_n)$ available to the neural controller. (B) Summary of evidence of locomotion-mediated tactile sensing for wall following in the American cockroach, *P. americana*. We illustrate that the physical interactions between an organism and its environment when locomoting can lead to a reconfiguration (white arrow) of the sensor state (state x_1 [forward] to state x_2 [backward]) via passive mechanics. Arrows between the neural controller and musculoskeletal system indicate neural feedback whereas arrows between the body dynamics and musculoskeletal system indicate mechanical feedback.

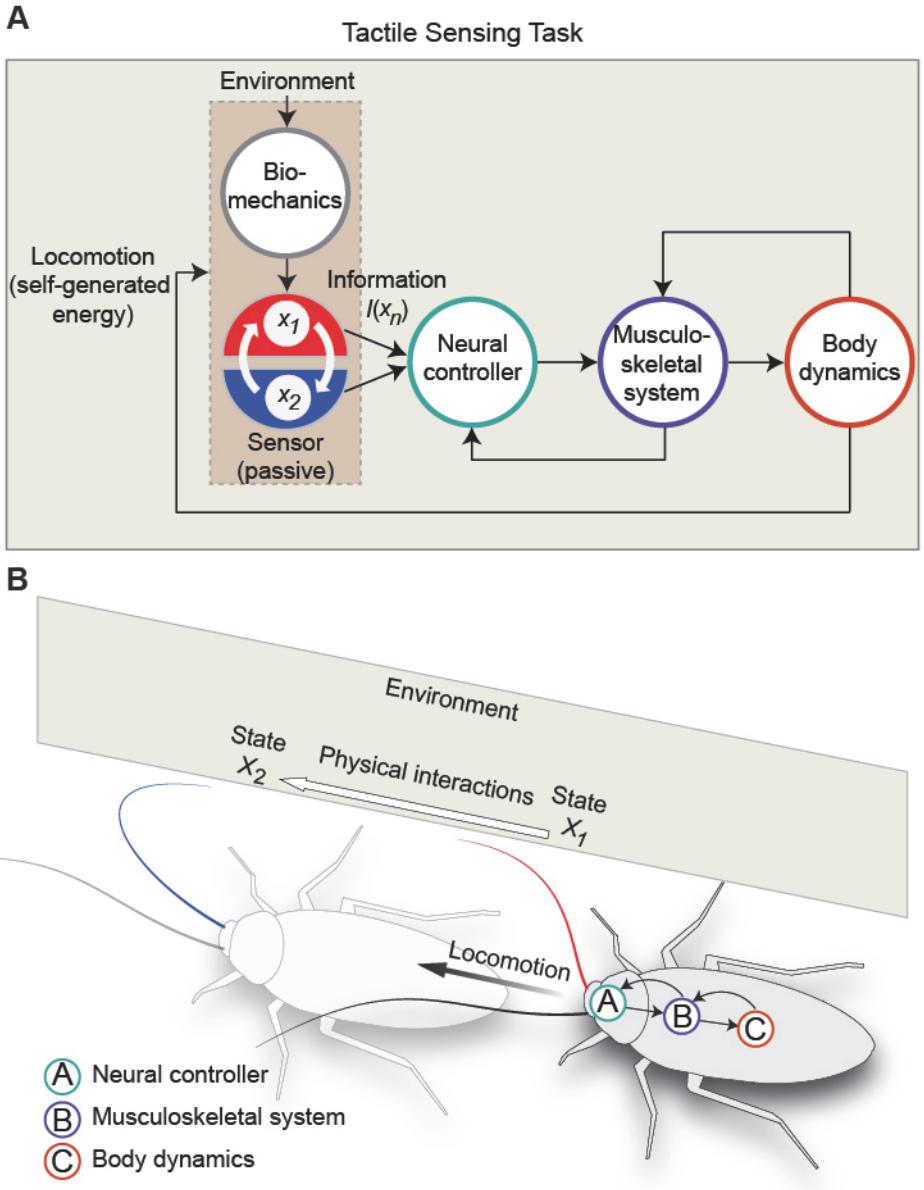
A
Tactile Sensing Task
Environment
Bio-
mechanics
Locomotion
(self-generated
energy)
Information
$I(x_n)$
x_1
x_2
Sensor
(passive)
Neural
controller
Musculo-
skeletal
system
Body
dynamics
B
Environment
State
X_2
Physical interactions
State
X_1
Locomotion
A
B
C
A Neural controller
B Musculoskeletal system
C Body dynamics

Figure 2. Experimental setup to study high-speed wall following. (A) Arena with a turn perturbation for eliciting high-speed escape and wall following in cockroaches *P. americana*. We recorded the time prior and after a turn using two synchronized high-speed video cameras. Adapted from Cowan et al., 2006. (B) Kinematic parameters evaluated for wall following. We digitized the two markers on the cockroach body (large white dots) to extract the point of rotation (POR; small dot with arrow) and body angle θ relative to the wall. v is the forward velocity of the animal.

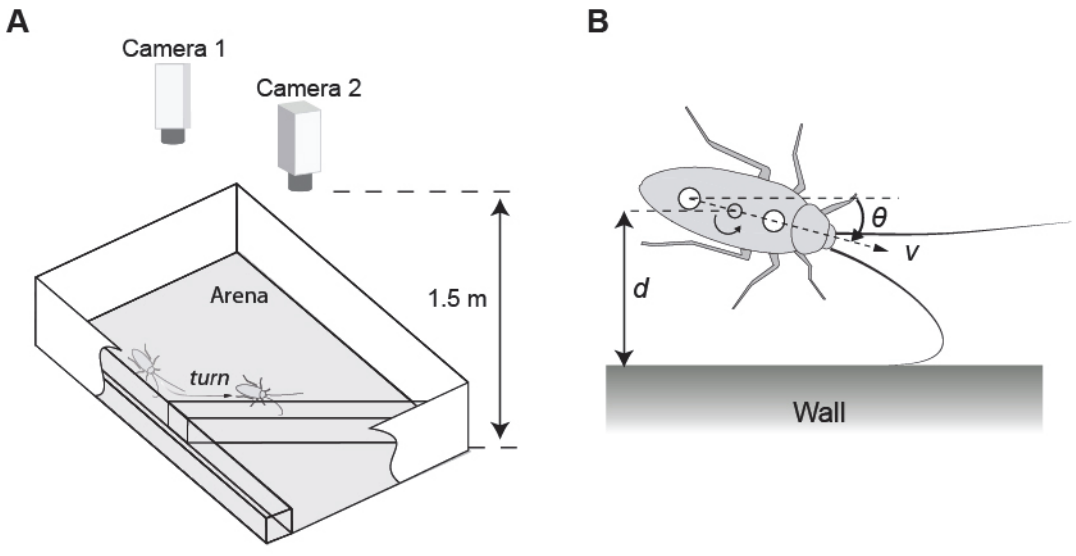
A
Camera 1
Camera 2
Arena
1.5 m
turn
B
θ
v
d
Wall

Figure 3. Methods for determining mechanical role of hairs. (A) Procedure for laser hair ablation. The body and antennae of cockroaches were restrained on an x-y stage while we applied laser pulses at the tip of the antenna on both the ventral and dorsal sides. The inset shows high-resolution images of the three distal-most annuli of a cockroach antenna viewed from the ventral position. The top image shows the antenna before hair ablation and the bottom image shows the same antenna annuli after laser hair ablation. The scale bar is 40 μm. (B) Experimental procedure for determining the role of hairs in reconfiguring the antenna. We mounted body and antenna-fixed animals on a platform and allowed the tip of the antenna to slide along a rough (paraffin) wall mounted on a motorized stage. The inset shows a drawing of a treated antenna prior to interacting with the wall.

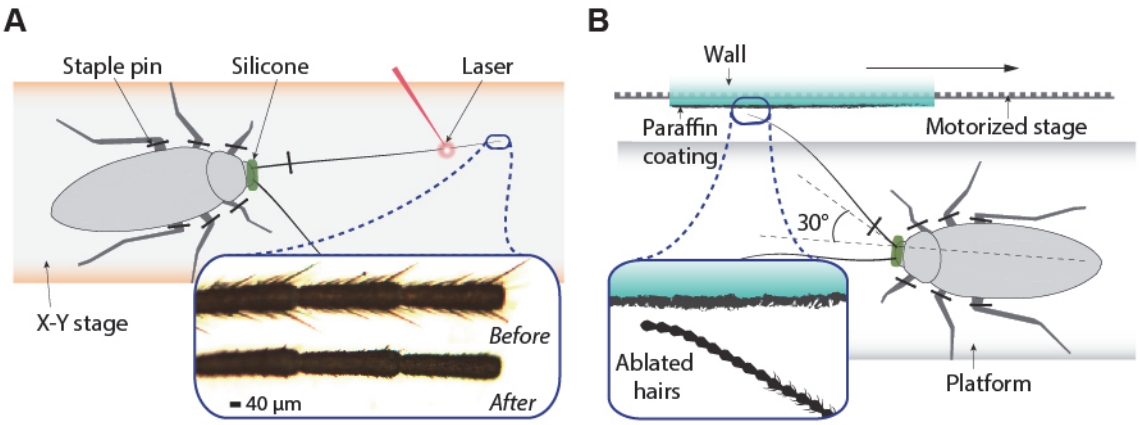
A
Staple pin
Silicone
Laser
X-Y stage
Before
After
40 µm
B
Wall
Paraffin coating
Motorized stage
30°
Ablated hairs
Platform

Figure 4. Physical model of antenna. (A) Physical model for independently testing the hypothesis that hairs facilitate the passive reconfiguration of an antenna. The 8-segment robotic antenna with anisotropic hairs is tangent to a felt-cloth covered wall in the forward-projecting posture. (B) Close-up of the robotic antenna showing the inter-segmental joints and the collapsing direction of a hair. (C) CAD rendering of a single antenna segment with anisotropic hairs: 1: NiTi hair tip and stiffness element; 2: Hair; 3: Hair 45° hard stop; 4: Segment cover; 5: Hair slots; 6: Contact sensor.

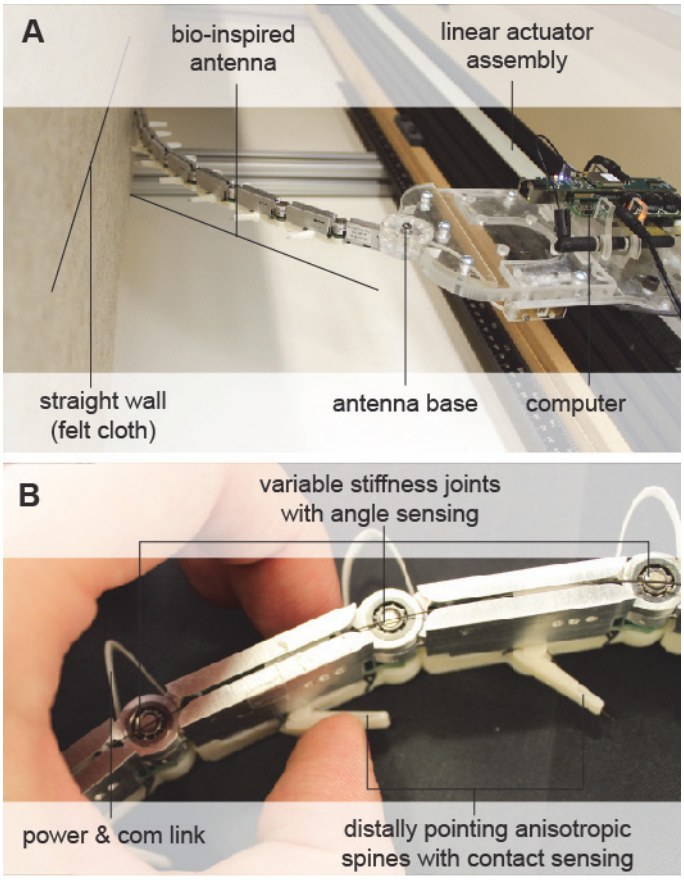
A
bio-inspired antenna
linear actuator assembly
straight wall (felt cloth)
antenna base
computer
B
variable stiffness joints with angle sensing
power & com link
distally pointing anisotropic spines with contact sensing
C
1
2
3
4
5
6

Figure 5. Effect of wall properties on antenna mechanical state. (A) Two wall following sequences during a turn perturbation recorded from high-speed video. The left panel shows a cockroach running with its antenna bent, projecting backward, whereas the right panel shows the same animal in a different trial running with the antenna straight, projecting forward. Wall properties are the same for both trials. Boxes with dotted lines highlight the shape of the antenna as it interacts with the wall. (B) Proportion of antennae pointing forward, backward or flipping for smoother and rougher wall surfaces. Wall surfaces categorically affected the antenna state. (C) Transition probabilities within and between states by modeling antenna reconfiguration as a two-state discrete Markov chain. Transition probabilities calculated from the transition matrices for both smoother and rougher walls are shown by arrows.

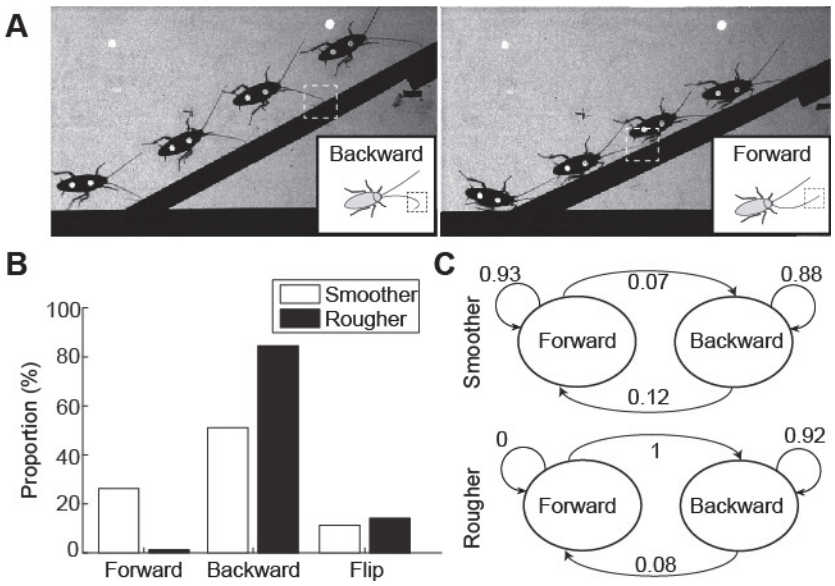
A
Backward
Forward
B
Smoother
Rougher
Proportion (%)
100
80
60
40
20
0
Forward
Backward
Flip
C
Smoother
0.93
0.07
0.88
Forward
Backward
0.12
Rougher
0
1
0.92
Forward
Backward
0.08

Figure 6. Locomotor performance as a function of antenna mechanical state. (A) Body-to-wall distances of cockroaches wall following for antennae projecting backward or forward as a function of time following a turn perturbation. The shaded blue and red regions show the full range of body-to-wall distances while individual lines represent single trials. Animals running with an antenna projecting forward following a turn ran significantly closer to the wall than animals running with an antenna projecting backward ($p<0.001$). (B) The box plot summarizes body-to-wall distances shown in (A) for backward and forward groups. (C) Proportion of trials where the leg and/or body contacted the wall for strides with forward and backward projecting antennae. Overall, the antenna state had a statistically significant association on the frequency of leg and body contacts ($p<0.001$). (D) (top) Body angles for animals running while the antenna flipped from forward to backward projecting. Individual lines represent single trials. The vertical dashed line represents the onset of the antenna flip. (bottom) Body angles for non-flip control group. Individual lines are randomly selected trials where the antenna remained backward. The vertical dashed line represents randomly selected time events. Positive angles indicate the cockroach was turning away from the wall and negative angles indicate the cockroach was turning toward the wall. (E) The box plot summarizes the bootstrapped body angles following a flip and for non-flip controls. Angles were statistically significant when comparing 95% confidence intervals. For box plots in (B) and (F) the central line is the median, the bottom and top edges of the box are the 25^{th} and 75^{th} percentiles and the whiskers extend to ± 2.7 standard deviations. Red crosses represent outliers lying outside whiskers.

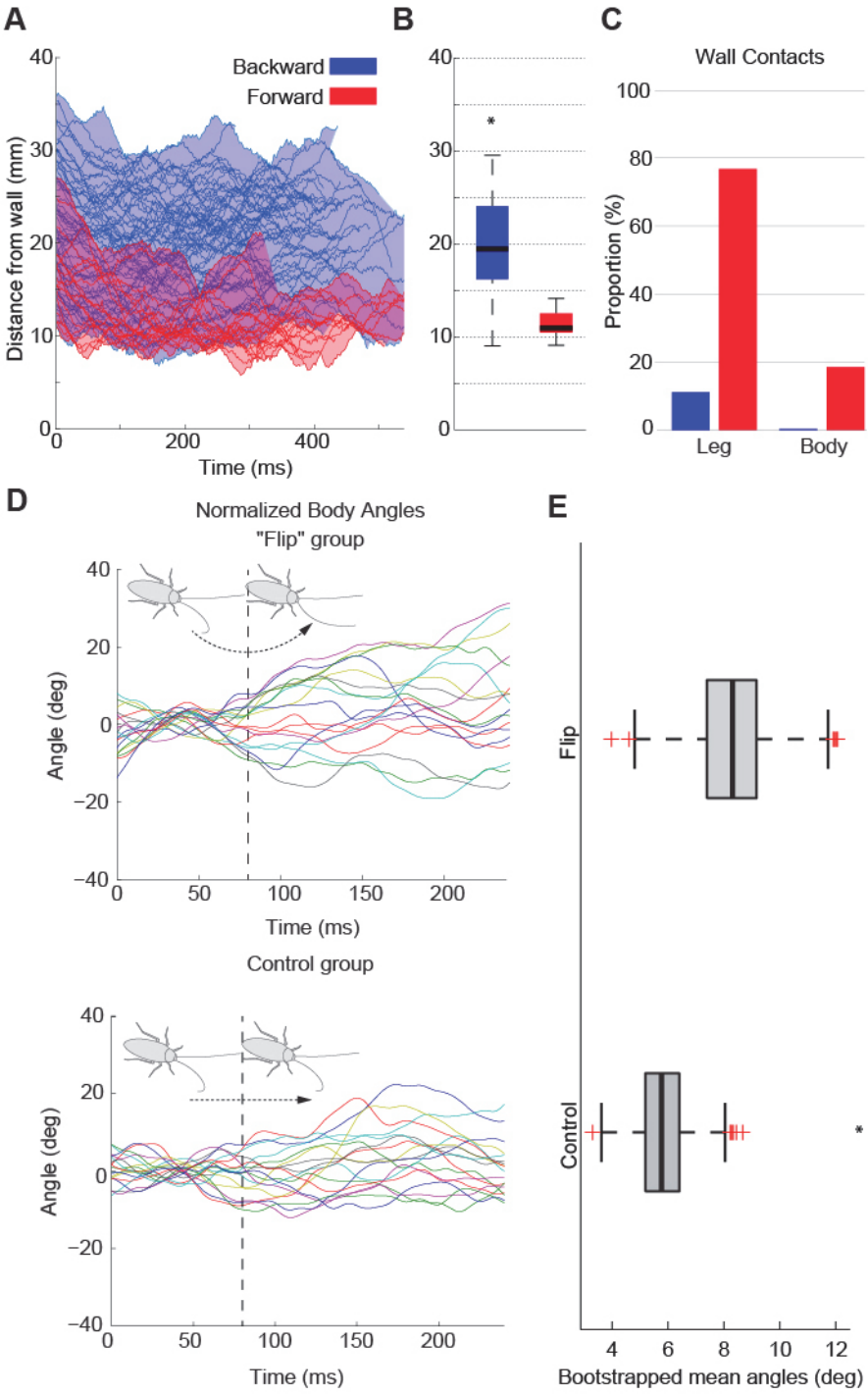
A
B
C
Backward
Forward
Distance from wall (mm)
Time (ms)
Wall Contacts
Proportion (%)
Leg
Body
D
Normalized Body Angles
"Flip" group
Angle (deg)
Time (ms)
Control group
E
Flip
Control
Bootstrapped mean angles (deg)

Figure 7. Sufficiency of antenna hairs in mediating an antenna "flip" from forward to backward state in biological and robotic experiments. (A) Sequence of a flip from a non-treated, intact cockroach antenna. The antenna is initially in a forward-projecting state. As the wall moves, the antenna catches and flips to a backward-projecting state. (B) Proportion of flips between non-treated and treated cockroach antennae. Non laser-treated (intact) antennae flipped at a statistically higher proportion than treated antennae ($p<0.001$). (C) and (D) depict data from individual joint angle sensors from the robotic antennna during an experimental trial starting from t_0 until t_{final} where d is the distance between the base of the antenna and the wall. A "flip" is registered when the anchored segment (most distal) is perpendicular to the wall. In (C), at t_{flip} the distally oriented hairs engage in the wall which results in the antenna transitioning (yellow) from a forward (pink) to a backward (green) projecting position. During this trial the wall was covered with rough, felt cloth and the hairs were oriented distally. In (D), the wall was covered with felt cloth and the three distal-most hairs of the robotic antenna were removed. This panel shows a failed transition from experimental data as the antenna remains forward projecting (pink) during the entire trial. When the antenna interacted with the felt-cloth wall, it resulted in a failed transition (arrow). (E) Data from one trial in which robotic antennal hairs ipsilateral to the wall were pointing distally while those on the other side were pointing proximally. After the antenna flipped, the proximally pointing hairs engaged causing the contact point to move behind the base thus significantly affecting the preview distance.

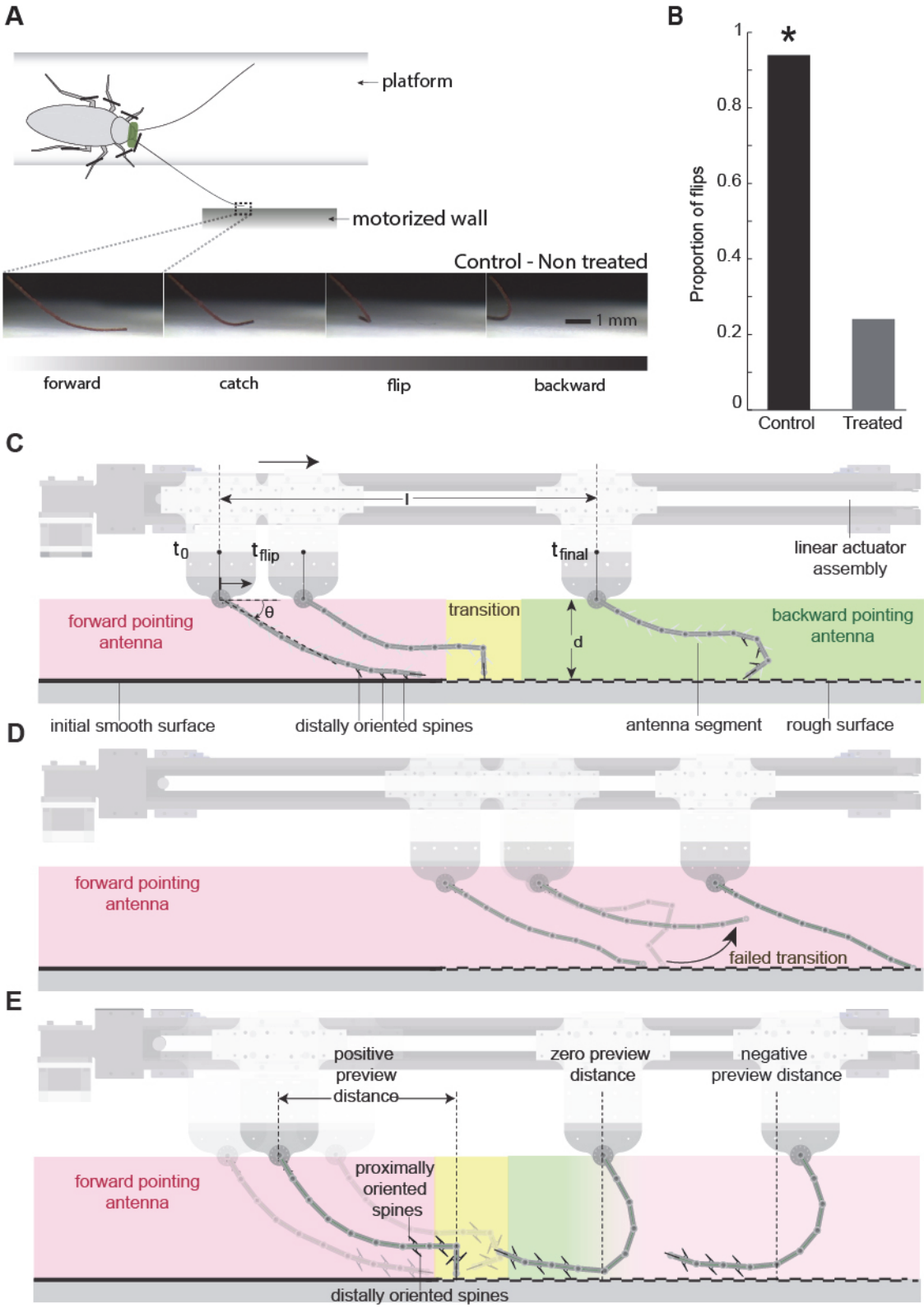
A
platform
motorized wall
Control - Non treated
1 mm
forward
catch
flip
backward
B
Proportion of flips
1
0.8
0.6
0.4
0.2
0
*
Control
Treated
C
l
t_0
t_{flip}
t_{final}
linear actuator assembly
θ
forward pointing antenna
transition
d
backward pointing antenna
initial smooth surface
distally oriented spines
antenna segment
rough surface
D
forward pointing antenna
failed transition
E
positive preview distance
zero preview distance
negative preview distance
forward pointing antenna
proximally oriented spines
distally oriented spines

Chapter 2

Sensory conditioning for neuromechanical control arises from neuronal processing in distributed antennal mechanosensory array

Summary

Motor control requires animals not only to acquire the relevant information from their environment but also to integrate sensory signals with the ongoing motor program. A control theoretic model of high-speed wall following in the American cockroach predicted that antennal tactile sensing of wall position (P) and the derivative of position (D) was sufficient for stable control. Previous whole-nerve recordings from the antenna during a simulated turning experiment demonstrated a population response consistent with P and D encoding, and suggested that the temporally-filtered response was preconditioned for task-level control. We hypothesized that individual mechanoreceptors distributed along the antenna's flagellum encoded P and D signals and that variable-latency responses from each neural unit would be sufficient to generate a conditioned population response. Multi-unit extracellular recordings revealed P and D sensitivity and variable-latency responses with delays matching the timing of turning behavior and population response. A sensory encoding hypothesis, derived from neuromechanical models of a closed-loop behavior, predicts the filtering properties of antenna mechanoreceptors. During wall following, both the information and the temporal filtering properties of the population of afferents may be matched to the dynamic requirements of control. Sensory conditioning could simplify or reduce necessary downstream neural computations since it provides signals that can be transmitted to the motor system with little or no further processing. Conditioning could be critical during behaviors where the reactions are rapid and when the dynamics of movement impose significant constraints on sensorimotor control.

Introduction

During high-frequency sensorimotor control tasks such as predatory escape, the neuromechanical system of animals is pushed to operate near its fundamental limit due to *both* neural conduction delays and locomotor dynamics. Since sensorimotor control bandwidth constraints impose fundamental limits on gains for stable closed-loop control, animals could benefit from having a tuned control system (Cowan et al., 2006; Elzinga et al., 2012). Conditioning of sensory information to match the animal's requirement for control could simplify processing and reduce delays in transforming the stimulus into motor action. The term "conditioning", analogous to signal conditioning in control engineering, implies that the sensory signal is transformed in such a way as to match the requirements of the next stage of processing, thus having a constructive effect. Here we use this term within a biological context to signify something more precise: this signal processing operates to match the dynamic requirements of control of an organism's body. Specifically, we refer to processing occurring at the level of afferents prior to synaptic integration at interneurons and/or motor neurons. We contend that it is critical to interpret sensory neural responses with respect the dynamics of the behavior as the control system of rapid

locomotion is embedded within neural circuits and animals' mechanics. As recently demonstrated in studies of refuge tracking in the electric fish, connecting stimulus and sensory responses with body dynamics is necessary to correctly predict coding properties of sensors (Cowan and Fortune, 2007).

To study sensory conditioning in animals requires control theoretic models of sensorimotor closed-loop behavior integrating detailed knowledge of locomotor dynamics. Fortunately, the American cockroach *Periplaneta americana* is an ideal system to study sensory conditioning as there exists a well-developed characterization of its locomotor dynamics that has been integrated into a closed-loop control theoretic model of high-speed tactile navigation (Lee et al., 2008). During this escape behavior, termed "wall following", *P. americana* navigates using sensory feedback from its antennae – predominantly the flagellum – to track surfaces at speeds up to 80 cm s^{-1} (Figure 1A; Camhi and Johnson, 1999). The antenna's flagellum has a distributed array of about 270,000 sensillae along its length that are sensitive to mechanical and chemical stimuli (Schafer and Sanchez, 1973; Schaller, 1978). As the flagellum bends in response to wall projections, the antenna generates a reference signal for wall position, allowing the cockroach to control its body angle. *P. americana* can generate body rotations of up to 25 times per second and respond to impulse-like perturbations in as little as 30-40 ms (Camhi and Johnson, 1999). These fast responses suggest that neural delays impose severe constraints on sensorimotor control bandwidth.

A closed-loop, control theoretic model of wall following predicted thes sensory information that is required for stable running (Cowan et al., 2006). This model hypothesized that the cockroach controls its distance to the wall d (sensed with antenna) and generates a turning torque u to control body angle (Figure 1B,C). Testing a controller operating on a mechanical model with realistic running dynamics revealed that the cockroach executes the most effective control for stability and maneuverability by detecting not just the relative or proportional (P) distance from the wall, but also wall velocity, the derivate (D) of position (Cowan et al., 2006; Lee et al., 2008). We hypothesized that at the level of afferents, conditioning of the antennal bending stimulus operates to match the information requirement for stable control of wall following, as predicted from a control theoretic model.

Extracellular tungsten recordings of the whole antenna nerve during a simulated turning experiment revealed evidence for proportional (P) encoding of wall position as well as derivative (D) encoding in the bulk population response (Figure 1D; Lee et al., 2008). Specifically, the root mean square (RMS) power of the neural response had directionally-dependent tonic and phasic components, respectively suggestive of P and D control. Explicit dependence on velocity was not demonstrated and the question remains whether P and D signals are encoded at the level of individual receptors or the population. We observed a surprising feature of the whole antenna response: while a neural response was evident almost immediately following the onset of wall movement, it was sustained for ~300 ms even after a brief 40 ms stimulus was concluded (Figure 1D). Assuming antennal conduction delays of 20 ms, as suggested by Camhi and Johnson (1999), one would have expected the neural response to decay quickly following termination of the stimulus, declining within 60-80 ms. This delay in the response suggests that is does not match the time course of the stimulus. Instead, since the cockroach takes several strides (each ~70 ms) to complete a turn, we contend that this temporal filter in the antennal nerve transforms

the sensory stimulus into a time course that matches the animal's turn behavior (Lee et al., 2008). We hypothesize that this processing could have a constructive effect for the control of rapid locomotion.

It remains an open question how upstream conditioning of the stimulus arises from primary afferents. Specifically, how do the individual mechanoreceptive neurons encode the necessary information for stability and subsequently sum to generate the population response? We hypothesized that individual mechanoreceptive neurons would demonstrate explicit position and velocity dependence in response to stimulation from an actuated wall segment moving to simulate a turn. We predicted that individual neurons would express the same temporal filtering characteristics as the population response. Alternatively, the population-level processing could arise from combined action of multiple neurons with different delays and filtering properties. In this study, for the first time, we record neural responses from individual afferents *and* link these responses to the dynamic requirements of control, as predicted from a closed-loop neuromechanical model.

Materials and Methods

Animals

Adult male American cockroaches, *Periplaneta americana*, were acquired from a commercial vendor (Carolina Biological Supply Company) and housed in plastic cages maintained at a temperature of 27 ºC. Cockroaches were exposed to a L:D cycle of 12h:12h and given fruits, dog chow and water ad libitum. We performed a total of 19 recordings (n = 12 animals, mass = 0.78 ± 0.13 g; right antenna length = 4.17 ± 0.38 cm; body length = 3.37 ± 0.16 cm; mean ± std).

Preparation

Animals with intact antennae were first sedated on ice for approximately 30 minutes and then weighted. Cockroaches were restrained dorsal side up on a Sylgard (Dow Chemical) gel plate by placing insect pins in all six legs and one or two staple pins along the abdomen (Fig. 2). We placed an additional staple pin between the pronotum and head, i.e. on the neck, such that the ventral side of the head was flush with the plate. We placed additional small staple pins to hold the antenna of interest at an angle of 30 degrees from the midline using a protractor. This is the angle that cockroaches typically maintain during wall following (Camhi & Johnson, 1999). We carefully fixed the region of the antenna covering the gel plate (including the scape and pedicel as well as the sides of the head) using epoxy glue with a 1 hour drying time to ensure complete fixation. As the flagellum has been shown to be necessary and sufficient for stable wall following (Camhi & Johnson, 1999), we mechanically isolated the scape and pedicel. We then measured and recorded the antenna and body length.

Dissection

Under a dissection microscope, we used a fine dissection knife to cut a small window through the cuticle near the base of the antenna. After cutting the entire plate of cuticle, we removed surrounding tissues to expose the antennal nerve. Once the nerve was well-exposed, a petroleum-jelly well was made to hold a pool of cockroach saline around the nerve (Bech et al., 1960). After preparation, we mounted the animal at a distance of approximately 2.5 cm from the body midline to the actuated wall. The antenna was bent in an inverted J-shape characteristic of thigmotaxis in cockroaches (Camhi & Johnson, 1999; Cowan et al., 2006) and the distal-most segments were fixe to the wall with a small piece of wax to prevent the antenna from slipping laterally during our experiment.

Stimulus generation

To test our hypothesis about proportional (P) and derivative (D) encoding at the level of individual mechanoreceptors, we developed a system for precise position control, mimicking antennal displacements experience during a turn while wall following (Cowan et al., 2006). In short, this system allowed us to simulate turning with the animal held in a fixed state. We attached an acrylic wall segment mounted to a plastic funnel that fit snugly around the cone of a larger speaker (Goldwood GW-1248). We controlled wall position using the speaker's voice coil actuator driven by a current amplifier (Quanser LPAM-1). To monitor the actual position output, a DC-DC Linear Variable Differential Transformer (LVDT; Trans-Tek Incorporated model 0242-0000) was mounted parallel to the base of the wall. The current waveforms used to drive the speaker were generated using a custom Matlab script (Mathworks Inc.) and sent through a data acquisition board (National Instruments BNC-2090) at 40,000 Hz.

Extracellular recording

We performed *en passant* extracellular suction recordings from the antennal nerve. Micropipettes (Sutter Instruments Co., model #B150-86-10) were prepared using a custom recipe on a pipette puller (Sutter Instruments Co. model P-97) to form a short and gradual taper with diameter at the tip near 100 μm, narrower than whole nerve suction electrodes. Silver/Silver-chloride microelectrodes were mounted into the pipettes. The pulled pipettes had an impedance less than 1 MΩ. A reference silver electrode was inserted in the saline pool, away from the recording site. The approach angle of the pipette was approximately 45° from horizontal. We were able to maintain stable recordings for about 3 hours with sufficient signal-to-noise to resolve individual units. Recordings were passed to a high input-impedance probe (Grass Instruments, HIZ probe) before filtering and amplification (Grass Instruments P5 series AC pre-amplifier). Recordings were band-pass filtered from 100-10 KHz with a 60 Hz notch filter. Neurophysiological and LVDT position data were recorded at a sampling rate of 40,000 Hz.

Experimental protocol

After we obtained a stable recording, variable position and velocity ramps were played through the actuated wall. In variable-position rampa, position amplitudes ranged from 0.5-6 mm in steps of 0.5 mm, and the velocity was fixed at 1 mm s^{-1}. The variable-velocity ramps ranged from 10 to 110 mm s^{-1} in steps of 10 mm s^{-1} and were fixed at a position of 10 mm. These ranges of positions and velocities are within the behaviorally-relevant range for wall following as measured by (Cowan et al., 2006) for a 30° turn while running at a rate of approximately 7-17 strides s^{-1}. Each ramp was held at the desired position for a total of two seconds before returning to its neutral zero position for two seconds. We randomized the presentation of variable position and velocity ramps. We collected a total of 10 trials per recording, which lasted for a total of about 1 hour. For the subsequent data analysis, the actual position outputs from the LVDT were used to analyze the neural response to position and velocity ramps. For each recording we performed a control experiment in which the antenna was not in contact with the wall while we played the ramp stimuli. This was in order to determine if chemo- or helio-sensitive receptors were activated during our experiments. We did not find effects of chemical or wind stimuli on our multi-unit recordings.

Data analysis

To identify and sort individual units from our extracellular recordings, we used supervised spike sorting based on wavelet decomposition and superparamagnetic clustering (SPC) algorithms developed by (Quiroga et al., 2004). Prior to processing, we digitally filtered the neural data with a 2^{nd} order Butterworth bandpass filter within a bandwidth of 3-20 kHz. To detect spikes we set a 1 ms absolute refractory period and used an amplitude threshold 5 times the estimated standard deviation of the background noise, as described by (Quiroga et al., 2004). After detection, we stored a total of 3.2 ms of data for each spike. To cluster spikes, we used a total of 300 Monte Carlo iterations and set the minimum cluster size to 20 units. After a round of unsupervised clustering, we carefully went through each individual trial to determine the quality of the clustering process by determining inter-trial repeatability and the stability of the clusters over a range of temperature. We rejected individual trials within a recording session by determining the stability and reproducibility of clusters when compared to the average of trials within the same recording session. These outliers were detected infrequently (11/191 trials) and were most likely due to gradual loss in suction in the electrode during an individual recording session.

To determine if individual units were responsive to the ramp stimuli, we computed a Gaussian-convolved firing rate from binary spikes using a Gaussian window with a standard deviation of 10 ms, cut off after 6 standard deviations. For variable-position ramp trials, we calculated the firing rate after the ramp reached its commanded position and was held; specifically, 0.5 s after and 0.5 s before it returned to its baseline position, for a total of 1.5 s. For variable-velocity ramp trials, we calculated the firing rate from the onset of the ramp to the point when it reached its final position. We computed the median firing rates during these intervals and subtracted these rates from the median baseline firing rate, which we computed over a 10 s interval after all ramp presentations for each recording.

To determine which units were responsive to our ramp stimuli, we used a non-parametric one-way ANOVA test (Kruskal-Wallis) at a significance level of 0.001 between the Gaussian-convolved firing rates and the individual ramp positions and velocities. Only units responsive to variable-velocity ramps were used in the latency and summation analysis (Figure 3,4). For these units, we measured the delays from the onset of a ramp presentation to the maximum spike rate and to the first spike. We measured the decay rates by computing the half-life from maximum Gaussian-convolved firing rates following the ramp presentation. Finally, we summed individual unit responses and compared the temporal characteristics of the summed response to the whole-nerve response reported in (Lee et al., 2008). We summed the averages of each unit for multiple trials and report the average of the averages. To determine if the summed response was consistent with the presence of sustained tonic activity in some units, we compared the plateau regions of the response after stimulus onset. We defined the plateau region as 1.0 to 1.5 s after stimulus and the baseline as -0.5 to -0.1 s before stimulus.

Results

From 19 recordings, the majority of neurons (65%, 30/46) increased their firing rate in proportion to a changing wall velocity, indicating D encoding (Figure 3C). Only a few neurons (4%, 2/54) demonstrated position dependence or P encoding to variable wall positions (Figure 3C). For D-sensitive neurons, our results show that the mean spike rate increased from 0 to ~60 spikes s^{-1} with a plateau beyond a wall velocity of about 60 mm s^{-1} and a linear region from 0 to 60 mm s^{-1} (linear regression: $p < 0.001$).

To test the hypothesis that individual neurons have the same temporal filtering properties as the population response reported in Lee et al. (2008; Fig. 1D), we characterized the properties of the neural response for D-encoding neural units. First, we measured the delays from the onset of a wall presentation to the first spike. We found a broad range of latencies (range: 5.90 to 103.88 ms; 31.22 ± 24.50 ms; mean ± std unless otherwise specified) with a median of 22.54 ms (Figure 4B). Delay to maximum firing rate was similarly variable (70.43 ± 21.36 ms) with a median of 76.87 ms. The median half-life from peak maximum rate for all neurons was 0.033 seconds with some falling off very rapidly and others demonstrating sustained activity (range: 0.014 to 1.16 s). When comparing across individual neural units, we determined variable unit responses to wall movements (Figure 4,5). In addition to the variable latencies and half-lives, one subset (11) of neurons exhibited double peaks in their firing responses, corresponding to the periods of acceleration and deceleration of the wall.

To test if individual D-encoding neural unit differences were sufficient to account for the population level response, we summed the individual unit responses and compared their time courses to the whole nerve recording from Lee et al. (2008; Fig. 1D). Direct summation of individual units (peak time = 100 ms; half-life = 150 ms) approximated the temporal dynamics of the population response (peak time = 90 ms; half-life = 138 ms), with 87% of the variance of the population response explained by the summation (Figure 4D). To determine if the summed response was consistent with the presence of sustained, directionally-dependent tonic activity in the population, we compared the plateau regions of the response 1.0 to 1.5 s after stimulus onset (Fig. 3B). The plateau region for the wall moving towards the animal was significantly more

positive than the baseline firing rate (13% increase; paired *t*-test $p<0.001$), suggesting sustained phasic-tonic responses firing above baseline firing rates for well beyond the brief 70-80 ms stimulus. The plateau region of the spike rate for the wall moving away from the animal – following the wall moving towards the animal and holding for two seconds – was significantly more negative than the baseline spike rate (10% decrease; paired *t*-test $p<0.001$) . These shifts in plateau firing rates compared to baseline firing rates are consistent with directionally-dependent tonic activity in the summed response of units.

Discussion

Our data support the hypothesis that individual mechanoreceptive neurons provide velocity encoding, consistent with the D signal of the proposed controller (Figure 1C). The majority of neurons responded to variable velocity signals with a characteristic fast phasic response. In insects, it is has been shown that tactile hairs, such as hair sensillae, exhibit primarily phasic responses (Chapman, 1998). Many fewer neurons responded with P dependence and a sustained tonic response (Figure 3A,C). However, these were sufficient to reconstruct the sensitivity to wall direction that was present in the whole- nerve population response (Figure 4A,D). The few explicitly position-sensitive units could be sufficient for this response. Alternatively, small changes in firing rate in D units that were not statistically distinguishable in isolation could have aggregate effects at the population level, as no pure P sensors were identified. Insect sensors involved in proprioception, such as campaniform sensillae, have been shown to primarily exhibit phasic-tonic responses, suggesting that these are responsible for the mixed P and D neurons (Chapman, 1998; Okada & Toh, 2001). A P signal could also be obtained downstream by the integration of time-delayed D signals. Further downstream processing to compute a P signal would inevitably increase delays, but a P signal may require lower bandwidth to reduce errors between the desired state and actual state, while D control corrects for rapidly changing perturbations.

The population-level processing of tactile information arises from the combined effect of many neurons with different latencies and individual filtering properties. Different neural units along the antenna of cockroaches have different latencies, both in terms of time to first spike and time to peak firing rate (Figure 4B). While some neurons (2) have activity sustained for the full 300 ms of the turning response, by combining variable latencies and half-lives of all neurons, they produce a summed response that reflects the whole-nerve recording and the timing of the turning behavior (Fig. 4D). The majority of our measured latencies are within the expected range (0-50 ms) for action potentials traveling from mechanoreceptors distributed along the length of the flagellum (up to ~ 5 cm in length), with a conduction velocity of 1-4 m s^{-1} as suggested by (Chapman & Pankhurst, 1967; Pumphrey & Rawdon-Smith, 1937). Given that antennal axons have similar cross-sectional areas, without any known giant afferents (Baba & Comer, 2008), the conduction velocities should be comparable, further supporting that variable latencies arise at least in part from the spatial distribution of sensors on the flagellum.

However, some neurons' latencies (5 of 30) were longer than the 50 ms maximum expected simply due to conduction delays. This property, along with the variable half-lives and the double maxima present in some neurons, indicates that neurons likely also have different filter functions

between stimuli and responses. These differences could arise neurally, from encoding properties of different sensillae, or mechanically, as a function of the local strains and stresses at the sensors's location or material properties of each individual sensillum. Further studies will need to address whether the variable-latency responses in *P. americana* antennae are due primarily to individual neurons' axonal conduction velocities, the spatial arrangement of mechanosensors, and/or individual mechanoreceptors' transfer functions. Revealing the static and dynamical properties of the antenna will be necessary to identify how mechanical filtering contributes to the overall conditioning at the level of afferents (Staudacher et al., 2005). While characterization of specific mechanoreceptor populations on the antenna could identify further spatial organization, isolation of these neurons via backfilling is currently limited because of the long diffusion distances required (Nishino et al., 2005).

Conceptually, the antenna implements delay-line-like processing, indicating that information about the relative timing of arrival of spikes could be used for downstream processing. Interestingly, crickets' cerci — a sensory system analogous to antennae — implement delay-line processing based on the spatial arrangement of filiform afferents (Mulder-Rosi et al., 2010). Our finding, demonstrating that the antenna in *P. americana* may implement delay line processing, parallels a number of studies in vertebrates such as in rapid sound localization in barn owls (Carr and Konishi, 1988), bats (Saitoh and Suga, 1995) and cats (Beckius et al., 1999). To identify if the antenna implements delay-line processing would require further experiments, with simultaneous recordings at known distances from one another or a single recording site with a variety of stimulation sites.

We noted that some units (11) exhibited doubled peaks in firing rate corresponding to periods of wall acceleration and deceleration (or absolute value of acceleration). This suggests that for some units, acceleration information may be provided at the level of afferents. It is important to note that the PD control hypothesis from Cowan et al. (2006) does not preclude the existence of a more complicated controller, including additional acceleration and/or integral terms. Additional experiments would be necessary to identify rigorous acceleration encoding. An integral term could reduce steady state errors that could occur with a pure PD controller in the presence of a constant perturbation. Integral information could be obtained by integrating P signals further downstream; such information may only be necessary a lower bandwidth to correct steady state error. However, this processing would come at a cost of adding additional delays.

With respect to controlling high-speed wall following, the variable latency and half-lives of individual neurons were sufficient to generate a conditioned signal that provides a response consistent with the timing of a turn maneuver (Lee et al., 2008). The conditioned response starts with a rapid increase in firing rate, peaking near 100 ms, consistent with the timing of the onset of turning after the antenna starts to bend. This is followed by sustained tonic activity that extends well beyond the stimulus for about 300-500 ms, the approximate time it takes for the animal to complete a turn (Cowan et al., 2006; Lee et al., 2008). Sensory conditioning arising from the integration of responses from a distributed array of mechanoreceptors, could simplify or reduce computations necessary by downstream neural circuits, since it provides signals that can be transmitted to the motor system with little or no further processing. Conditioning could be critical during behaviors where the reactions are rapid and when the dynamics of movement

impose significant constraints on closed-loop control, such as in flying, swimming and running (Dickinson et al., 2000).

References

Baba, Y., & Comer, C.M. (2008). Antennal motor system of the cockroach, *Periplaneta americana*. *Cell Tissue Res.* **331**, 751-762.

Becht, G., Hoyle, G. & Usherwood, P. (1960). Neuromuscular transmission in the coxal muscles of the cockroach. *J. Insect Physiol.* **4**, 191–201.

Beckius, G. E., Batra, R. and Oliver, D. L. (1999). Axons from anteroventral cochlear nucleus that terminate in medial superior olive of cat: observations related to delay lines. *J. Neurosci.* **19**, 3146–61.

Carr, C. and Konishi, M. (1988). Axonal delay lines for time measurement in the owl's brainstem. *Proc. Natl. Acad. Sci. U.S.A.* **85**, 8311–8315.

Camhi, J. M. & Johnson, E. N. (1999). High-frequency steering maneuvers mediated by tactile cues: antennal wall-following in the cockroach. *J. Exp. Biol.* **202**, 631–643.

Chapman, K. & Pankhurst, J. (1967) Conduction velocities and their temperature coefficients in sensory nerve fibres of cockroach legs. *J. Exp. Biol.* **46**, 63–84.

Chapman, R. F. (1998). The Insects: Structure and Function. 4th edn. *Cambridge University Press*.

Cowan, N. J. and Fortune, E. S. (2007). The critical role of locomotion mechanics in decoding sensory systems. *J. Neurosci.* **27**, 1123–8.

Cowan, N. J., Lee, J., Full, R.J. (2006). Task-level control of rapid wall following in the American cockroach. *J. Exp. Biol.* **209**, 1617-1629.

Dickinson, M.H., Farley, C.T., Full, R.J., Koehl, M.A.R., Kram, R., Lehman, S. (2000). How animals move: an integrative view. *Science.* **288**, 100-106.

Elzinga, M. J., Dickson, W. B. and Dickinson, M. H. (2012). The influence of sensory delay on the yaw dynamics of a flapping insect. *J. R. Soc. Interface.* **9**, 1685–96.

Lee, J., Sponberg, S., Loh, O. Y., Lamperski, A. G., Full, R. J. & Cowan, N. J. (2008). Templates and anchors for antenna-based wall following in cockroaches and robots. *IEEE Trans. Robot.* **24**, 130–143.

Mulder-Rosi, J., Cummins, G. I. & Miller, J. P. (2010). The cricket cercal system implements delay-line processing. *J. Neurophysiol.* **103**, 1823–1832.

Nishino, H., Nishikawa, M., Yokohari, F. & Mizunami, M. (2005). Dual, multilayered somatosensory maps formed by antennal tactile and contact chemosensory afferents in an insect brain. *J. Comp. Neurol.* **493**, 291–308.

Okada, J. & Toh, Y. (2001). Peripheral representation of antennal orientation by the scapal hair plate of the cockroach *Periplaneta americana*. *J. Exp. Biol.* **204**, 4301–4309.

Pumphrey, R. & Rawdon-Smith, A. (1937). Synaptic transmission of nervous impulses through the last abdominal ganglion of the cockroach. *Proc. R. Soc. Lond. B Biol. Sci.* **122**, 106–118.

Quiroga, R. Q., Nadasdy, Z. & Ben-Shaul, Y. (2004). Unsupervised spike detection and sorting with wavelets and superparamagnetic clustering. *Neural Comp.* **16**, 1661–87.

Saitoh, I. and Suga, N. (1995). Long delay lines for ranging are created by inhibition in the inferior colliculus of the mustached bat. *J. Neurophys.* **74**, 1–11.

Schafer, R. & Sanchez, T. V. (1973). Antennal sensory system of the cockroach, *Periplaneta americana*: postembryonic development and morphology of the sense organs. *J. Comp. Neurol.* **149**, 335–54.

Schaller, D. (1978). Antennal sensory system of *Periplaneta americana L*. *Cell Tissue Res.* **191**, 121–139.

Staudacher, E., Gebhardt, M. and Durr, V. (2005). Antennal movements and mechanoreception: neurobiology of active tactile sensors. *Adv. In Insect Phys.* **32**, 49-205.

Figure 1. Control of wall following in the cockroach *Periplaneta americana*. (A) Sequence of turning as a blinded cockroach encounters a wall projection and responds to antenna bending. A complete turn takes about 300 ms to complete. (B) Diagram of wall following cockroach. The body-to-wall distance *d* is the putative control variable estimated from the long axis vector with velocity *v* to the wall contact point. (C) Control diagram of wall following where *u* is the control input and *s* is a complex variable. P: Proportional. D: Derivative. Adapted from Cowan et al. (2006). (D) Bulk, population response from the antennal nerve. Despite a brief 40 ms ramp and hold wall stimulus, activity was sustained for ~300 ms, thus matching the time course of the animal's turn behavior. Modified from Lee et al. (2008).

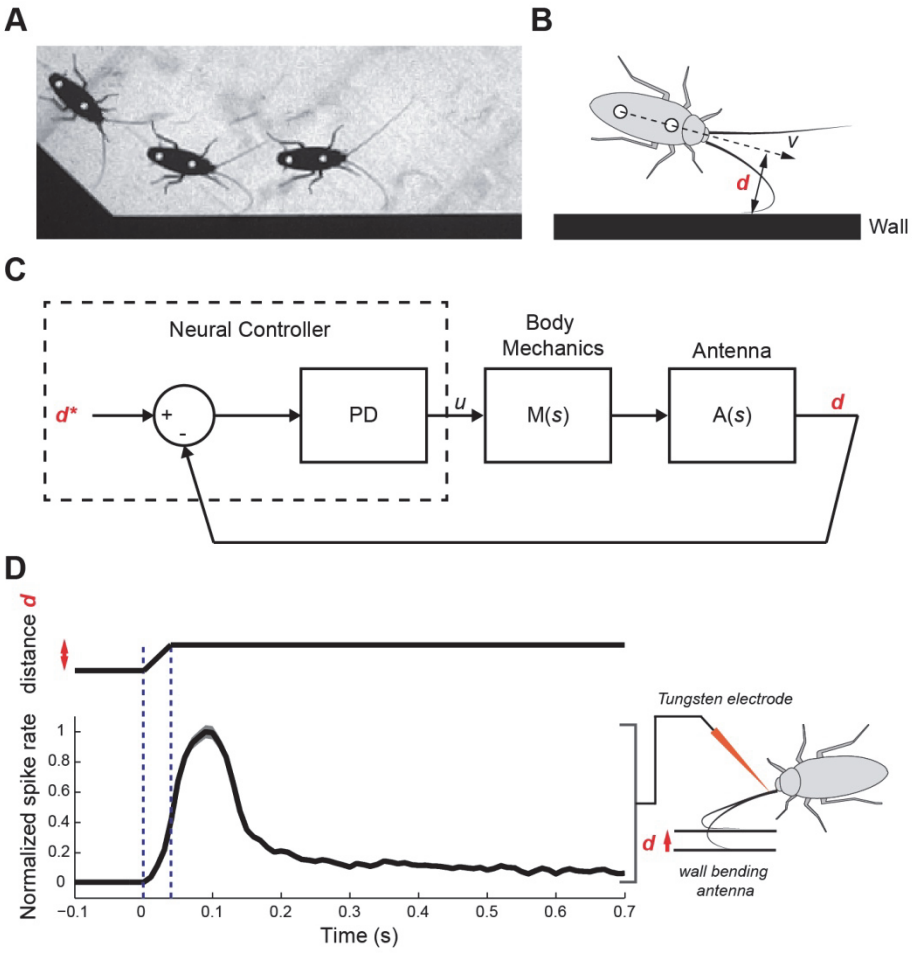
A
B
v
d
Wall
C
Neural Controller
Body
Mechanics
Antenna
d*
+
-
PD
u
M(s)
A(s)
d
D
distance d
Normalized spike rate
1
0.8
0.6
0.4
0.2
0
−0.1
0
0.1
0.2
0.3
0.4
0.5
0.6
0.7
Time (s)
Tungsten electrode
d
wall bending
antenna

Figure 2. Extracellular recording apparatus. We performed en passant extracellular recordings from the antennal nerve while simultaneously bending the antenna flagellum at prescribed position and velocities with a voice coil actuator to simulate the animal encountering wall projections. A Linear Variable Differential Transformer (LVDT) sensor, mounted in parallel with the actuator, measured the actual position of the wall. We fixed the legs and body of the animal to a platform with insect pins. The head, scape and pedicel segments of the antenna were fixed with glue. The inset shows the recording site at the base of the antenna, relative to anatomical landmarks of the cockroach.

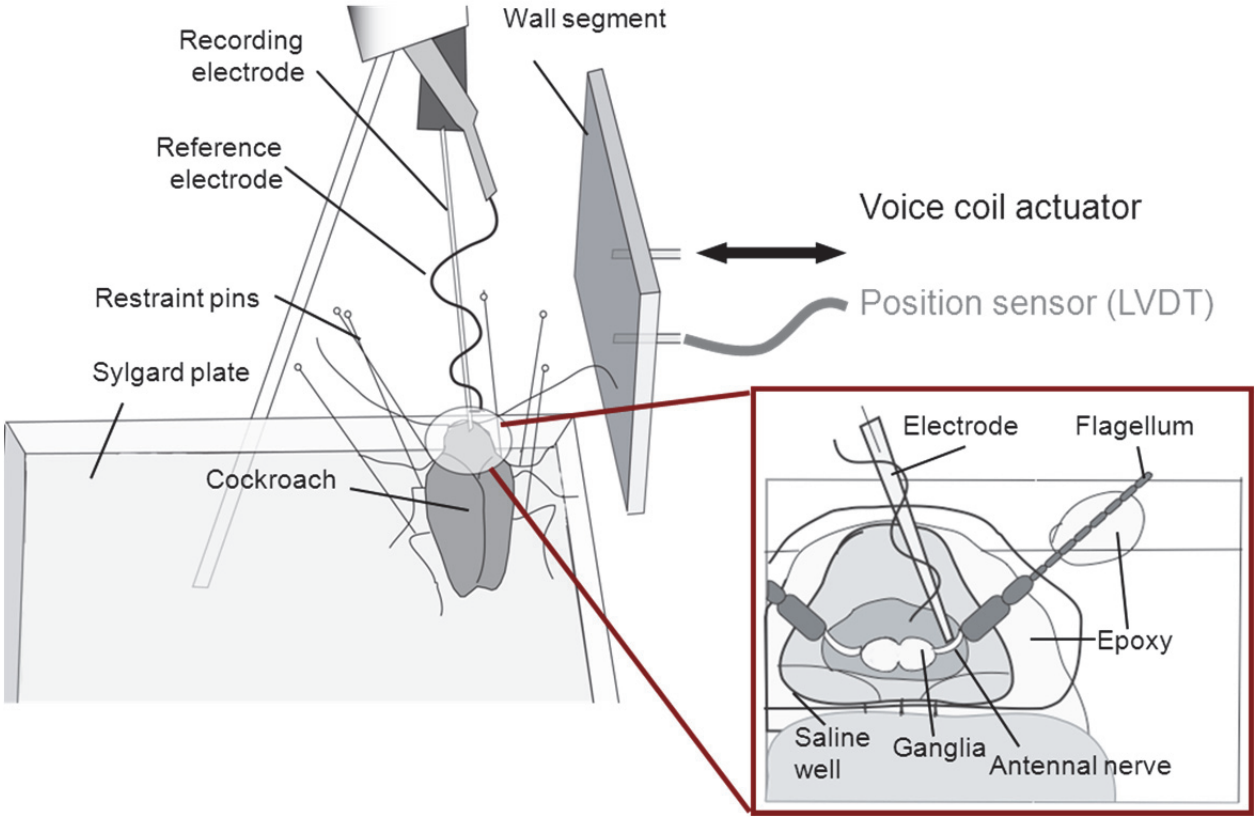
Wall segment
Recording electrode
Reference electrode
Voice coil actuator
Position sensor (LVDT)
Restraint pins
Sylgard plate
Cockroach
Electrode
Flagellum
Epoxy
Saline well
Ganglia
Antennal nerve

Figure 3. Proportional (P) & Derivative (D) encoding of individual neurons. (A) Multi-unit extracellular recording (gray) during a ramp-and-hold wall stimulus (blue) as a function of time. The largest amplitude neuron shows a characteristic phaso-tonic response. (B) Spike clustering for one wall stimulus presentation showing wall position (i) and neural responses (ii). We detected individual spikes (lines; ii) from the raw neural data (gray). From individual spikes we calculated Gaussian-convolved spike rates shown in (iii). Spike rates for three units (blue, red and green) are shown in (iii). The bottom panel (iv) shows spike data from identified clusters from multiple trials. (C) Neural firing rate is sensitive to position P (left) and derivative D (right) information (Kruskal-Wallis test, $\alpha<0.001$). Each colored line is a separate neural unit. For P-sensitive neurons, mean ± 1 standard error are shown. For D-sensitive neurons, the mean spike rate averaged across neurons is shown by the bold line with the shaded region equal to ± 1 standard error.

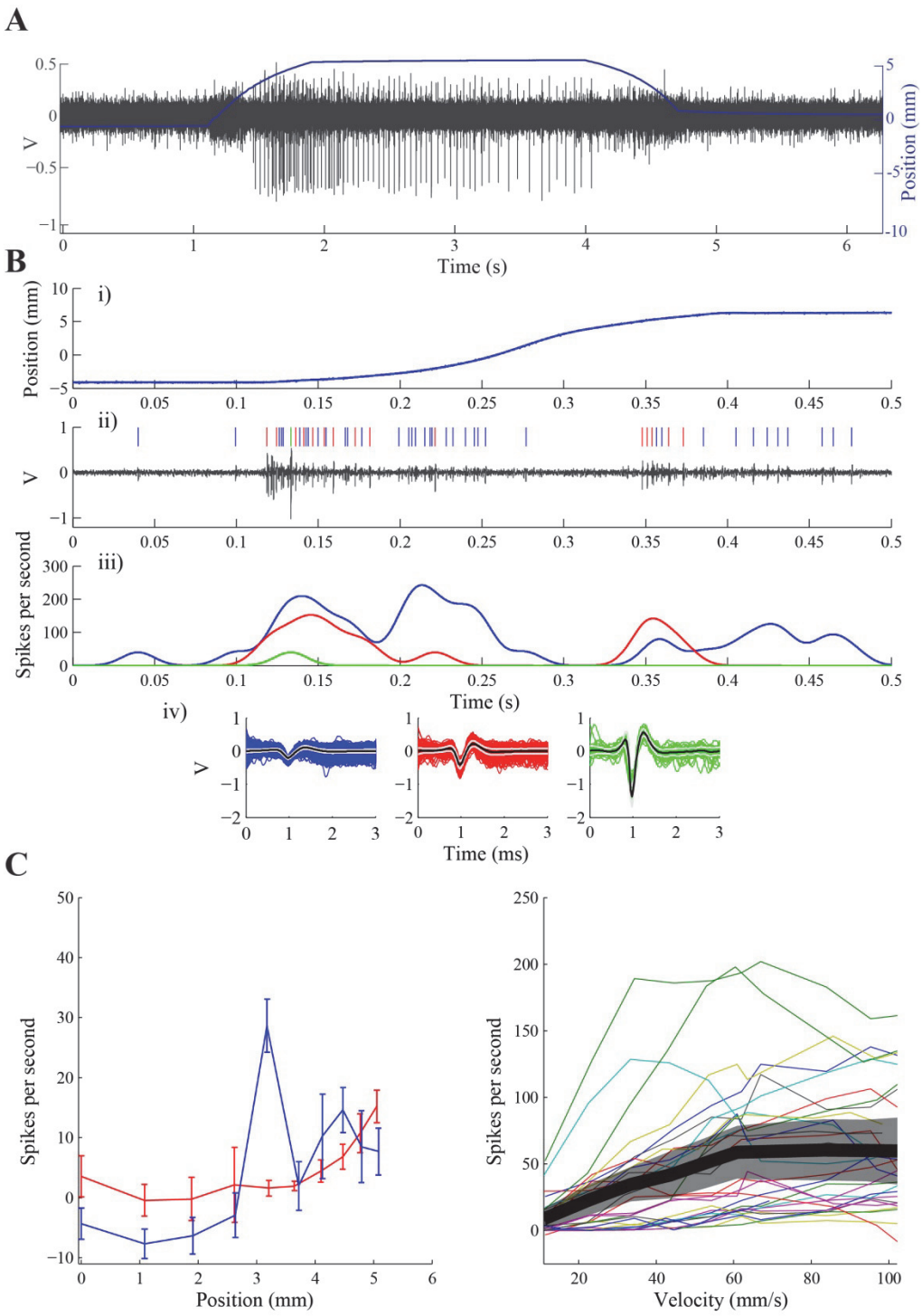
A
Position (mm)
V
Time (s)
B
i)
Position (mm)
ii)
V
iii)
Spikes per second
Time (s)
iv)
V
Time (ms)
C
Spikes per second
Position (mm)
Spikes per second
Velocity (mm/s)

Figure 4. Neural unit temporal processing and summation. (A) (i) Wall position and velocity for fastest-moving wall stimulus (mean velocity ~ 110 cm s^{-1}; wall moving towards cockroach). (ii) Mean responses for n = 30 D-encoding neurons. Unit spike rates are normalized according to their respective maximum spike rate. From top to bottom, neurons are sorted according to their delay to maximum firing rate. (iii) Summation of individual spike rates. (B) (i) Three units (1, 15, 24) are plotted to demonstrate the variation in delay to maximum firing rate (from 10 trials). Histograms show the distribution of delays to maximum firing rate (ii) and first spike (iii) for all D-sensitive neurons. Envelopes are ± 1 standard error around mean firing rates. (C) (i) One unit (29) is plotted to demonstrate slow decay rates (from 10 trials). Envelopes are ± 1 standard error around mean firing rates. (ii) The histogram shows the distribution of half-lives for all D-sensitive neurons. (D) Summation of Gaussian-convolved spike rates for variable-velocity neurons shown in A for wall moving towards (green) and away (red) from animals. Envelopes are ± 1 standard error. The average root-mean square power of the whole-nerve (population) reported in (Lee et al., 2008) is shown for comparison (black: toward animal; blue: away from animal).

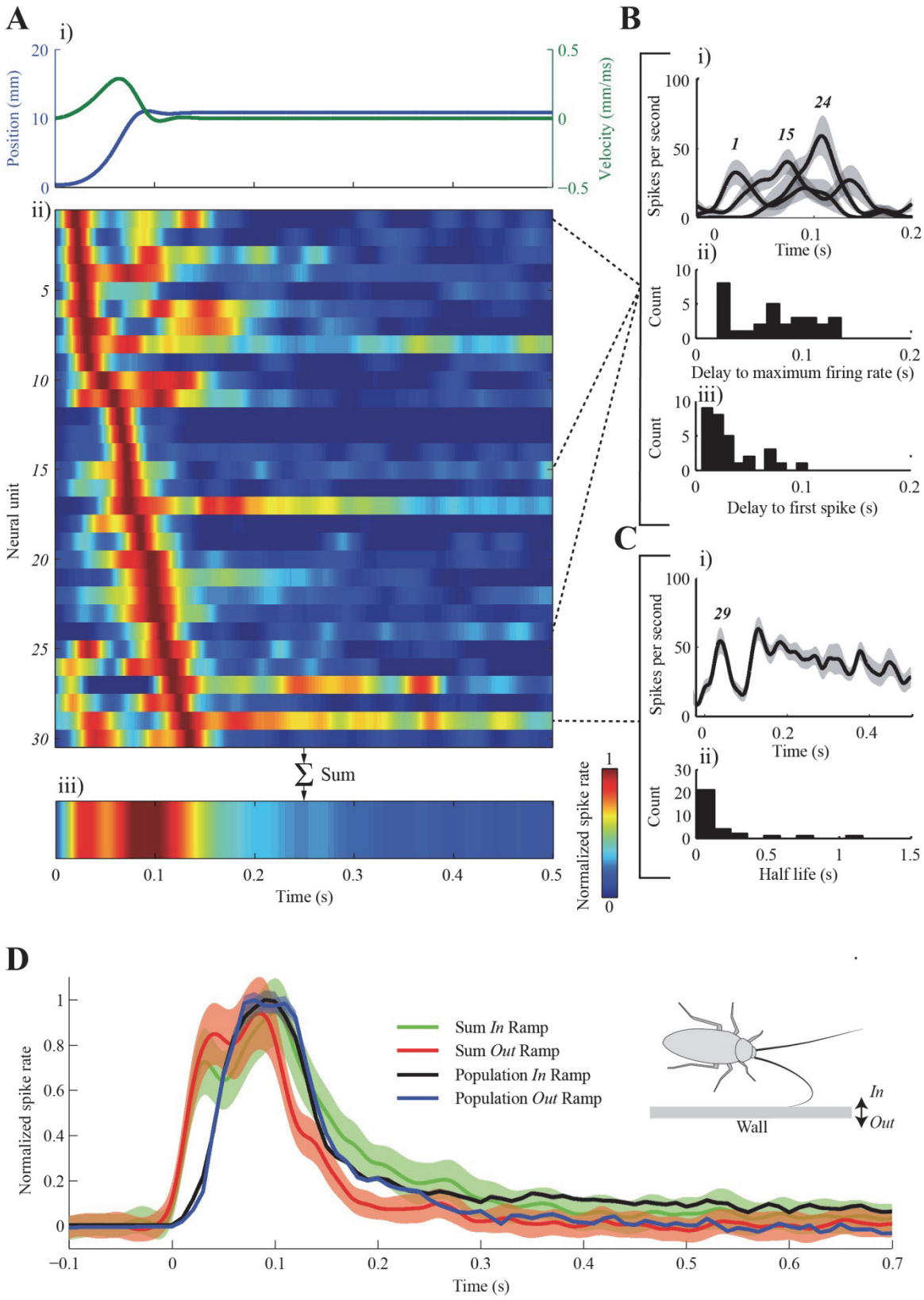
A
i)
Position (mm)
Velocity (mm/ms)
ii)
Neural unit
iii)
Sum
Time (s)
Normalized spike rate
B
i)
Spikes per second
1
15
24
Time (s)
ii)
Count
Delay to maximum firing rate (s)
iii)
Delay to first spike (s)
C
i)
29
Half life (s)
D
Sum In Ramp
Sum Out Ramp
Population In Ramp
Population Out Ramp
Wall
In
Out
Normalized spike rate

Figure 5. D-encoding neural units with phasic and phasic-tonic responses. The wall onset is at t = 0. Blue line are averages and red lines are ± 1 standard error. From top to bottom, neurons are sorted in increasing order according to their delay to maximum firing rate (same order as Figure 3).

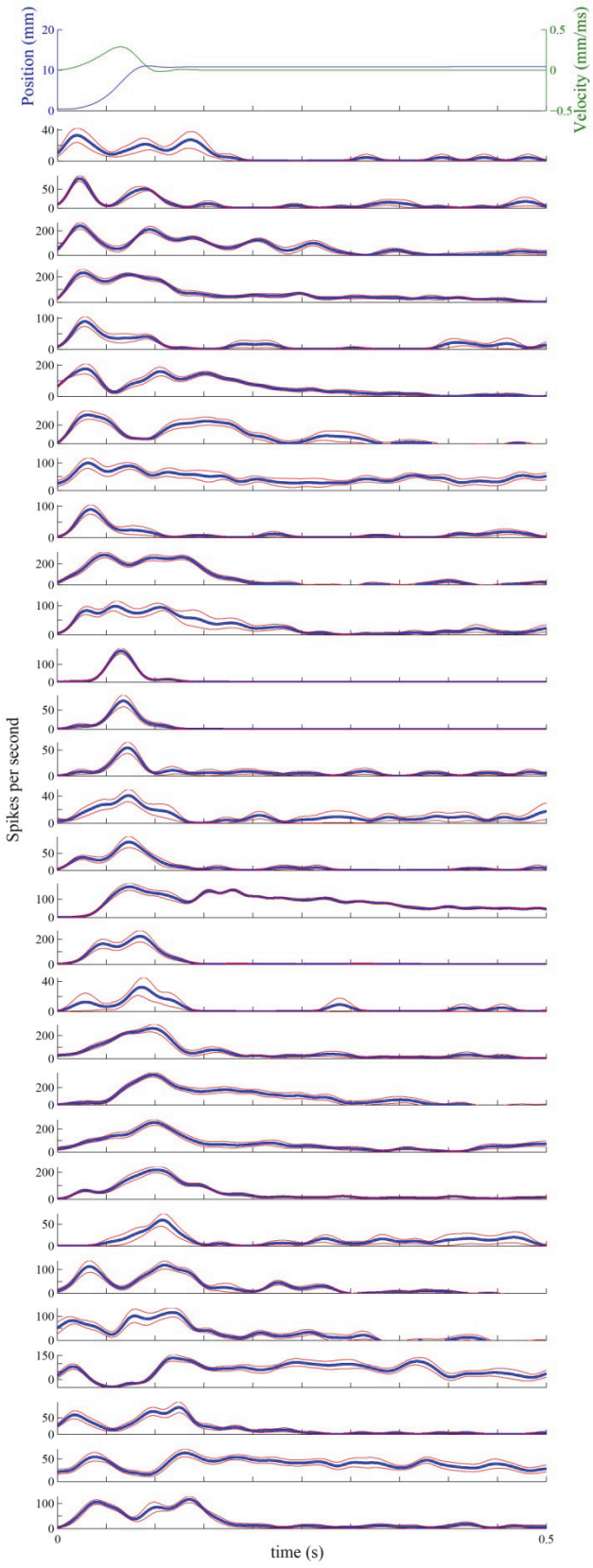
Position (mm)
Velocity (mm/ms)
Spikes per second
time (s)

Chapter 3

Mechanical processing of tactile sensor during rapid running: static and dynamical properties of the antenna flagellum of the American cockroach

Summary

The integration of information from dynamic sensory structures operating on a moving body is a challenge for locomoting animals and engineers seeking to design agile robots. Tactile sensors are physical linkages mediating mechanical interactions between body and environment. We took the first step in revealing the static and dynamical response of a tactile sensor by studying the antennae of the American cockroach, *Periplaneta americana*, an animal that escapes predators by integrating information from antennae during rapid tactile navigation. High-resolution geometrical measurements, combined with static bending experiments, revealed an exponentially decreasing flexural stiffness profile from base to tip. We found that the elastic modulus did not vary along the measured length and averaged 6.46 x 10^6 Pa. We provide evidence that a decreasing second moment of area may simplify sensing for tactile navigation. Measurement of the transient response at the tip of the antenna following step deflections revealed a mean damped natural frequency of 18 Hz and damping ratio of 0.52. As the antenna was under-damped, approximately 93% of the perturbation was rejected within the first cycle (~70 ms), which corresponds to within one stride period during high-speed running. An impulse-like perturbation near the antennal tip revealed dynamics characteristic of a near perfect inelastic collision, allowing the antenna to "stick" to obstacles. Further elucidation of antennal mechanical tuning will lead to hypotheses integrating distributed mechanosensory inputs from a dynamic sensory appendage operating on a moving body.

Introduction

When animals move rapidly through the environment, sensors must work with the dynamics of the body to be most effective. This is particularly critical for sensory appendages such as antennae, whiskers and legs that project outside the body and therefore must counteract gravitational and inertial forces (Nelson and MacIver, 2006). These appendages are the physical linkages between organism and environment. A major challenge of tactile-mediated sensorimotor integration is to determine how these projecting neuromechanical appendages should be tuned mechanically when operating on a moving body interacting with a complex environment. During mechano-sensation, mechanical forces are processed at different stages. Information from stimuli flows from whole sensory appendages to individual mechanosensors and finally, by way of mechanosensory transduction pathways, into all-or-none neural spike events (Sane and McHenry, 2009). Therefore, mechanics condition neural processing. To understand sensory processing, we must possess a more complete characterization of how appendage mechanics condition information flow. Exploiting this interaction remains a challenge not only for biologists, but also for engineers seeking to design tactile probes on agile robots.

Motion of sensory appendages driven by rapid body motion can be sensed and used to stabilize the body, as with halteres in fruit flies (Frye and Dickinson, 2001). In moths, antennae can help stabilize the body during high-speed aerial maneuvers by sensing gyroscopic forces (Sane et al., 2007). However, antennae or halteres experience less direct physical contact with the environment than appendages used during rapid terrestrial locomotion. Many studies to date in tactile sensing in terrestrial arthropods such as stick insects (Dürr et al., 2001), cockroaches (Comer et al., 2003; Okada and Toh, 2004), and crayfish (Sandeman and Varju, 1988) have focused on object localization tasks where animals directly contact objects, while moving slowly. Likewise, research on whiskers has been conducted within the context of slow, active exploration, but even in these studies the role of passive mechanics appears important at the first stage of mechanosensory processing (Hartmann et al., 2003; Neimark et al., 2003). The manner in which antennal and whisker mechanics influence sensorimotor control when animals navigate at high speed remains unclear. Here we explore how environment-appendage interactions influence tactile sensing during rapid running to determine if passive mechanical tuning (static and dynamic) could simplify sensorimotor control.

When the body is moving at high speed, tactile appendages are propelled rapidly through the environment. An ineffectively tuned sensory appendage (e.g., a sensor with low damping) could oscillate excessively when driven by the body of a rapidly running animal. These oscillations could interfere with the sensing task by making it difficult to separate information due to self-motion versus sensor contact with the environment. When coming into contact with an object – during collision or when losing contact during slipping – the passive mechanical properties can determine a sensor's response. Flexibility and small size, which lessen the kinetic energy upon impact, may be desirable features, but the tactile structures must be stiff enough to support their own weight (Loudon, 2005). Without sufficient damping, a tactile sensor could bounce back from an object upon impact and oscillate excessively upon release. A sensor that is too stiff could cause forces to be transmitted to the body and potentially alter its course. A sensor with large moment of inertia (mass x length^2) could affect the dynamic stability of the body, much like a tail (Libby et al., 2012). Furthermore, frictional properties of the appendage could influence the mechanical interaction with the environment (see Chapter 1). Poorly tuned passive mechanical properties could have undesirable consequences by introducing excessive noise into the sensorimotor transfer function.

To study the effect of passive mechanics on sensing, we studied both static and dynamic properties of the antenna of *Periplaneta americana*. This animal escapes predators by integrating information from antennae in tasks such as wall following and collision avoidance while running rapidly at speeds up to ~ 80 cm s^{-1} (Baba and Tsukada, 2010; Camhi and Johnson, 1999; Cowan et al., 2006). Specifically, we measured the response of the flagellum, the long (~1.3X body length), non-actuated part of the antenna which has been implicated in high-speed navigation and collision avoidance with little-to-no contribution from basal segments (Camhi and Johnson, 1999). Extreme variations in antenna geometry and material properties in the insect world make it difficult to predict mechanical performance (Chapman, 1998). We hypothesized that flexural stiffness (EI) of the flagellum, the determinant of the bending response to static or quasi-static forces, would be determined primarily by a change in geometry or second moment of area (I). We estimated I by measuring the change in radius along the length of the antenna. Geometrical measurements revealed a highly-tapered structure predicting that it would be more difficult to

bend the antenna at the base than at the tip. We measured resistance-to-bending forces along the antenna. Forces suggest that the flagellum has an exponentially decreasing stiffness profile consistent with predictions from geometry, thus supporting our initial hypothesis. To measure the dynamic response of the antenna, we treated the antenna as a cantilever beam and imposed biologically-relevant deflections, measuring their corresponding responses. This method allowed us to estimate the first-mode natural frequency and damping ratio of the flagellum. Finally, to simulate high-speed collisions of the antenna with objects, we developed an impulse-like perturbation and measured the recovery of the flagellum.

Materials and Methods

Animal husbandry

Adult male American cockroaches, *Periplaneta americana*, were acquired from a commercial vendor (Carolina Biological Supply Company, Burlington, NC, USA) and housed in plastic cages maintained at a temperature of 27°C. Cockroaches were exposed to a L:D cycle of 12h:12h and given fruits, dog chow and water *ad libitum*. All experiments were conducted at room temperature (25–26°C).

Geometrical measurements

Geometrical properties were obtained from 10 male *Periplaneta americana* antennae *ex vivo*. After sedation of an animal with CO_2 for approximately 5 minutes, we cut at the base of the flagellum of the antenna, i.e. at the scape-head joint, and weighed it to the nearest 0.1 mg (Mettler AE 50, Mettler-Toledo International Inc., Columbus, OH, USA). The first few segments of the flagellum were glued to a microscope glass slide using epoxy to mount the antenna as flat as possible and minimize hemolymph loss. The slide was rigidly mounted on a single axis micro-positioning stage and placed under a microscope, with backlighting to maximize contrast of the flagellum against background. The flagellum was then photographed in overlapping segments of about 15 annuli with a high-definition camera (Canon Vixia HF S20; 3264 x 2456 pixels) mounted on an optical microscope. Starting at the antenna base, images were taken along the length of the antenna with care taken to ensure that there were overlapping features across images. Frames were calibrated with an objective micrometer with a resolution of 0.010 mm (Fine Science Tools 290025-02, Foster City, Ca, USA). Single images ranged from 428 to 460 pixels per mm in spatial resolution and were used to manually reconstruct an entire high-resolution image of the flagellum (Adobe Photoshop CS3, Adobe Systems Inc., San Jose, CA, USA). We used a high-resolution image of the entire flagellum reconstructed from individual segments to evaluate the geometrical properties. Due to the images' high contrast, with minimal processing, we were able to subtract the background and convert the flagellum to a binary image using the proper threshold with the *graythresh* function in Matlab (The MathWorks Inc., Natick, MA, USA). To correct for the inherent curvature of the flagellum, the central axis of the flagellum was approximated by finding the median point along the antenna from the detected

boundary. We then used a spatial moving average filter spanning 400 pixels (~ 2000 μm) to remove noise due to segment intersections.

This image processing allowed for determination of the radius of the antenna and approximations of the second moment of area, a determinant of flexural stiffness which can predict the resistance to bending of the antenna along its length. We estimated the second moment of area I of antennae by assuming a circular cross section, thus

$$I = \frac{\pi r^4}{4} \tag{1}$$

where r is the radius along the length of the antenna directly measured from high-resolution images of the flagellum. The assumption of a circular cross section is strongly supported by morphological studies of Kapitskii (1984). While the flagellum is a hollow structure with an inner (epithelium) and outer radius (cuticle), this relationship gives us an upper bound on I. Since both the thickness of the epithelium and cuticle co-vary with the radius of the antenna, our estimates are a good approximation of the upper bound (Kapitskii, 1984).

Static bending experiment - Animal preparation

We built an apparatus to characterize flexural stiffness along the length of the antenna (Fig. 1A). Cockroaches were first cold anesthetized for 30 minutes and weighed. We then fixed neck-lesioned cockroaches onto the edge of a platform using epoxy glue so that the flagellum projected outside the platform surface, unobstructed. This procedure left the antenna auxiliary hearts intact. We fixed the head, scape and pedicel joints with epoxy glue to prevent movement of the antenna during an experiment. The platform was mounted rigidly to a linear micro-translation stage operating in closed loop with a minimum step size of 50 nm (M112.1DG, Physik Instrumente, Palmbach, Germany).

Experimental setup

We measured the resistance-to-bending forces generated by the antenna flagellum at different positions along its length, similar to the method employed by Sandeman (1989) to characterize the mechanical properties of crayfish antennae (Fig. 1A). First, we clamped the antenna using fine forceps while a digital microscope camera (Dino-Lite Premier AD4113TL, AnMo Electronics Corp., Taiwan) was used to visually confirm that the flagellum was held rigidly. We carefully brought a rigid arm attached to a force sensor (Series 300, Aurora Scientific Inc., Ontario, Canada) in contact with the antenna using the micron-resolution stage. The arm was brought in contact as close as possible to the antenna while the measured force remained at baseline. For all experiments, the arm was carefully positioned 1 mm distally from the fixation point of the antenna (Fig. 1A). The first, proximal fixation point was taken five annuli distal from the pedicel-flagellum joint. The force lever was then driven into the antenna, perpendicularly, with a fixed displacement of 1 mm and speed of 2 mm s^{-1} using a linear translation stage with submicron resolution (M112.1DG, Physik Instrumente, Palmbach,

Germany), while forces were sampled at 1000 Hz (Fig 1A). This position was held for 15 seconds and then the lever was returned to its original position. Three trials were obtained for each position per plane. The antenna was positioned within a small groove etched at the base of the arm to minimize out-of-plane motion (Fig 1A). We measured the resistance-to-bending force in steps of 2 mm, which required releasing the antenna and clamping at a new position at every point 2 mm distally from the previous measurement point. We repeated this procedure until measured forces became lower than the 0.3 mN resolution of the force lever, which provided coverage of over 1/3 the length of the flagellum from the base. We recorded forces for both the lateral and medial planes. After a completed experiment, we measured the length of the antenna. Only flagella with more than five measurements along the length were included in the final analysis. The 1 mm displacement imposed large angle (45°) deflections of the antenna, similar to what an antenna may experience when contacting an object when running. We smoothed the data by convolving a moving average window of 200 ms with the response. For statistical analysis, we used the peak forces of the response averaged over three trials, thus giving an upper bound on estimates of the elastic modulus.

Cantilever beam model

To estimate the order of magnitude and variation of the elastic modulus along the antenna, we modeled our experimental conditions using cantilever beam theory. Since we imposed deflections of ~45º in our experiment, we used a 2D Euler-Bernoulli beam model to test our hypothesis that the elastic modulus E did not significantly vary along the antenna. We made estimates of E by numerical integration, which required approximating

$$\kappa(x) = \frac{\left|\frac{d^2y}{dx^2}\right|}{\left[1+\left(\frac{dy}{dx}\right)^2\right]^{3/2}} = \frac{M(x)}{E(x)I(x)} \tag{2}$$

where $\kappa(x)$ is the curvature, y and x are the 2D position of the antenna, $M(x)$ is the moment along the antenna, $E(x)$ is the elastic modulus and $I(x)$ is the second moment of area (Timoshenko, 1934). We briefly describe the procedure for numerically solving this equation.

We adapted the numerical simulation method of Quist and Hartmann (2012) to relate the flagellum deflection to the measured force. The model is quasi-static and assumes that the material of the flagellum remains within the elastic limit during an experiments. The model also assumes that the antenna is inextensible such that the arc length after deflection is equal to the initial length of the flagellum. For the purpose of this simulation, the cockroach flagellum is modeled as a 2D continuously tapering cantilever with a circular cross-section (Kapitskii, 1984) under the action of a point force acting perpendicular to the contact at a distance s measured along the length L of the flagellum from the clamp position. The simulation computes the flagellum's local curvature at the location of the applied force and then successively computing changes in the local curvature back to the base of the cantilever (or the clamp position). As a first

step, the flagellum was discretized into a series of rigid links connected by elastic torsional springs (Fig. 2). At a given node *i*, the change in curvature, $d\kappa_i$, is related to the applied moment M_i, by the equation

$$\kappa_i = \frac{M_i}{E_i I_i} \tag{3}$$

where E_i is the elastic modulus and I_i is the second moment of area of node *i* using the experimentally-determined relationship between radius and flagellum length. Using the above computed curvature information at each node, the algorithm iterates until the final flagellar shape can be computed passing through the experimentally defined deflection (y_{def} = 1 mm) at the point of force application (s = 1 mm). We assume that the elastic modulus, within each experimental condition [$F_i(s)$, $y_{def}(s)$] does not change along the length, and therefore $E_i = E(s)$, is constant for each simulated condition and $E(s)$ is left as a free parameter to be optimized for obtaining the unique flagellar shape with the least deviation from the desired point [$y_{def}(s)$]. The effect of the continuously changing clamp positions in the experiments is replicated in simulation by using an equivalent flagellum truncated at the clamp position.

Dynamic testing - Animal preparation

We evaluated the dynamic properties of the antenna by treating the flagellum as a cantilever beam fixated at one end and free to vibrate at the other. Since fast running cockroaches hold their antennae relatively still at the base while their flagella bend in response to upcoming perturbations (Camhi and Johnson, 1999; Cowan et al., 2006), we tested intact antennae with immobilized head-scape and scape-pedicel joints, while leaving the flagellum unrestrained (Fig. 1B). A cockroach was first anesthetized with ice for 30 min (without direct contact between animal and ice) and mounted *in toto* to a rotatable platform. The head and the untested antenna were secured to the platform with dental silicone (Coltene light body, Coltène/Whaledent AG, Altstätten, Switzerland), while both the head-scape and scape-pedicel joint of the tested antenna were immobilized using 5-minute epoxy glue after an additional anesthesia with CO_2 for 1.5 min. Animals were given at least 1 h to recover from the procedure and to ensure that the epoxy glue had fully set. Prior to experimentation, we confirmed that the antenna was intact by lightly probing the antenna and visually confirming the initiation of a stereotypical escape response evidenced by the leg and body twitching.

Experimental setup: natural frequency and damping identification

We fixed the proximal 0.5 cm of the antenna with a pair of fine forceps, leaving the major part (~90 %) of the flagellum unrestrained (Fig. 1B,C). A microscope camera (Dino-Lite Premier AD4113TL, AnMo Electronics Corp., New Taipei City, Taiwan) was used to visually confirm that the flagellum was not clamped too tightly. We recorded the passive recovery from either a step deflection or an impulse-like collision with a high-speed camera (Phantom v10, Vision Research Inc., Wayne, NJ, USA), mounted to view the vertical motion of the flagellum (side

view). We obtained recordings at 1000 Hz, with a shutter speed of 400 µs and a resolution of 10 pixels per mm. A second camera (X-PRI, AOS Technologies AG, Baden Daettwil, Switzerland) directly above the antenna (top view) additionally recorded the horizontal motion of the flagellum at 250 Hz. These recordings allowed us to discard trials in which motion exceeded the resting, horizontal position of the flagellum by more than ± 15° and thus allowing a small-angle approximation when tracking positions from the side view. The experimental apparatus was mounted on a vibration isolation table to isolate flagellar responses from environmental vibrations. A control experiment showed that our results were not affected by air flow in the experimental room.

We characterized the damping properties of the flagellum by analyzing the transient response to an initial step deflection (Fig. 1C). The flagellum was deflected manually and held by a second pair of fine forceps 1 cm distal to its fixation site. These forceps were closed above the flagellum. The resulting contact force caused the flagellum to bend in the region between the two pairs of forceps. After a brief hold time of a few seconds, the flagellum was abruptly released and snapped back passively to its starting position. To account for possible directional anisotropies of the flagellum, the animal was rotated such that the flagellum could be deflected ventrally, dorsally, medially, and laterally. To further investigate possible effects of initial conditions, the flagellum was deflected to 20°, 35°, and 50° (Fig. 1C). The amount of deflection is well within the biologically relevant range for high-speed tasks like wall following and collision avoidance. To account for possible effects of order, the sequence of orientations and angles of deflection was varied pseudo-randomly for each insect. Testing the flagellum in four orientations with three angles of deflection per orientation and three repetitions per angle resulted in a total of 36 trials per animal.

Experimental setup: collision dynamics

Since the antennae are held in front of the body during high-speed running, the antennal tip is likely the first part to contact an object. During collision avoidance, for instance, the antenna bumps into an object and drives past it. To characterize how the antenna rejects such a perturbation, we analyzed the response of the flagellum to an impulse-like collision (Fig. 1D). We were specifically interested in the dynamic characteristics at the instant of impact and the motion transfer along the flagellum. Therefore, the flagellum was deflected close to the tip (at ~95 % of its unrestrained length) with a 5 mm LED light mounted to a lever arm. The use of an LED with a plastic casing allowed for an almost friction-less contact and created sufficient contrast to clearly identify the flagellar shape in each video frame. The lever arm was released manually and rotated in the sagittal plane. Accelerated by gravity, the collision object hit the flagellum at a speed of 60 cm s^{-1}, similar to average running speeds during wall following (Cowan et al., 2006). Since the radius of the lever arm was large, the motion during impact following its pendular trajectory was quasi-linear. As the lever arm was multiple orders of magnitude heavier than the flagellum, this experiment simulated a collision of a running animal with a fixed object, in a reverse reference frame. As the first experiment provided no evidence for a directional anisotropy (see Results), the flagellum was deflected only in the ventral direction in the second experiment. We recorded 10 trials per animal.

Data Analysis

We analyzed displacements in response to a step or impulse-like deflection using the video from the side view camera. The position of the flagellum was then automatically tracked for each frame using a custom Matlab script (The MathWorks Inc., Natick, MA, USA). Our tracking method allowed us to test the intact flagellum since the tracking algorithm did not require any antennal markers. The script identified the contour of the antenna in each frame after converting images from grayscale to binary. The contours were smoothed using a low-pass Butterworth spatial filter of second order with a cut-off of 100 pixels (~10 mm). The algorithm then set 21 equally spaced points along the unrestrained flagellum (from the proximal fixation site to the tip, corresponding to 5 % length intervals) and determined their displacement relative to the positions prior to deflection. In the case of the step response, the flagellum was partly obscured (~5 % of the unrestrained length) by the second pair of forceps during the first few frames; we reconstructed the missing porting using polynomial fitting. To analyze the transient response after a step deflection, we measured the displacement of the tip. At least two distinct overshooting peaks could be identified in each trial and were therefore used to estimate the damping ratio, which determines how much the system oscillates as the response decays toward steady state, and the damped natural frequency, which determines how fast the system oscillates during the transient response. We began our analysis by assuming the antenna behaved as linear time-invariant (LTI) system. Specifically, we posit the following, single degree of freedom mechanical model:

$$\ddot{x} + 2\zeta\omega_0\dot{x} + \omega_0{}^2 = 0 \tag{4}$$

This model is appropriate assuming we excite a single vibrational mode of the antenna dynamics. As we show below, we use multiple distinct methods to estimate model parameters, providing some assurance that this simplified model captures the results of the experiments.

We first measured the damping ratio using the maximum overshoot (M_p) method as

$$\zeta_{M_p} = \frac{\log\left(M_p/100\right)}{\left(\pi^2 + \log\left(M_p/100\right)^2\right)^{1/2}} \tag{5}$$

where M_p is defined as the maximum difference between the transient and steady state response. To independently determine another damping ratio value and hence assess the linearity of our system, we studied under-damped oscillations of the flagellar response by means of the logarithmic decrement Δ method (Tongue, 2002). For the first period $n = 1$ we calculated

$$\Delta = \log\left(\frac{A_1}{A_2}\right) \tag{6}$$

where A_1 and A_2 correspond to the amplitudes of the first two peaks, so that in the under-damped case

$$\zeta_1 = \frac{\Delta}{\left(4\pi + \Delta^2\right)^{1/2}} \tag{7}$$

To further characterize the properties of the transient response, we measured standard engineering performance specifications including the delay time t_d, rise time t_r, peak time t_p, maximum overshoot M_p and settling time t_s. These variables are defined in Appendix 2.

To compare our results with theoretical predictions from cantilever beam theory, damped natural frequencies f_d, directly obtained from the peak-to-peak durations of the measured time courses, were transformed into natural frequencies f_n, assuming linear second order damping (Tongue, 2002):

$$f_n = \frac{f_d}{\left(1 - \zeta^2\right)^{1/2}} \tag{8}$$

We then compared the average natural frequency with the natural frequency predicted from a truncated-cone cantilever beam model fixed at one end and free to vibrate at the other (Conway et al., 1964):

$$f_{n,predicted} = \frac{\lambda_n}{L^2}\left(\frac{EI}{\rho A_b}\right)^{1/2} \tag{9}$$

where λ_n are tabulated eigenvalues determined by boundary conditions, L is the length of the cone, E is Young's modulus, A_b is the cross-sectional area at the base of the cone, I is the cross-section moment of area at the base of the cone ($A_b^2/4\pi$), and ρ is the density of the material.

In addition to the step deflection experiment, the collision response allowed us to obtain a qualitative measure of the dynamic characteristics at the instant of impact (elastic or inelastic collision) and another quantitative measure of motion transfer along the flagellum. For the latter, we identified the position of maximum bending by first fitting a polynomial to the automatically tracked points on the flagellum at the time of maximum deflection (see Fig 4) and then calculating the curvature $\kappa(x)$ for each point as

$$\kappa(x) = \frac{\left[1 + \left(\frac{df(x)}{dx}\right)^2\right]^{3/2}}{\left|\frac{d^2 f(x)}{dx^2}\right|} \tag{10}$$

where x denotes the horizontal coordinate of a tracked point in the side view recording and $f(x)$ its vertical counterpart from the polynomial fit. The smallest R along the flagellum corresponds to the position of maximum bending. See Table 2 for a list of all symbols.

Results

Geometrical properties

From n = 10 animals (body mass = 0.81 ± 0.12 g; mean ± std unless otherwise specified), we determined a mean flagellum length of 47.16 ± 3.97 mm and a mass of 0.0023 ± 0.0001 g (Fig. 3A). The length of annuli remained constant until about the 30th segment, after which there is a marked increase in annulus length up to the 80th segment followed by a plateau (Fig. 3B). This sigmoidal increase in annulus length is consistent with observations by Kapitskii (1984). The number of segments ranged between 134 and 152 with a median of 146. When averaged across individual animals, the flagella had a base radius of 0.22 ± 0.01 mm, whereas the tip was almost five times finer with a radius of 0.05 ± 0.01 mm. In contrast to a perfect cone, the radius decreased exponentially from base to tip (Fig. 3C). Under the model of a logarithmically decreasing radius from base to tip, all slopes were statistically significant from 0 at a level of α = 0.01. When averaged across individuals, an exponential model ($\alpha e^{-\beta x}$; α = 0.22 mm, β = -0.017) captured 99.6% of the variance in radius. From our measurements of the radii, we estimated an upper bound of the second moment of area using Equation 1. In addition, we estimated an average volume of 2.60 ± 0.21 mm^3. This measurement of volume is consistent with measurement from Kapitskii (1984) who estimated the volume to be 2.1 mm^3 on specimens who had undergone cryofixation and dehydration with ethanol. From our estimate of volume we estimated an average density of 0.88 ± 0.07 mg mm^{-3} across individuals.

Static bending

We performed static bending experiments on the flagellum of n = 5 adult male *P. americana* (mass = 0.97 ± 0.15 g; antenna length = 4.82 ± 0.39 cm; 3 left, 2 right). As predicted from our approximation of the second moment of area, estimated from our measurements of the radius of the antenna, the antenna's bending resistance was higher at the base than at more distal positions along the antenna (Fig. 3D). We found an exponential decrease in resistance-to-bending force as a function of distance from base. Under the model of a logarithmically decreasing force profile, all slopes were statistically significant from 0 at a level of α = 0.01. We found no statistically significant effect of plane (lateral vs. medial) on the resistance-to-bending forces after correcting for the continuous covariate *distance* and random factor *animal* using a logarithmic transformation of *force* (mixed effect model: *F test* p = 0.570). Solving for *EI* using a 2D Euler-Bernoulli model yielded a mean of 5.67 x 10^{-9} ± 4.46 x 10^{-9} Nm^2 over the measured length. To determine whether the resistance-to-bending measurements could be explained by geometry alone, i.e. second moment of area, we used our cantilever beam model to estimate how the elastic modulus E varied along the measured region of the antennae, using an upper bound estimate of I from geometrical measurements. We found that E was not statistically different for distances along the length of the antenna when correcting for the effect of individuals (mixed effect model: F test, p = 0.996). When pooling E across different measurement distances along the antenna, we found a mean elastic modulus of 6.46 x 10^6 ± 3.37 x 10^6 Pa.

Dynamics: natural frequency and damping identification

Damping properties were determined by measuring the passive return of $n = 5$ intact flagella after a step deflection (body mass = 0.79 ± 0.12; antenna mass = 0.0022 ± 0.0001 g; antenna length = 44.74 ± 2.56 mm; 3 right, 2 left antennae). After an initial step deflection, the flagellum quickly returned to its starting position (Fig. 4A). Accordingly, time courses of the tip displacements showed clear characteristics of an under-damped system: the amplitude decreased to zero rapidly within 100 to 125 ms and showed two clearly identifiable overshoots in each trial (Fig. 4B). Analysis of the average maximum displacements along the length of the unrestrained flagellum revealed that most of the motion occurs at the tip, while the more proximal parts of the flagellum remained stationary and exhibited only small or no overshoots (Fig. 4E). The maximum displacement during trials appears to increase somewhat exponentially with flagellum length, although initially the flagellum was bent in an almost linear fashion (values below zero in Fig. 4E). As expected, an increase in initial deflection resulted in an increase in maximum displacement.

For these two identifiable positive peaks, we found a mean damped natural frequency of 18 ± 3.0 Hz and a mean damping ratio ζ_1 of 0.52 ± 0.09 (Fig. 4D,F). Using the maximum overshoot method (Eq. 5), we found a mean damping ratio ζ_{Mp} of 0.27 ± 0.07 (Fig. 4E). Since ζ_1 and ζ_{Mp} were significantly different (*t*-test, $p<0.001$), this suggests that the flagellum transient response is non-linear. Oscillatory time courses were highly consistent within and across animals, and higher mode oscillations were not observed. On average, the flagellum tip rejected 93.3 % of the initial deflection within the first oscillation cycle (69 ms on average from trough to trough). Deflection directions did not have a significant effect on damped natural frequencies (ANOVA *F*-test, p = 0.255) and damping ratios (ANOVA *F*-test for ζ_1 and ζ_{Mp}, p=0.812 & $p=0.477$, respectively). When taking into account the effect of individuals using a mixed effect model, the effect of initial deflection direction on damped natural frequency (*F*-test, p = 0.0923) and damping ratios (*F*-test for ζ_1 and ζ_{Mp}, p=0.452 & p=0.431, respectively) remained insignificant.

The time characteristics of the response were affected by the initial deflection angle. An increase in deflection resulted in a significant decrease in damped natural frequency (mixed effect model: *F*-test, $p<0.001$) and a significant increase in damping ratios (mixed effect model: ANOVA *F*-test for ζ_1 and ζ_{Mp}, p=0.066 & $p<0.001$, respectively), after accounting for the effect of individuals. We therefore present these pooled data across animals and orientations, but not across angles. Likewise, transient response properties including delay time, rise time, peak time, and settling time were dependent on the initial angle (mixed effect model: *F*-test, $p<0.001$ for all) even after correcting for the possible effect of individuals. Maximum overshoot, however, was not dependent on angle (mixed effect model: *F*-test, p=0.239) even after correcting for individual effects. Transient response properties are summarized in Table 1.

To predict the mean natural frequency based on vibration analysis of tapered, truncated-cone cantilevers, we chose the boundary condition according to Georgian (1965), who tabulated eigenvalues λ_n in terms of $(A_t/A_b)^{1/2}$, where A_t is the cross-sectional area at the tip of the cone and A_b at the base. We estimated λ_n to be ~4.7 in our experiment by linearly interpolating the tabulated eigenvalues for each $(A_t/A_b)^{1/2}$. We used an average value of $E = 6.46 \times 10^6$ Pa, as determined in the static bending experiments. All other model parameters for Equation 9 were

obtained from our geometrical measurements (see above). Using average values for r_b (0.23 mm), L (46.12 mm), and ρ (0.79 mg/mm^3) as model inputs resulted in a predicted natural frequency of 23 Hz, which falls within the range of natural frequencies obtained in our experiments (15–31 Hz).

Dynamics: collision response

We measured collision dynamics via an impulse perturbation on $n = 5$ intact flagella (3 right, 2 left antennae; Fig. 5A). Similar to the step deflections, flagella showed highly consistent collision responses (Fig. 5B). After an impulse-like perturbation near the antennal tip, the flagellum remained in contact with the colliding object for up to 20 ms before slipping and rapidly flipping back to its starting position (Fig. 5). At the instant of impact (Fig.5 at $t = 0$ ms) and throughout the deflection period, there was no observable separation between object and flagellum, which is characteristic of a near perfect inelastic collision; the flagellum effectively stuck to the colliding object. Moreover, antennal bending showed peak curvatures close to the site of impact. The point of greatest curvature κ at the instant of maximum deflection (e.g. Fig. 5A at $t = 20$ ms) was always found between 80 % and 90 % of the unrestrained flagellum length (80 %: 12/50 trials; 85 %: 18/50 trials; 90 %: 20/50 trials), while the perturbation was at ~95 % of the unrestrained length. Consistent with the results from the step deflection experiment, motion appeared to be transferred only marginally from tip to base.

Discussion

The present study takes a first step in elucidating interplay between a dynamic tactile sensory appendage and a rapidly moving body. Here we speculate on how the antenna mechanics described above could be considered tuned for effective tactile-mediated sensorimotor control of a rapidly moving body. To begin to define these tuning properties, we analyzed the main tactile sensor of one of the fastest land invertebrate runners — the antenna of the American cockroach, *P. americana* — and characterized the antenna's static and dynamic response.

Static bending properties

From estimates of the second moment of area, derived from geometrical measurements, we hypothesized that the flexural stiffness of the flagellum should decrease rapidly from base to tip (Fig. 3A-C). We tested this hypothesis by measuring the resistance-to-bending forces along the flagellum while imposing large deflections. We found that the forces decreased exponentially whereas the elastic modulus did not change significantly, suggesting that geometrical properties are the main determinant of flexural stiffness (Fig. 3D). Using a 2D Euler-Bernoulli beam model matching the boundary conditions of our experiment, we estimated the average elastic modulus E to be 6.46×10^6 Pa. This approximation gives us an upper bound on E, as it is based on the upper bound of the second moment of area and peak forces during displacements. This estimate is similar to measurements of the elastic modulus of resilin, which lies between approximately 3.0

x 10^5 to 3.0 x 10^6 as reported by Vincent and Wegst (2004). Solving for *EI* instead of *E* – i.e. without prior knowledge of *I* – for each point along the length and averaging, yielded a flexural stiffness of 5.67 x 10^{-9} Nm^2. Our results are the same order of magnitude as Kellogg (2007), who reported a flexural stiffness of approximately 10 x 10^{-9} Nm^2 in the house cricket *Acheta domesticus L.* – an insect with a flagellum with morphology similar to *P. americana* – for dorsal and ventral directions at 0.5 cm from the base. Interestingly, compared to Wistar (*Rattus norvegicus*) rat whiskers, made of keratin, the flagellum of *P. americana* is less stiff by 3 orders of magnitude (whiskers were reported at 3.34 x 10^9 Pa; Quist et al. (2011)). This difference in stiffness suggests that rat whiskers will transmit forces differently than in antennae of *P. americana*, requiring greater forces for the same deflection at the tip.

Our results, demonstrating that the resistance-to-bending forces decrease exponentially from base to tip, are consistent with antennal static bending experiments in another arthropod, the crayfish *Cherax destructor*, which uses its antennae for tactile localization (Sandeman, 1989). In fact, by geometry alone, we would expect setaceous or filiform antennae in other insects to exhibit this mechanical property because of the tapered geometry from base to tip. Similar to *P. americana*, crayfish antennae are articulated by annuli and highly tapered. However, in crayfish, it was shown that the flagellum is stiffer when bent medially than laterally. In our experiment, we found no statistically significant differences between lateral and medial planes, consistent with dynamic measurements.

For *P. americana*, *I* at the base (2.06 x 10^{-15} m^4) is three orders of magnitude greater than *I* at the tip (9.48 x 10^{-18} m^4). Having a tip that is highly flexible could increase spatial acuity during object localization (Comer et al., 2003) and perhaps improve the reliability of tactile flow computation during high-speed running tasks such as wall following (Cowan et al., 2006; Lee et al., 2008) or, more generally, obstacle avoidance. In terrestrial mammals, it has been suggested that the conserved taper of whiskers provides selective advantages, for instance enabling discrimination of finer surface features in contrast to un-tapered whiskers (Williams and Kramer, 2010). Using a physical model of arthropod antennae, Demir et al. (2010) demonstrated that a compliant tip increases spatial acuity during spatial mapping tasks. In addition, for arthropods, having a flexible antenna may be a desirable feature for self-cleaning, which requires manipulation with significant bending before passage through the mouth (Smith and Valentine, 1985).

Implications for sensing and control

During wall following in cockroaches, Camhi and Johnson (1999) observed that cockroaches initiate turns when the antenna bends in response to wall projections. They noted that as the cockroach moves closer to an object, the straight portion of the antenna (region from base of antenna to bend) shortens. That is, the bend or contact point "moves" towards the base. The same observation was reported in the crayfish antenna by Sandeman (1989). Camhi and Johnson (1999) hypothesized that this parameter, the point of bend, could constitute a one-dimensional map along the length of the antenna that could provide a cue to induce a change in body angle. The point of bend is where the radius of curvature *R* will be smallest, and thus curvature κ will be greatest. For a discretized beam with a force near the tip and with constant stiffness, κ will

vary according to I^{-1} (Eq. 2), such that curvature κ (and therefore amount of bending) will be greatest where I is smallest, assuming first-mode bending. Thus, more bending should be expected at the tip than at the base. The fact that the point of bend (or point of greatest curvature) is always closest to the wall and appears to "move" considerably as the animal changes its distance to the wall can be attributed to a decreasing second moment of area. In contrast, we would expect the point of bend for a beam or antenna with a constant I to remain constant. Thus, we contend that these observations in the literature can be attributed to geometrical properties (I) and that these properties could enable and simplify detection of sensory cues to evoke a turn, as suggested by Camhi and Johnson (1999).

Another advantage of a decreasing second moment of area, given sufficient friction, is to provide an increase in preview distance as the bending occurs closest to the point of contact. In contrast, an antenna with a constant second moment of area would assume an inverted "U" shape where the contact point would be closer to the head. To our knowledge, the second moment of area has never been linked to preview distance. Preview distance is a critical component for stabilizing closed-loop tactile navigation, as demonstrated in control theoretic studies of wall following using simple (Cowan et al., 2006) and dynamically-representative (Lee et al., 2008) models of running *P. americana*.

Dynamic properties

To study flagellar dynamics, we treated the flagellum as a cantilevered beam. We imposed step deflections and measured tip displacements to characterize natural frequency and damping properties (Fig. 4). Following a step deflection, the flagellum oscillated at first mode natural frequency as the transient response decayed. The tip exhibited two overshoots and recovered almost entirely after as little as 70 ms (Fig. 4B). The time course of the tip displacement (Fig. 3B) classified the antennal flagellum of *P. americana* as an under-damped system that allows a fast return to its original position after deformation in ~70 ms. Interestingly, this return time of 70 ms corresponds to approximately one stride period during high-speed running (Full and Tu, 1991). The statistically significant difference in the two independent measurements of damping ratio – based on the maximum overshoot and the logarithmic decrement methods – revealed that the flagellum response is non-linear, quickly settling following a large overshoot (~40-50 above stead state; Table 1). The dynamic response showed no signs of directional anisotropy when comparing dorsal, ventral, lateral and medial planes. This directional anisotropy corroborates findings in stick insect antennae (Dirks and Dürr, 2011). The variance in frequencies observed in the present study can mainly be attributed to different initial deflection angles. Surprisingly, an increase in the deflection resulted in a significant decrease in the estimated damped natural frequency (Fig. 4E,F). While one would expect a larger deflection to cause an increase in amplitude in a linear system, a change in time characteristics points towards some non-linearity. Assuming a truncated-cone cantilever beam with geometrical properties similar to that of the flagellum, the model described in Equation 9 predicted a natural frequency of 23Hz, which falls within the observed natural frequency range (15.8–31.0 Hz). It should be noted that the lengths of the analyzed flagella varied by as much as 12 mm. Although care was taken to select animals with intact antennae, missing distal segments were common, e.g. due to aggressive behavior with conspecifics. Nevertheless, the dynamic responses were highly consistent and differences in

length (factor *animal*) did not account for a significant part of the variance found in the tip recovery.

Since the flagella were held rigidly near the base (fixed base, free end boundary condition), which is presumably more stiff than the antenna operating on the animal, measurements of (damped) natural frequencies are upper bounds and measurements of damping ratios are lower bounds. The head-scape, scape-pedicel, and pedicel-flagellum joints may dampen some of the motion, though it is unclear at present how the fixed-base boundary condition contributes to overall tip displacements. Activation of muscles attaching to these segments could vary the compliance at the base and hence vary the boundary conditions. Thus, active neural control may modify damping and natural frequency. However, studies of wall following suggest little-to-no contribution from basal segments; therefore, it is unclear if active control is present at the base during rapid running, besides tonic muscular activity to maintain antennal angles (Camhi and Johnson, 1999). Additional experiments with unrestrained antennae would be necessary in order to test the contribution of basal segments. At present, it is difficult to assess how the antenna responds to step-like perturbations in the behaving animal. Specifically, as the dynamics of the body also drive antenna motion towards the tip, it is a challenge to separate passive antenna dynamics from body-driven dynamics during recovery. In fact, 3D tracking of the tip in freely-running *P. americana* show maximum dorso-ventral amplitude displacements of over 2 cm (Mongeau, unpublished), despite the center of mass having vertical excursions of only 0.3 mm (Full and Tu, 1991).

A factor which may affect the damping and stiffness of the flagellum during high-speed running in *P. americana* is the active regulation of fluid pressure within the antenna via pumping of the antennal heart. However, we think this scenario is unlikely. The antennae of *P. americana*, unlike other pressurized systems like the proboscis of Lepidoptra (Krenn, 1990), is an open circulatory system with no identified valve that prevents backflow to the head (Pass, 1985), thus it is unlikely that a static pressure can be held. However, the heart could build a dynamic pressure due to instantaneous changes in flow rate of hemolymph. However, return fluid flow velocity, which has been estimated as 50 $\mu m\ s^{-1}$ from distal to basal end by Kapitskii (1984), is very slow. This is consistent with measurements of hemolymph exchange in the antennae, taking approximately 10 minutes (Pass, 1985). However, additional experiments with animals in different behavioral states (e.g. at rest vs. running) would be necessary. Decapitation, which eliminates the possible contribution of the body cavity in regulating antennal pressure, has no effect on antennal damping in the stick insect *Carausius morosus* (Dirks and Dürr, 2011). However, in that study the antennal heart remained intact.

Collision response

To understand how the flagellum physically interacts with the environment, we simulated an antenna colliding with an obstacle near running speed. We determined that the flagellum is highly flexible at the tip, with little to no perturbation transmitted to the base when impacting an object (Fig. 5). In accordance with observations from collision avoidance behaviors such as wall following (Camhi and Johnson, 1999), both step and impulse responses indicate that most of the motion occurs towards distal parts of the antenna. The amount of motion decreases roughly

exponentially towards the base, with the proximal regions exhibiting no macro scale vibrations (Fig. 4C; i.e., vibrations with amplitudes larger than our resolution of 0.1 mm). This result is consistent with our findings showing that the antennae of *P. americana* have a decreasing, non-linear flexural stiffness profile from base to tip. Furthermore, the collision response showed dynamics characteristic of a nearly perfect inelastic collision; that is, the antennal tip did not move away from the colliding object at the instant of impact (Fig. 5A, at $t = 1$ ms), but was dragged along until increased bending caused it to slip and snap back rapidly (Fig. 5A, at $t = 20$ ms). These findings support the notion that *P. americana* does not sense macro-scale antennal deflections at the base, but rather that information may be encoded in the shape of the flagellum itself (Camhi and Johnson, 1999). Along the flagellum, the distal part appears to be critical for sensing. Its flexibility may increase the overall contact area with an object and maintain contact during high-speed running from the instant of impact. This property reduces high-frequency oscillations of the flagellum, which may in turn decrease mechanical noise propagating through the sensory array.

In summary, the tip displacement classifies the flagellum as a highly damped system with exponentially decreasing flexural stiffness, which may simplify neural control for tactile sensing: (1) the flagellum can maintain contact with an object from the instant of impact, which may increase the reliability of tactile information while isolating the contact event from body motion; (2) the flagellum can dampen high-frequency macro-vibrations and associated sensory noise that arise after the antenna loses contact and (3) the flagellum allows a rapid, passive recovery of the original antennal shape within about one stride period without the need for neural control, such that the animal can rapidly respond to a new impending obstacle. Our results suggest that antennae of *P. americana* are less damped than those of slowly walking stick insects (Dirks and Dürr, 2011), but more damped than vertebrate vibrissae (Hartmann et al., 2003). However, direct comparison of damping values with measurements from Dirks and Dürr (2011) are difficult due to different experimental designs. Their damping measurements are not based on antennal tip displacements, as in the present study, but on different points along the antenna. Furthermore, for each successive experiment, Dirks and Dürr (2011) changed the boundary conditions, thus altering the overall dynamics of the antenna's response.

Further elucidation of antennal mechanical tuning will lead to neural hypotheses which integrate distributed mechanosensory inputs from a dynamic sensory appendage operating on a rapidly moving body. Future research in predicting stresses along the flagellum will help to reveal how information from different mechanoreceptors (e.g. stress-sensitive campaniform sensilla) is integrated during tactile tasks. In addition, measurements of the frequency response of antennae will help to further characterize its mechanical filtering properties (i.e., its transfer function) and help identify the frequency ranges beyond the natural frequency that may be excited during different tasks. Finally, in future studies, it will be important to investigate the neuromechanical role of the two actively-controlled segments of the antenna, the scape and pedicel.

For roboticists seeking to design tactile probes to add new capabilities to mobile robots, choosing mechanical design parameters that integrate with the body remains a challenge. The next generation of agile and multifunctional robots will undoubtedly benefit from building sensors with the body in mind. Our collaborative work transferring biological principles to engineering is informing the design of statically and dynamically tunable bio-inspired tactile antenna (Demir et

al., 2010). In return, this physical model may allow us to test biological hypotheses that would otherwise be extremely difficult to test in live, behaving animals.

References

Baba, Y., Tsukada, A. and Comer, C. M. (2010). Collision avoidance by running insects: antennal guidance in cockroaches. *J. Exp. Biol.* **213**, 2294–302.

Camhi, J. M. and Johnson, E. N. (1999). High-frequency Steering Maneuvers Mediated by Tactile Cues: Antennal Wall-Following in the Cockroach. *J. Exp. Biol.* **202**, 631–643.

Chapman, R. F. (1998). *The Insects: Structure and Function*. 4th ed. Cambridge University Press.

Comer, C. M., Parks, L., Halvorsen, M. B. and Breese-Terteling, A. (2003). The antennal system and cockroach evasive behavior. II. Stimulus identification and localization are separable antennal functions. *J. Comp. Phys. A.* **189**, 97–103.

Conway, H. D., Becker, E. C. H. and Dubil, J. F. (1964). Vibration Frequencies of Tapered Bars and Circular Plates. *J. Appl. Mech.* **31**, 329.

Cowan, N. J., Lee, J. and Full, R. J. (2006). Task-level control of rapid wall following in the American cockroach. *J. Exp. Biol.* **209**, 1617–1629.

Demir, A., Samson, E. and Cowan, N. J. (2010). A tunable physical model of arthropod antennae. *IEEE International Conference on Robotics and Automation*. 3793-3798.

Dirks, J.-H. and Dürr, V. (2011). Biomechanics of the stick insect antenna: damping properties and structural correlates of the cuticle. *J. Mech. Behav. Biomed. Mater.* **4**, 2031–42.

Dürr, V., König, Y. and Kittmann, R. (2001). The antennal motor system of the stick insect Carausius morosus: anatomy and antennal movement pattern during walking. *J. Comp. Phys. A.* **187**, 131–144.

Frye, M. a and Dickinson, M. H. (2001). Fly flight: a model for the neural control of complex behavior. *Neuron* **32**, 385–8.

Full, R. J. and Tu, M. S. (1991). Mechanics of a rapid running insect: two-, four- and six-legged locomotion. *J. Exp. Biol.* **156**, 215–231.

Georgian, J. (1965). Vibration frequencies of tapered bars and circular plates. *J. Appl. Mech.* **32**, 234–235.

Hartmann, M. J., Johnson, N. J., Towal, R. B. and Assad, C. (2003). Mechanical characteristics of rat vibrissae: resonant frequencies and damping in isolated whiskers and in the awake behaving animal. *J. Neurosci.* **23**, 6510–9.

Kapitskii, S. V. (1984). Morphology of the antenna of the male American cockroach *Periplaneta americana*. *J. Evol. Biochem. Physiol.* **20**, 59–66.

Kellogg, D. (2007). Antennal Biomechanics of House Crickets (*Acheta domesticus L.*). *ProQuest*. M.A. University of Kansas, 31 pages; 1447112.

Krenn, H. W. (1990). Functional morphology and movements of the proboscis of Lepidoptera (Insecta). *Zoomorphology.* **110**, 105–114.

Lee, J., Sponberg, S., Loh, O. Y., Lamperski, A. G., Full, R. J. and Cowan, N. J. (2008). Templates and Anchors for Antenna-Based Wall Following in Cockroaches and Robots. *IEEE Trans. Robot.* **24**, 130–143.

Libby, T., Moore, T. Y., Chang-Siu, E., Li, D., Cohen, D. J., Jusufi, A. and Full, R. J. (2012). Tail-assisted pitch control in lizards, robots and dinosaurs. *Nature.* **481**, 181–4.

Loudon, C. (2005). Flexural stiffness of insect antennae. *American Entomologist.* 48–49.

Neimark, M. a, Andermann, M. L., Hopfield, J. J. and Moore, C. I. (2003). Vibrissa resonance as a transduction mechanism for tactile encoding. *J. Neurosci.* **23**, 6499–509.

Nelson, M. E. and MacIver, M. A. (2006). Sensory acquisition in active sensing systems. *J. Comp. Phys. A.* **192**, 573–86.

Okada, J. and Toh, Y. (2004). Antennal system in cockroaches: a biological model of active tactile sensing. *International Congress Series* **1269**, 57 – 60.

Pass, G. (1985). Gross and fine structure of the antennal circulatory organ in cockroaches (Blattodea, Insecta). *J. Morphol.* **185**, 255–268.

Quist, B. W. and Hartmann, M. J. Z. (2012). Mechanical signals at the base of a rat vibrissa: The effect of intrinsic vibrissa curvature and implications for tactile exploration. *J. Neurophys.* **9,** 2298–2312.

Quist, B. W., Faruqi, R. a and Hartmann, M. J. Z. (2011). Variation in Young's modulus along the length of a rat vibrissa. *J. Biomech.* **44**, 2775–2781.

Sandeman, D. C. (1989). Physical properties, sensory receptors and tactile reflexes of the antenna of the australian freshwater crayfish cherax destructor. *J. Exp. Biol* **141**, 197–217.

Sandeman, D. C. and Varju, D. (1988). A behavioural study of tactile localization in the crayfish *Cherax destructor*. *J. Comp. Phys. A.* **163**, 525–536.

Sane, S. P. and McHenry, M. J. (2009). The biomechanics of sensory organs. *Integr. Comp Biol.* **49**, 8–23.

Sane, S. P., Dieudonné, A., Willis, M. A. and Daniel, T. L. (2007). Antennal mechanosensors mediate flight control in moths. *Science.* **315**, 863–6.

Smith, B. J. B. and Valentine, B. D. (1985). Phylogenetic Implications of Grooming Behavior in Cockroaches (Insecta: Blattaria). *Psyche.* **92**, 369–385.

Timoshenko, S. (1934). *Theory of Elasticity*. 1st ed. McGraw-Hill book company, Inc.

Tongue, B. H. (2002). *Principles of Vibration*. 2nd ed. Oxford University Press.

Vincent, J. F. V. and Wegst, U. G. K. (2004). Design and mechanical properties of insect cuticle. *Arthro. Struct. Dev.* **33**, 187–99.

Williams, C. M. and Kramer, E. M. (2010). The advantages of a tapered whisker. *PloS ONE* **5**, e8806.

Figure 1. Setup for static bending and dynamic response measurements of the flagellum. (A) Apparatus for determining the variation in flexural stiffness of the antenna. We immobilized the head, scape, and pedicel with silicone (green). The flagellum was held near the base with a pair of fine forceps. A force sensor 1 mm away from the forceps mounted on a motorized stage deflected the flagellum laterally (away from the midline) by 1 mm while measuring the resistance-to-bending force. A small notch at the base of the arm of the force sensor prevented out-of-plane motion. This procedure was repeated for different points along the flagellum by moving the platform in steps of 2 mm to the left. This procedure was also repeated for the medial plane (toward the midline). (B) Apparatus for determining the dynamic response of the flagellum. Animals were mounted on a rotatable platform with their heads and first two antennal segments (scape and pedicel) immobilized. The flagellum was fixated 0.5 cm away from the base with a pair of fine forceps. Two high-speed cameras recorded horizontal and vertical motions during recovery from either (C) a step deflection or (D) an impulse-like collision. For the step deflection, a second pair of forceps was used to deflect the flagellum to different initial angles (20°, 30º, and 50°). We measured the response by tracking the tip for the lateral, medial, dorsal and ventral planes. In the case of the collision response, a small cylinder hit the flagellum dorsally at ~ 60 cm s^{-1} near the tip to simulate obstacle contact during high-speed running. Antenna not drawn to scale.

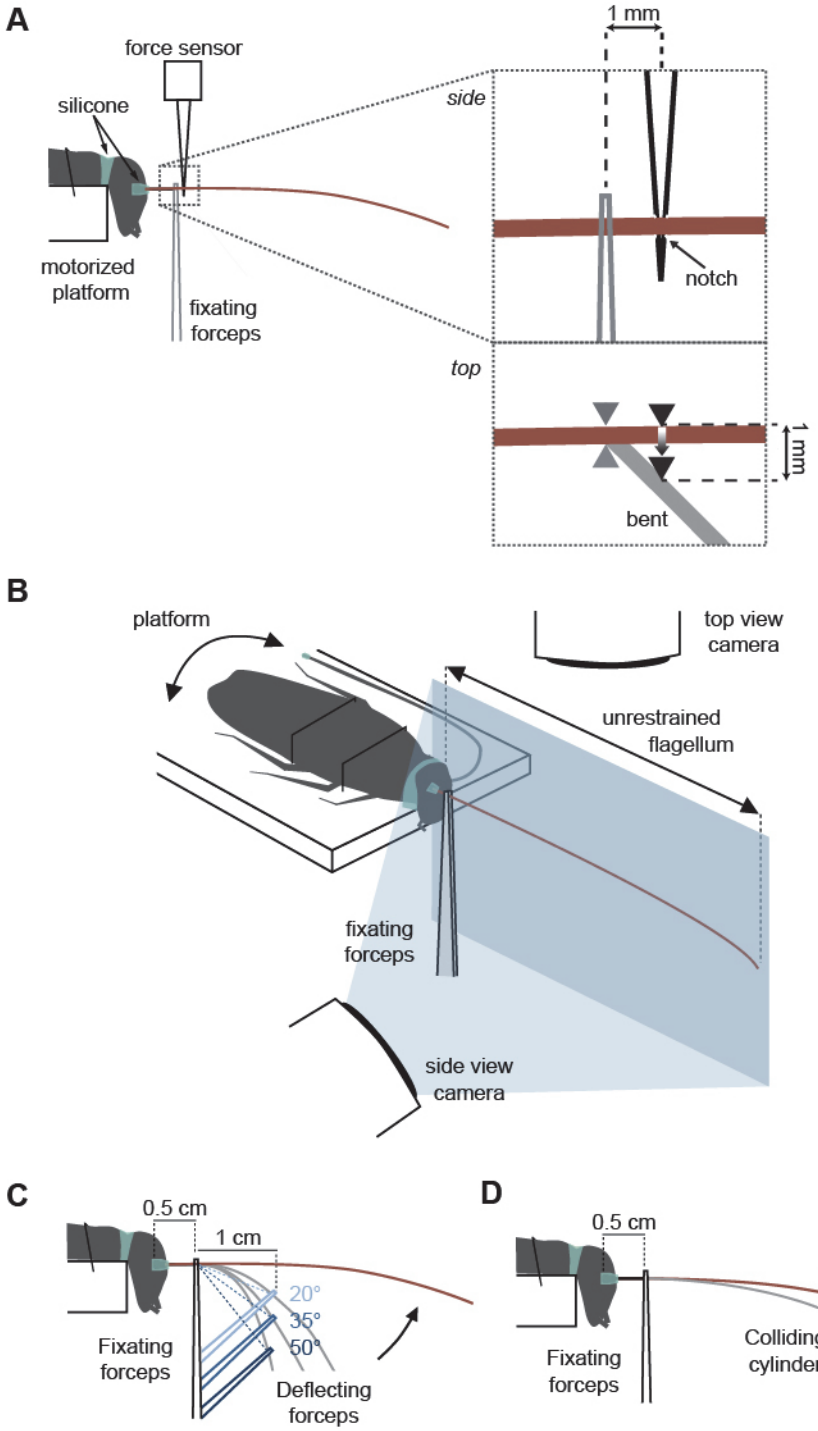
A
force sensor
silicone
motorized
platform
fixating
forceps
side
1 mm
notch
top
1 mm
bent
B
platform
top view
camera
unrestrained
flagellum
fixating
forceps
side view
camera
C
0.5 cm
1 cm
20°
35°
50°
Fixating
forceps
Deflecting
forceps
D
0.5 cm
60 cm/s
Fixating
forceps
Colliding
cylinder

Figure 2. Diagram of 2D Euler-Bernoulli beam model. The flagellum of length L is modeled as a tapering conical cantilever beam under the action of a point force F at distance s from the clamp, with the prescribed deflection y_{def}. The flagellum is discretized into a series of rigid links with nodes labeled in the inset. Antenna not drawn to scale.

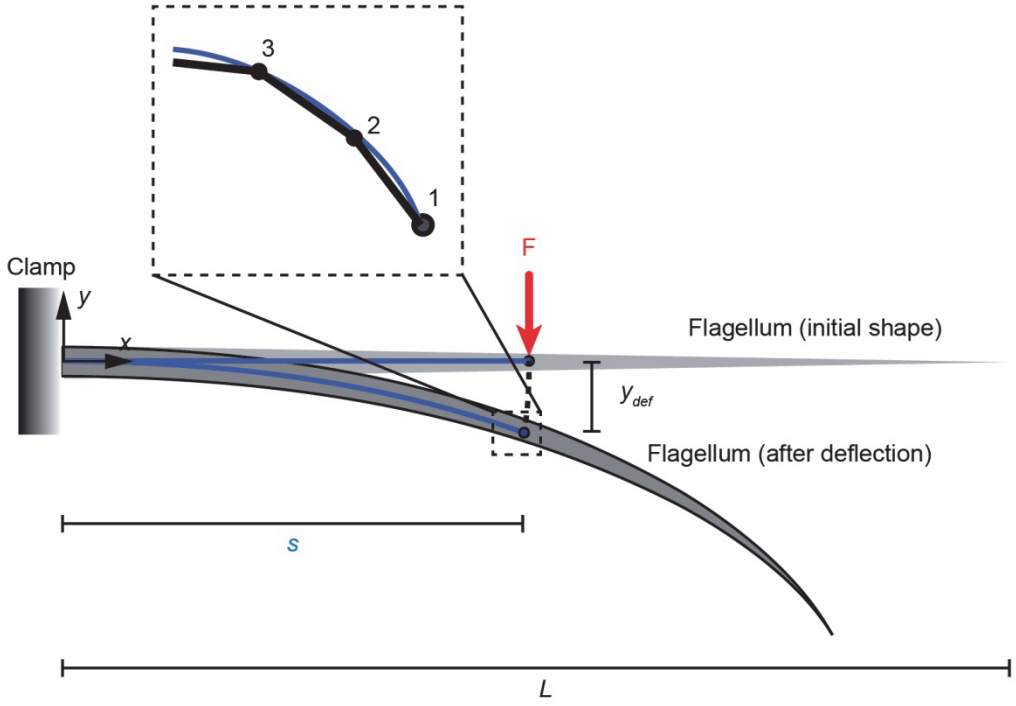
3
2
1
F
Clamp
y
x
Flagellum (initial shape)
y_{def}
Flagellum (after deflection)
s
L

Figure 3. Flagellum geometry and resistance-to-bending force. (A) High-resolution image of flagellum constructed from multiple frames (dark boxes). (B) Length of annuli for 3 flagella out of $n = 10$ flagella measured. The length of annuli increase from base to tip, with a transition near 20 % of the antenna length. (C) Variation in radius along the length for 3 flagella out of $n = 10$ flagella measured. The radius decreases exponentially from base to tip. Using a logarithmic model, all slopes are significantly different from 0 with $\alpha = 0.01$. (D) Log of resistance-to-bending force vs. distance from base for $n = 5$ flagella. The force exponentially decreased from base to tip. Using a logarithmic model, all slopes were significantly different from 0 with $\alpha = 0.01$. Results are consistent with predictions of second moment of area estimates from measurements of the change in radius from base to tip.

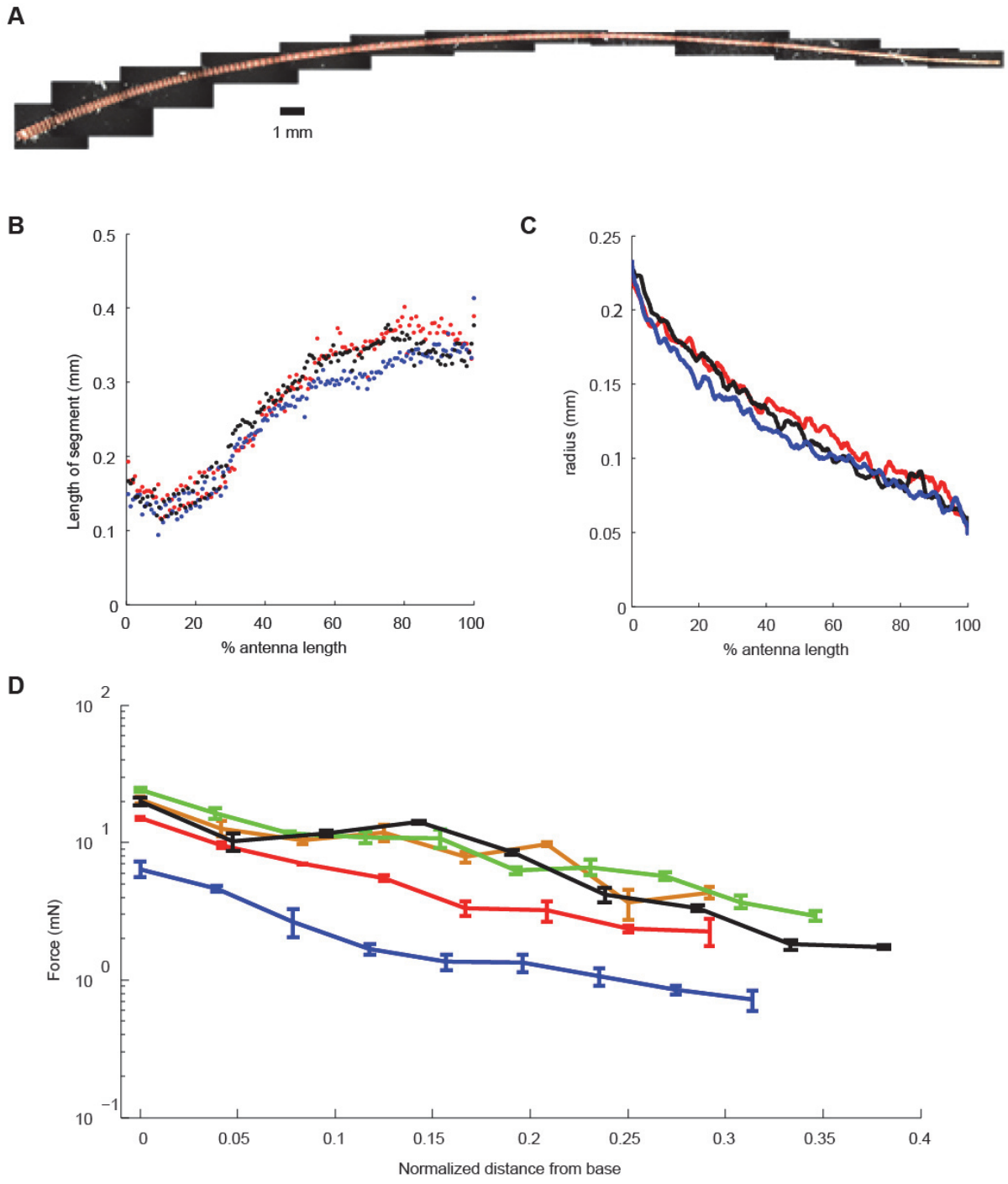
A
1 mm
B
Length of segment (mm)
% antenna length
C
radius (mm)
% antenna length
D
Force (mN)
Normalized distance from base

Figure 4. Antenna step deflection response. (A) Sequence of flagellum recovery from a step deflection of 50º with 20 automatically tracked points overlaid in blue. (B) The tip of the antenna recovered rapidly after an initial deflection of 20º, 35 º, or 50º and exhibited only two overshoots. Most of the perturbation was rejected within the first oscillation cycle (~70 ms on average). Deflection directions did not have a significant effect on damped natural frequencies (*F*-test, p = 0.255) and damping ratios (*F*-test, p = 0.812). (C) Analysis of the maximum displacement of different parts of the flagellum during recovery revealed large deflections toward the tip, with little-to-no motion transferred at the base. Dark lines represent the mean, and the shaded region is ± 1 standard deviation. The under-damped system is characterized by (D) a mean damped natural frequency f_d of 18 Hz and mean damping ratios ζ_{Mp} (E) of 0.27 (based on overshoot method) and ζ_1 (F) of 0.52 (based on logarithmic decrement method). For box plots, the central line is the median, the bottom and top edges of the box are the 25th and 75th percentiles and the whiskers extend to ± 2.7 standard deviations. Outliers are shown as small colored dots.

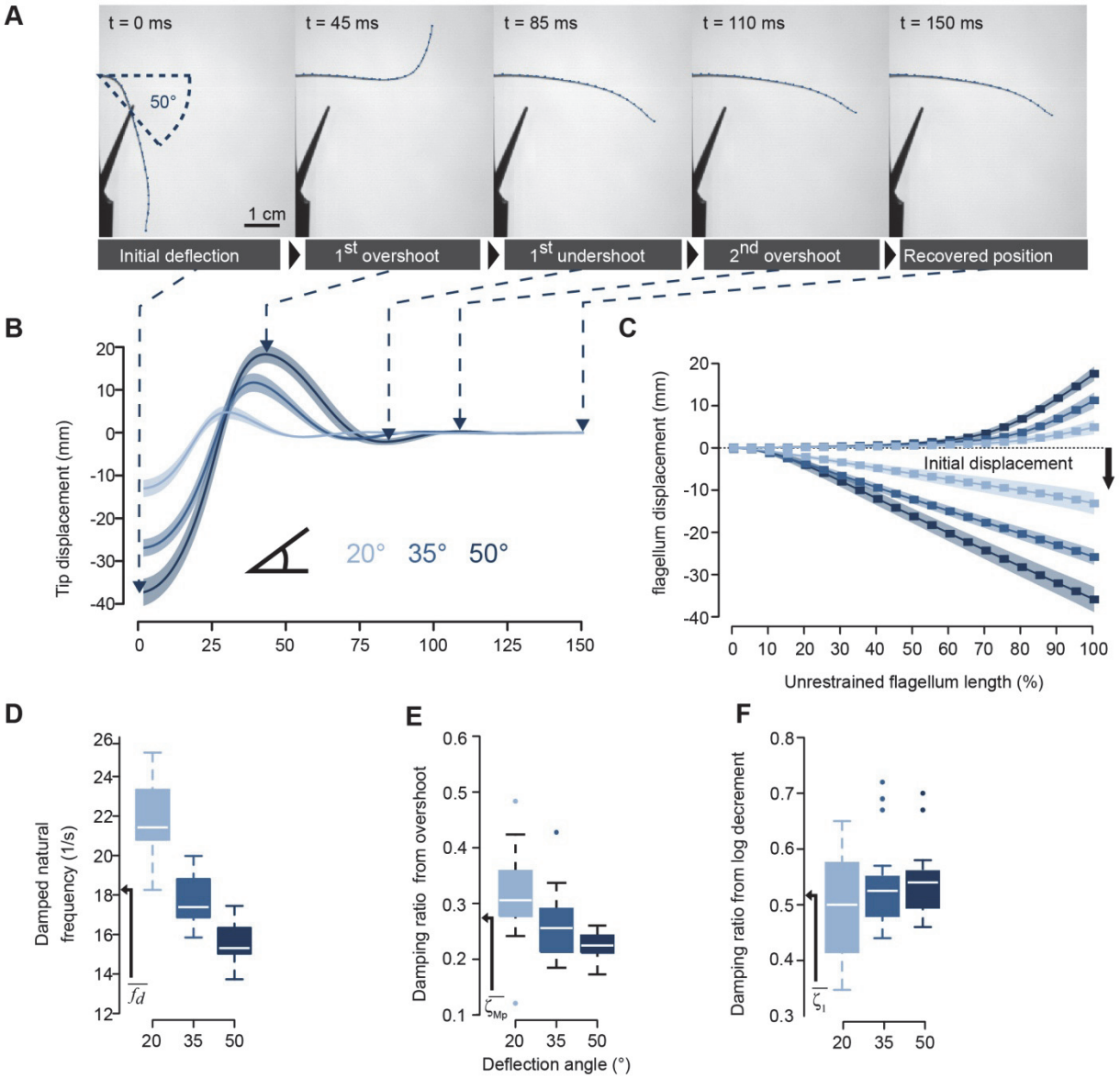
A
t = 0 ms
t = 45 ms
t = 85 ms
t = 110 ms
t = 150 ms
50°
1 cm
Initial deflection
1st overshoot
1st undershoot
2nd overshoot
Recovered position
B
Tip displacement (mm)
20°
35°
50°
C
flagellum displacement (mm)
Initial displacement
Unrestrained flagellum length (%)
D
Damped natural frequency (1/s)
E
Damping ratio from overshoot
Deflection angle (°)
F
Damping ratio from log decrement

Figure 5. Impulse collision response. (A) Sequence of flagellar recovery with automatically tracked points overlaid. (B) Time course of tip recovery. The response shows dynamics characteristic of a near perfect inelastic collision (at t = 1 ms) and antennal bending with peak curvatures close to the site of impact (at t = 20 ms). Similar to the step deflection (Fig. 3), the collision response indicates that motion at the tip is only marginally transmitted to proximal regions. Data were pooled across animals (n = 5; 10 trials per individual). Dark lines represent the mean and the shaded region is ± 1 standard deviation.

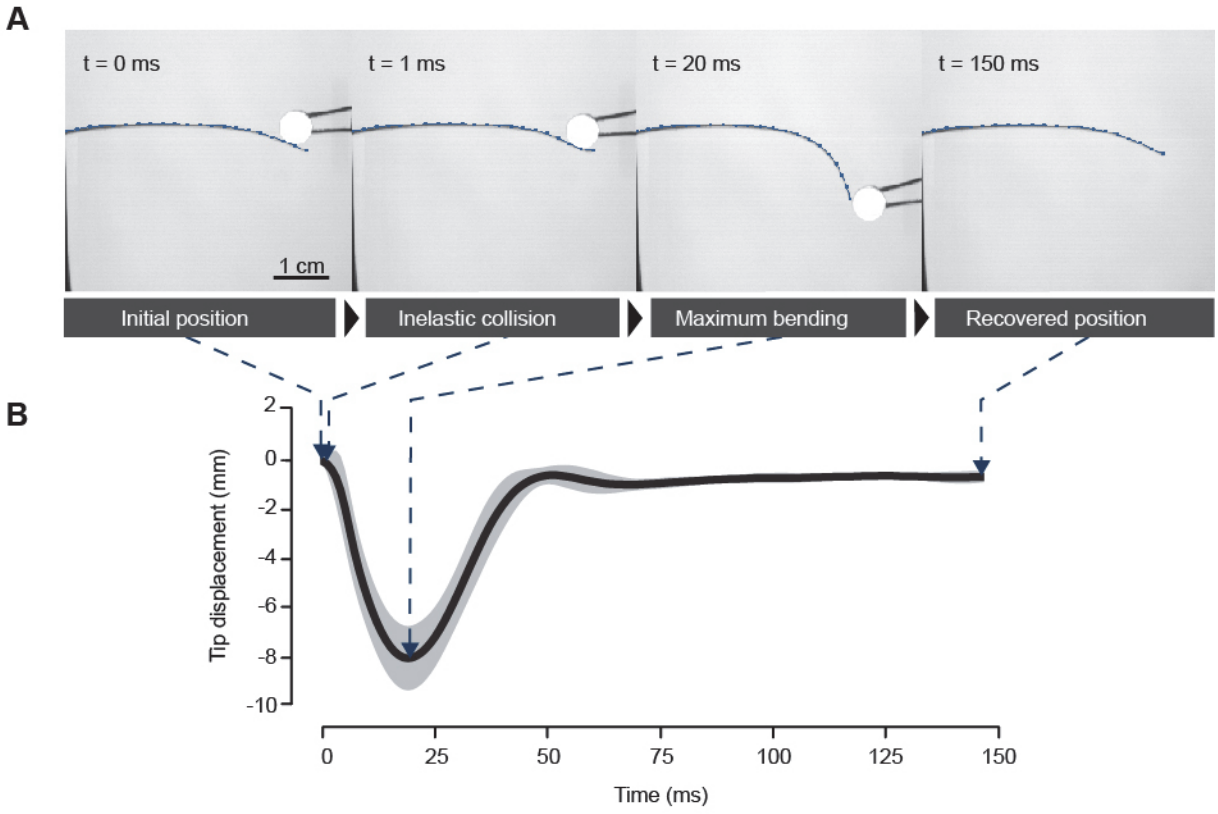
A
t = 0 ms
t = 1 ms
t = 20 ms
t = 150 ms
1 cm
Initial position
Inelastic collision
Maximum bending
Recovered position
B
Tip displacement (mm)
2
0
-2
-4
-6
-8
-10
0
25
50
75
100
125
150
Time (ms)

Table 1. Transient response specifications.

	Angles		
	20°	**35°**	**50°**
Delay time t_d (ms)	15 ± 3	20 ± 2	23 ± 2
Rise time t_r (ms)	21 ± 4	27 ± 3	30 ± 2
Peak time t_p (ms)	30 ± 5	39 ± 2	45 ± 3
Maximum overshoot M_p (%)	43 ± 15	46 ± 13	51 ± 13
Settling time t_s (ms)	69 ± 13	76 ± 10	89 ± 12

Table 2. List of symbols

κ	curvature
ζ	damping ratio
Δ	logarithmic decrement
ρ	mass density of antenna
ω_0	undamped angular frequency
A_b	cross-sectional area at base
A_t	cross-sectional area at tip
E	elastic or Young's modulus
EI	flexural stiffness
F	force applied on antenna
f_d	damped natural frequency
f_n	undamped natural frequency
I	second moment of area
L	length of antenna
M	moment or torque
R	radius of curvature
r	radius of antenna
r_b	radius at base of antenna
s	distance from clamp to force application
x, y	Cartesian coordinates
y_{def}	deflection of antenna in y direction

Chapter 4

Rapid inversion: running cockroaches, geckos and robots swing like a pendulum under ledges

Summary

Escaping from predators often demands that animals rapidly negotiate complex environments. The smallest animals attain relatively fast speeds with high frequency leg cycling, wing flapping or body undulations, but absolute speeds are slow compared to larger animals. Instead, small animals benefit from the advantages of enhanced maneuverability in part due to scaling. Here, we report a novel behavior in small, legged runners that may facilitate their escape by disappearance from predators. We video recorded cockroaches and geckos rapidly running up an incline toward a ledge, digitized their motion and created a simple model to generalize the behavior. Both species ran rapidly at 12–15 body lengths-per-second toward the ledge without braking, dove off the ledge, attached their feet by claws like a grappling hook, and used a pendulum-like motion that can exceed one meter-per-second to swing around to an inverted position under the ledge, out of sight. We discovered geckos in Southeast Asia can execute this escape behavior in the field. Quantification of these acrobatic behaviors provides biological inspiration toward the design of small, highly mobile search-and-rescue robots that can assist us during natural and human-made disasters. We report the first steps toward this new capability in a small, hexapedal robot.

Introduction

Fundamental laws of scaling in biology reveal why small animals have the opportunity to employ maneuvers that simply are unavailable to large animals. Turning ability and angular acceleration are largely dependent on rotational inertia (Walter & Carrier, 2002; Carrier et al., 2001). If we assume that animals are geometrically similar, then rotational inertia scales with body mass$^{5/3}$. The rotational inertia of a 70 kg human is more than eight orders of magnitude greater than that of a 1 g insect, whereas their masses differ by only five orders of magnitude. In part, this explains why fruit flies during rapid saccades can execute a 90° turn in only 50 ms with 10 wingbeats (Dickinson, 2005). Two centimeter long mother-of-pearl caterpillars can recoil-and-roll backwards in 300 ms at 11 revolutions per seconds (Brackenbury, 1997; Brackenbury, 1999). Small lizards (3-6 g) running at high speed on artificial branches perform 90° turns with rotational velocities exceeding 600° per second (Higham et al., 2001). Small geckos (3g) can right themselves in mid-air in only 100 ms by a swing of their tail after falling upside down from the underside of a leaf (Jusufi et al., 2008). Small geckos (Autumn et al., 2006) and insects (Goldman et al., 2006) can race up vertical surfaces at speeds near one meter per second (25 body lengths s^{-1}) due to their advantageous strength to weight ratio (Alexander, 1985; Full et al., 1995) and the ability of their feet to engage the surface. The number of asperities available for claw-based climbing scales inversely with the radius of a claw's tip (Asbeck et al., 2006) allowing these animals to even run upside down (Larsen et al., 1995). These abilities conferred

by physical scaling laws can provide key advantages to small animals, especially during escape responses from predators that demand rapid negotiation of complex environments challenging the fastest neural reflexes (Spagna et al., 2007).

Fortunately, these behaviors we admire in animals can now provide biological inspiration for small, mobile robots due to advancements in fabrication and rapid prototyping. Previously, microrobots with dimensions at the centimeter scale have been difficult to design using precision machining or microelectromechanical systems (MEMS) technology because of the difficulty in constructing high-strength segments with low-loss joints on the millimeter and micron scale. Now, new fabrication processes such as smart composite microstructures (SCM) (Wood et al., 2008) can integrate rigid links and large angle flexure joints through laser micromachining and lamination. Using these new rapid prototyping approaches, multiple design hypotheses of microrobots (Hoover and Fearing, 2008; Hoover et al., 2008; Birkmeyer et al. 2009) and their parts can be tested and the unparalleled maneuverability we see in nature's smallest animals can begin to be realized.

To understand the opportunities provided by scaling on the strategies used to maneuver in complex natural and human-made environments, we began by studying high-speed running in animals negotiating transitions in terrains. First, we ran the American cockroach *Periplaneta americana* at high speeds along an inclined track with a gap. To our surprise, the animal did not clear the gap, but exhibited a new behavior, a rapid inversion using its hind legs to swing underneath the ledge. To explore the generality and biological relevance of high-speed transition strategies, we also studied geckos in the laboratory and in the field in forest reserves of Singapore. We hypothesized that small animals running at high speed can attain an advantage in maneuverability by managing the transfer and redirection of kinetic and potential energy, so we compared the rapid inversion behavior to a passive pendulum model as a null hypothesis and then to a pendulum model with an initial velocity comparable to the animals. Our findings inspired the beginnings of a similar behavior in a physical model, a small hexapedal, prototype robot.

Materials and Methods

Laboratory animal husbandry

Adult male American cockroaches, *Periplaneta americana*, were acquired from a commercial vendor (Carolina Biological Supply Company, Burlington, NC, USA) and housed in plastic cages maintained at a temperature of 27°C. Cockroaches were exposed to a L:D cycle of 12h:12h and given fruits, dog chow and water ad libitum. Flat-tailed house geckos, *Hemidactylus platyurus*, used in the laboratory were purchased from commercial vendors (The Reptile Company, Endicott, NY; Glades Herp, FL; California Zoological Supply, Los Angeles, CA, USA). Note that this is the species used in climbing experiments, but now resides in a different taxa (Zug et al., 2007). Geckos were housed in common cages in an animal care facility at UC Berkeley. They were fed with a diet of crickets with vitamin and mineral supplements as deemed suitable by veterinarians. Water was provided ad libitum. Geckos were kept in an environmental control room with 12 h of light per day and at a temperature of 25±2°C. Trials were conducted at

an average temperature of 30°C. The Animal Care and Use Committee at the University of California, Berkeley, whose activities are mandated by the U.S. Animal Welfare Act and Public Health Service Policy, approved all experimental procedures described for these research projects.

Track

We ran cockroaches and geckos at high speeds along an inclined track in an arena enclosed with Acrylic walls. For both species, the track abruptly ended. The track was inclined at approximately 30° and ended with a ledge whose undersurface matched the track substrate (cardboard for cockroach and cardboard with a thin layer of 40-grit sandpaper for geckos). Animals started from the bottom of the track and upon eliciting an escape response, they ran up the inclined track. Trials were conducted at room temperatures between 28-32°C.

Animal and robot kinematics in the laboratory

We captured high-speed videos of the animal using two cameras (X-PRI, AOS Technologies AG, Baden Daettwil, Switzerland) positioned at the top and the side of the arena. The cameras were synchronized and recorded at 500 frames per second. For the cockroaches and geckos, we tracked a 2-dimensional projection of the head and feet attachment positions to obtain kinematic measurements of the maneuver (ProAnalyst, Xcitex, Inc., MA, USA). All digitized data were filtered and analyzed with custom scripts (Matlab; The MathWorks Inc., Natick, MA, USA). All animal kinematics data used to calculate velocities and accelerations were low-pass filtered using a Butterworth filter at 75 Hz, which was about three times the stride frequency of *P. americana* for the recorded running speeds. For the robot, we used a low-pass filter at 50Hz which was also about three times stride frequency. To estimate the center of mass (COM) of *P. americana*, we manually tracked the head and dorsal region of the abdomen to define the body length and determined the COM to be 50% of body length based on previous measurements (Ting et al., 1994). For the gecko, we manually tracked the rostral and caudal region of the torso and took the COM to be between these points. We video recorded the robot, DASH, performing the maneuver using high-speed videography at 300 frames per second (Casio Exilim EX-F1) and tracked its motion for kinematic analysis. For the robot, we manually tracked the front and back region to define the body and length and determined the COM to be at 50% of body length. Note, speeds shown in Figure 2 were calculated using the rostral portion of the body for animal and robots, whereas velocities shown in Figure 4 are for the COM. Data are reported as means ± s.d. unless otherwise noted.

Claw ablation experiment

To study the role of claws, we performed claw-ablation surgeries on cold-anesthetized cockroaches. The pair of claws on each metathoracic leg was ablated under a microscope using fine dissection scissors. Care was taken to leave the membranous base, the arolium, intact.

Animals were allowed at least 24h to recover after the surgery. We then ran the animals with the same procedure as controls.

Field behavior

To establish the generality of our results on the incline running and ledge climbing performance of *H. platyurus* from the laboratory, we sought to relate it to the animal's ecology and natural history by conducting field research in the context of a South-East Asian lowland tropical rainforest habitat. For the field experiments, we used eleven wild-caught geckos (3.75±0.4 g).

The National Parks Board of The Republic of Singapore approved a request to study the locomotion of geckos with a field research permit and the Wildlife Reserves Singapore allowed us to capture house geckos *H. platyurus* (Specimen Collection Permit # NP/RP955B). We accommodated lizards in portable terraria with ambient humidity (ca. 85%) and temperature (ca. 38°C) for the shortest duration possible. As a medium for our experiment, we selected the "Bird's Nest Fern" *Asplenium cymbifolium* which is native to the lowland tropical rainforest at our field site in the Wildlife Reserves. It can be observed at great heights above ground and therefore lives in the same canopy habitat as *H. platyurus*. The mid-rib of this fern renders the overall leaf very rigid and capable of supporting the weight of *H. platyurus*.

We used three digital video cameras (X-PRI, AOS Technologies AG, Baden Daettwil, Switzerland) to capture simultaneously dorsal, sagittal and cranial views of the lizards running on the giant bird nest fern. Video frames from all three camera views were synchronized. The data were stored on a portable computer. The lighting conditions in the field can change rapidly due to patchy clouds temporarily obscuring the path of the sunlight. We responded to this situation by working with the lighting available and filmed at different frame rates ranging from 32-500 frames per second. We frequently adjusted the aperture on one 50 mm and two 25 mm lenses to ensure an adequate amount of light be made available to the high-speed video cameras in face of the dynamically changing lighting conditions.

To acquire individual morphometrics, the house gecko's length was measured while holding the animal in hand, whereas the mass was determined by placing the animal on a small scale. All animals were released at the region of capture after video recording. No harm was done to the animals or surrounding landscape during this process. All animals were released shortly after capture if they were deemed not suitable for the study. No detrimental effects resulted from the short confinement. All methods of capture and handling are well-established standard techniques used by herpetologists. Geckos were not recaptured.

Pendulum model

We determined the pendulum model trajectory by solving a nonlinear physical pendulum model of the form

$$\frac{d^2\theta}{dt^2} + \frac{mgL}{I}\sin\theta = 0 \quad (1)$$

using the ode45 solver in Matlab (The MathWorks Inc., Natick, MA, USA) where θ is the angle as defined in Figure 2a, m is the mass of the animal or robot, g is the acceleration due to gravity, L is the pendulum length and I is the moment of inertia.. We determined the pendulum length L by computing the average length from feet to center of mass during the swing of the animals and robot. By the parallel axis theorem, the moment of inertia I of the animals and robot was approximated as

$$I = I_{COM} + mL^2 \quad (2)$$

where I_{COM} is the moment of inertia at the COM and mL^2 is the parallel axis term. The moment of inertia of the animals and the robot was approximated as an ellipsoid and flat rectangular plate, respectively. Since the moment of inertia of the legs in the animals and robot were less than 5% of the parallel axis term, they were not included in the final calculations (see Appendix 1).

This model has two initiation conditions: initial angle θ and initial angular velocity $d\theta/dt$. We set the initial conditions such that the angle of the pendulum θ matched the initial angle of the animals and robot. We calculated θ by taking the angle between a vector defined by the point at the end of the ledge where the feet attach to the COM and a vector defined by the horizontal axis parallel to the ground (Fig. 2a). We defined the initiation of the swing maneuver as the time when the COM attained minimum speed (Fig. 4). For the model with no initial kinetic energy, we set $\dot{\theta}_i = 0$, where $\dot{\theta}_i$ is the angular velocity. For the pendulum model with initial kinetic energy, we set $\dot{\theta}_i$ equal to the tangential velocity of the center of mass at the transition between running and swinging by using experimental data (see Fig. 4c). Tangential velocity is equal to

$$\dot{\theta}_i = \frac{\vec{r}_i \times \vec{v}_i}{\left|\vec{r}_i\right|^2} \quad (3)$$

Where $\vec{r}_i$ is the vector from the ledge to the COM and $\vec{v}_i$ is the velocity at the transition from running to swinging. To compare the progression of the animals and robot in Figure 4, we linearly interpolated the animal and robot position data to attain a temporal resolution of 0.5 ms. We assumed aerodynamic drag forces to be negligible as calculations using a flat plate model perpendicular to flow yielded drag forces less than 5% for cockroaches and geckos (Appendix 1).

To measure the total energy transfer in the transition from running to swinging, we selected trials in which cockroaches used both feet to engage at the ledge and continued engaging both feet during inversion. These trials had very little out-of-plane motion, thus improving our estimate of the 2D-projected COM position. For geckos, we also selected trials in which the animal ran off the ledge with both feet engaged. In addition, we rejected trials in which the ventral region of the abdomen contacted the ledge which could contribute to energy losses due to friction. For the

robot, we selected three trials out of four in which both feet remained attached to the Velcro pad for the longest period during inversion to minimize out-of-plane motion.

Robot assembly

The cockroach-inspired DASH robot was used as the platform to recreate the claw action observed in the legged animals. The hexapedal robot is 10 cm long and has a mass of 16g with onboard electronics, actuation, and battery. It was constructed using the cardboard Smart Composite Microstructures manufacturing process which produces folded structures from rigid cardboard beams and polymer flexure joints. Velcro was bonded to compliant pads that were attached to the hind feet of the robot cantilevered in the aft direction. The Velcro enabled the robot to gain purchase at the edge of the substrate while the compliant pads provided the necessary degree of freedom to allow the robot to rotate to the inverted position. Velcro on the underside of the substrate, paired with matching Velcro bonded directly to the front feet of DASH, allowed the robot to perch inverted beneath the substrate after the inversion maneuver.

Results

Cockroaches

We discovered that American cockroaches (mass = 0.71 ± 0.07g, n = 6 animals, 32 trials) escaped at high speed (62.1 ± 9.1 cm s^{-1}) up an inclined track, dove forward and caught their tarsal claws, usually of both hind legs, on the substrate (Fig. 1a). The claws briefly disengaged from the substrate as the tibia contacted the tip of the ledge, but then quickly reengaged at the tip (Frazier et al., 1999). With the claws attached, cockroaches executed a pendulum-like swing with peak head velocities of 109 ±12 cm s^{-1} (head angular velocities > 1,200 deg s^{-1}) around towards the underside of the substrate in only 127±22 ms (Fig. 2a-c). Cockroaches experienced mean peak accelerations of 3.8±0.9 Gs during the swing. After the swing, they secured their position and took several steps forward in an inverted posture. In approximately one quarter of the trials, cockroaches used a single leg to perform the maneuver without detectable changes in performance. Animals ran at full speed off the incline without requiring substantial braking. In only a few trials the animals continued to run off the ramp. Either slippage of the hind legs, loss of ground contact on the front and middle legs, or rapid change in pitch appeared to initiate the claw engagement reflex (Frazier et al., 1999), suggesting active control. In all trials, the front and middle legs continued to cycle during the swinging maneuver. We attempted a balanced experimental design where we collected between 5 to 7 trials per individual.

To test whether claws are necessary for executing this behavior, we ablated the claws on the tarsi of both hind legs while leaving the sticky pads (arolium) intact. Using a paired comparison, we found that animals (n = 6 animals, 34 trials total with 5 to 9 trials per individual) with ablated claws failed 94% (32/34 trials) of the time at performing the maneuver while running at similar speeds (63.0 ± 9.4 cm s^{-1}) compared to the same animals with intact claws (*t*-test, p = 0.76). In two trials, animals succeeded at performing the maneuver. For animals with ablated claws, we

observed no change in strategy as the animals attempted to perform the same maneuver but failed.

Geckos

The rapid inversion behavior was not unique to cockroaches. House geckos, *Hemidactylus platyurus,* (mass = 5.26±0.67g, n = 5 animals, 17 trials) also running at high speeds (67.3 ±17.1 cm s^{-1}) used a similar strategy as they rapidly approached the ledge (Fig. 1b). During their dive, geckos engaged claws and sticky hairs (setae) near the tip of the ledge allowing them to swing around at high speeds (peak head velocity of 108 ±19 cm s^{-1}, head angular velocities > 900 deg s^{-1}) towards the underside of the substrate in only 156 ±38 ms (Fig. 2d). Geckos experienced peak accelerations of 3.0±0.8 Gs during the swing. We attempted a balanced experimental design where we collected between 2 to 4 trials per individual animal.

We observed the rapid inversion behavior in the gecko's natural environment, the forests of Singapore (Fig. 3). Geckos (mass = 3.75 ± 0.4g) ran over the lamina of ferns and stretched their forelimbs outwards as their torso went over the leaf's edge. We studied eleven animals and we observed the behavior in three animals. They anchored their rear legs within the blade of the fern, thus causing the body to swing around towards the underside of the leaf as a result of their inertia. The behavior was analogous to the discovery made in the laboratory and demonstrates its potential effectiveness in traversing the animal's native habitat.

Robot prototype

The novel rapid inversion behavior can provide initial inspiration for the development of new capabilities in running robots (Fig. 1c). Using the cockroach-inspired hexapedal robot DASH (Dynamic Autonomous Sprawled Hexapod; Birkmeyer et al., 2009), we simulated claw action by attaching a pad of Velcro hooks on the hind legs. We glued the "loop" side of the Velcro on the substrate near and underneath the ledge. DASH (mass = 16.0g, n = 4 trials) ran at high speed along a track (88.0 ± 3.5 cm s^{-1}) on a level track because at this early stage in design inclines resulted in slipping. DASH successfully swung around toward the underside of the track in only 221 ± 43 ms ("head" angular velocity > 600 deg s^{-1}) and then stuck to the ledge and underneath the track (Fig. 2e). Robots were exposed to peak accelerations of 5.2 ± 0.12 Gs during the swing.

Pendulum model

We tested the hypothesis that animals swung around to the underside of the ledge like a pendulum by first comparing the swing kinematics to a physical pendulum model with zero transfer of kinetic energy as a null hypothesis. We determined the parameters of the pendulum model using estimates of morphology and matching the initial conditions to the animal or robot position (see Methods). If we assume that the body or center of mass of the animal or robot represents the bob of a pendulum subject to only gravitational force and starting from rest with no added kinetic energy, then we can trace the trajectory from the time the animal engages its claw or the robot sticks until the swing underneath the ledge is complete (Fig. 4a; grey circles).

For both the cockroach and gecko, we found significant differences in body angle when comparing the animals or robot and model at different time intervals in the full cycle (Fig. 4a,b). Here we define a full swing cycle from when the animal reaches a minimum velocity in transition from running to swinging (see Fig. 4d) until at legs come in contact with the underside of the ledge. For example, the cockroach is approaching a near vertical orientation with respect to the body long axis in the swing at half cycle (50 ms; Fig. 4a red line) due to its more rapid initial velocity (Fig. 2c), while the passive pendulum model is just moving down from a horizontal position after the same time period. Therefore, we reject our null hypothesis that a passive pendulum with no transfer in kinetic energy explains the swing kinematics of the animals.

The rapid inversion behavior better approximates a pendulum model with initial kinetic energy (Fig. 4a). In fact, we found no evidence that the animals reached a velocity of zero in transitioning from inclined running to swinging (see Fig. 4c). To test whether animals swing like a pendulum with an initial velocity, we set $d\theta/dt$ equal to the angular velocity at the transition between running and swinging where speed was lowest using estimates from experimental data (Fig. 4b). We found that in the first half of the swing cycle, the pendulum model with an initial velocity accurately predicts the trajectories of both the cockroach and gecko suggesting that the animals may conserve energy in the transition from running to swinging. To quantify the possible conservation, we estimated the total energy transfer in the transition from running to initial swinging (see Methods). Total energy transfer for cockroaches (n = 5 trials) and geckos (n = 3 trials) was 78.1±10.0 % and 74.4±5.6%, respectively. Our DASH robot prototype (n = 3 trials) transferred 72.5±13.5 % of its energy.

Discussion

As first articulated by Galileo in *Two New Sciences*, scaling in biology can impose important constraints on performance as well as permit new opportunities. Non-linear physical forces governing movement can shape an animal's behavioral repertoire. The novel behavior we have discovered in small animals demonstrates an important effect of scale, specifically the scaling of rotational inertia and claw-substrate interactions that allow these animals to outmaneuver the best

human acrobats in the world. Using a pendulum-like swing with their hind legs as grappling hooks, these small, legged runners represent another example of using the natural dynamics of the body and appendages to effectively complete a maneuver (Fig. 1) (Highman et al., 2001; Jusufi et al., 2008; Libby et al., 2012). The rapid inversion behavior may provide important advantages for predatory avoidance by rapid disappearance in natural settings, as demonstrated by our study of wild geckos in South East Asia (Fig. 3). Moreover, the new capability may provide insights into how animals can negotiate complex environments requiring transitions that demand rapid transfer and redirection of energy. The study of high-speed transitions including, but not limited to inclines, gaps, and landing maneuvers represent a frontier in biomechanics research that will enable the unravelling of new principles behind rapid dynamic reconfiguration of bodies and appendages.

Comparison to Simple Pendulum Model and Brachiation

To test the hypothesis that cockroaches and geckos configure their legs and bodies during rapid inversion to swing like a pendulum, we applied a template based on pendulum dynamics that has been used to understand cyclic animal movements such as walking, running and brachiating. Inverted pendulum models for walking capture the exchange between kinetic and potential energy, as well as the collisions and energy redirection (Ruina et al., 2005; Srinivasan and Ruina, 2006). This is true not only for their applications to bipeds, but models for walking crabs (Blichan and Full, 1987) and lizards (Farley and Ko, 1997) show patterns consistent with pendular energy exchange reaching 51-55%. Pendular exchange has been proposed for the suspensory or bridging locomotion of spiders that walk upsidedown (Moya et al., 2008). Given the novelty of the rapid inversion behavior, we only can compare it to the other swinging behavior well studied, brachiation. Gibbons display two types of brachiation: continuous contact, similar to walking, and ricochetal, analogous to running that has a flight phase (Bertram et al., 2004). Even using the simplest possible model for a single swing, a point mass with a massless support arm, both brachiation gaits display substantial pendular exchange between kinetic and potential energy (Bertram et al., 1999). Applying a physical pendulum model with zero transfer of kinetic energy to rapid inversion revealed substantial deviations from the actual trajectories in both the cockroaches and geckos, especially at the onset of the swing (Fig. 4a). The same pendulum with nonzero initial kinetic energy angular velocities better represented the beginning portion of the swing cycle of both animal trajectories suggesting that energy is effectively transferred from running to swinging, but not without losses (Fig. 4a: see time 75 ms and 100 ms for the cockroach and gecko, respectively). Our results suggest that approximately 20% of the total energy is lost in the initial transition from calculations of total energy transfer at the COM.

A next step in modeling rapid inversion can be guided by the efforts to study brachiation. A fundamental feature of brachiation gaits is the minimization of collisional energy loss due to discontinuities in the center of mass trajectory. In the case of rapid inversion, it is also likely that energies losses occur due to discontinuity in trajectory, particularly during the transition from running to swinging which requires a redirection of the available kinetic energy. The trajectories

of animals studied here, although more rapid than a passive pendulum, lag behind a pendulum model with an initial velocity near the end of the cycle (Fig. 4a). Losses likely occur due to damping in the legs by muscles and joint membranes during the swing. At the same time, we might consider the possibility that the legs store and return energy like springs as observed during running gaits modeled by a spring-loaded inverted pendulum (Srinivasan and Ruina, 2006). More representative brachiation models include multiple links that approximate the gibbon's head, torso and legs (Gomes and Ruina, 2005). These models account for rotational kinetic energy and its effects. Our kinematic data show the possibility that the kinetic energy of running can be transferred to rotation body segments and appendages such as a tail. Much of brachiation modeling has focused on energy (Bertram et al., 1999; Gomes and Ruina, 2005) and reasonable passive models show the possibility of very low energetic cost. By contrast, more costly active brachiation using muscle power appears to have the advantage of recovering from perturbations in the natural environment using neural feedback (Bertram et al., 2004). Given that rapid inversion is not a repeated, sustained activity like brachiation, we hypothesize that energy saving is less important, whereas effective transfer of energy to complete the behavior as quickly as possible with a sufficient level of stability is paramount.

Neuromechanical Control

Future investigation of the stability and control of rapid inversion and similar acrobatic behaviors will uncover the role of active neural sensory adjustments versus the feedforward, passive dynamics we model here. During the transition from running to swinging, we observed that the middle and front legs of cockroaches continue to cycle in free air, while the hind legs remain attached to the ledge via claw engagement. Leg cycling was not observed in geckos, thus suggesting alternate control responses in a vertebrate of similar size. In the cockroach, we noted that front and middle legs continued to cycle out of phase in free air much like in an alternating tripod gait used for high-speed running. This suggests that cockroaches could complement the task-level feedback required for claw engagement with a feedforward mode during this high-speed behavior. Pattern generators providing signals to the muscle controlling limbs have a flexible control architecture capable of decoupling the action of individual or pair of legs consistent with studies in other insects moving more slowly (Bassler and Buschges, 1998).

Bio-inspiration

We used the rapid inversion behavior to inspire the initial design of a legged robot, named DASH that begins to demonstrate this new level of maneuverability (Fig. 1c, 2e; Libby et al., 2012). The preliminary design may not be as effective as the animals in redirecting into the swing as evidenced by the losses later in the cycle (Fig. 4b), but given the flexible manufacturing approach available (Wood et al., 2008), future adjustments are possible. We already are developing several active and passive, bio-inspired claw designs to replace the prototype Velcro

hooks. The new behavior emphasizes a major difference that remains between animals and our best robots. We have designed robots that can run or climb, but few can do both and effectively transition from one surface to another. We anticipate that the quantification of acrobatic behaviors in small animals will continue to provide biological inspiration resulting in small, more highly mobile sentinel and search-and-rescue robots that assist us during natural and human-made disasters.

References

Alexander R.M. (1985). The maximum forces exerted by animals. *J. Exp. Biol.* 115:231–238.

Asbeck A.T., Kim S., Cutkosky M.R., Provancher W.R., Lanzetta M. (2006). Scaling hard vertical surfaces with compliant microspine arrays. *International Journal of Robotics Research* 25:1165-1179.

Autumn K., Hsieh S.T., Dudek D.M., Chen J., Chitaphan C., Full R.J. (2006).The dynamics of vertical running in geckos. *J. Exp. Bio.* 209:260-272.

Bassler U., Buschges A. (1998). Pattern generation for stick insect walking movements—multisensory control of a locomotor program. *Brain Res Rev* 27:65-88.

Bertram JE. et al. (1999) A point-mass model of gibbon locomotion. *J. Exp. Biol.* 202:2609-17.

Bertram, JE et al. (2004). New perspectives on brachiation mechanics. *Am. J. Phys. Anthropol.* 39:100-17.

Birkmeyer P., Peterson K., Fearing R.S. (2009). DASH: A Dynamic 15g Hexapedal Robot. *IEEE Int. Conf. Intelligent Robots and Systems*.

Blickhan R., Full R.J. (1987). Locomotion energetics of the ghost crab: II. Mechanics of the center of mass during walking and running. *J. Exp. Biol.* 130:155-174.

Brackenbury J. (1997). Caterpillar kinematics. *Nature* 390:453.

Brackenbury J. (1999). Fast locomotion in caterpillars. *J. Insect. Physio.* 45:525-533.

Carrier D.R., Walter R.M., Lee D.V. (2001). Influence of rotational inertia on turning performance of theropod dinosaurs, clues from humans with increased rotational inertia. *J. Exp. Biol.* 204: 3917.

Dickinson M.H. (2005). The initiation and control of rapid flight maneuvers in fruit flies. *Integr. Comp. Biol*. 45:274–281.

Farley C. and Ko T. (1997). Mechanics of locomotion in lizards. *J. Exp. Biol.* 200:2177-2188.

Frazier S.F., Larsen G.S., Neff D., Quimby L., Carney M., DiCaprio R.A, Zill S.N. (1999) Elasticity and movements of the cockroach tarsus in walking. *J. Comp. Physiol. A* 185:157-172.

Full RJ., Yamauchi A., Jindrich D.L. (1995). Maximum single leg force production: cockroaches righting and running on photoelastic gelatin. *J. Exp. Biol.* 198:2441-2452.

Goldman D.I., Chen T.S., Dudek D.M., Full R.J. (2006). Dynamics of rapid vertical climbing in cockroaches reveals a template. *J. Exp. Biol.* 209:2990-3000.

Gomes M.W., Ruina A.L. (2005). A five-link 2D brachiating ape model with life-like zero-energy-cost motions. *J. Theor. Biol.* 237:265-78.

Higham T.E., Davenport M.S., Jayne B.C. (2001). Maneuvering in an arboreal habitat: the effects of turning angle on the locomotion of three sympatric ecomorphs of Anolis lizards. *J. Exp. Biol.* 204:4141–4155.

Hoover A., Steltz E., Fearing R.S. (2008). RoACH: An autonomous 2.4g crawling hexapod robot. *IEEE Int. Conf. on Intelligent Robots and Systems*.

Hoover A.M., Fearing R.S. (2008). Fast scale prototyping for folded millirobots. *IEEE Int. Conf. on Robotics and Automation*.

Jusufi A., Goldman D.I., Revzen S., Full R.J. (2008). Active tails enhance arboreal acrobatics in geckos. *Proc. Natl. Acad. Sci. USA* 105:4215–4219.

Kohlsdorf T., Biewener A.A. (2006) Negotiating obstacles: running kinematics of the lizard *Sceloporus malachiticus*. *Journal of Zoology* 270:359-371.

Larsen G.S., Frazier S.F., Fish S.E., Zill S.N. (1995). Effects of load inversion in cockroach walking. *J. Comp. Physiol. A* 176:229-238.

Libby T., Moore T., Chang-Siu E., Li D., Cohen D., Jusufi A., Full R.J. (2012) Tail assisted pitch control in lizards, robots and dinosaurs. *Nature* 481:181–184.

Moya-Larano J., Vinkovic D., De Mas E., Corcobado G., Moreno E. (2008). Morphological evolution of spiders predicted by pendulum mechanics. *PLoS ONE* 3(3): e1841.

Ruina, A., Bertram, J.E.A. , Srinivasan, M.A. (2005). A collisional model of the energetic cost of support work qualitatively explains leg sequencing in walking and galloping, pseudo-elastic leg behavior in running and the walk-to-run transition. *J. Theor. Biol*. 237(2)170-92.

Spagna J.C., Goldman D.I., Lin P.-C., Koditschek D.E., Full R.J. (2007). Distributed mechanical feedback in arthropods and robots simplifies control of rapid running on challenging terrain. *Bioinspir. Biomim.* 2: 9–18.

Srinivasan M., Ruina A. (2006). Computer optimization of a minimal biped model discovers walking and running. *Nature* 439: 72-75.

Ting L.H., Blickhan R., Full, R.J. (1994). Dynamic and static stability in hexapedal runners. *J. Exp. Bio.* 197:251-269.

Walter R.M., Carrier D.R. (2002). Scaling of rotational inertia in murine rodents and two species of lizard. *J. Exp. Biol*. 205:2135-2141.

Wood R.J., Avadhanula S., Sahai R., Steltz E., Fearing R.S. (2008). Microrobot design using fiber reinforced composites. *ASME Journal of Mechanical Design* 130 Issue 5.

Zug GR et al. (2007). Burmese hemidactylus (Reptilia, Squamata, Geckkonidae): Taxonomic notes on tropical Asian Hemidactylus. *Proceedings of the California Academy of Sciences* 58:387-405.

Figure 1. Sequence of rapid inversion behavior in cockroaches, geckos, and a robot prototype. Panels a and b show a high-speed 180-degree inversion behavior on an incline for cockroaches, *P. americana* and house geckos, *H. platyurus*, respectively. Panel c shows a cockroach-inspired hexapedal robot, DASH, successfully performing a similar maneuver from a horizontal platform with small Velcro hooks attached at the end of the hind legs.

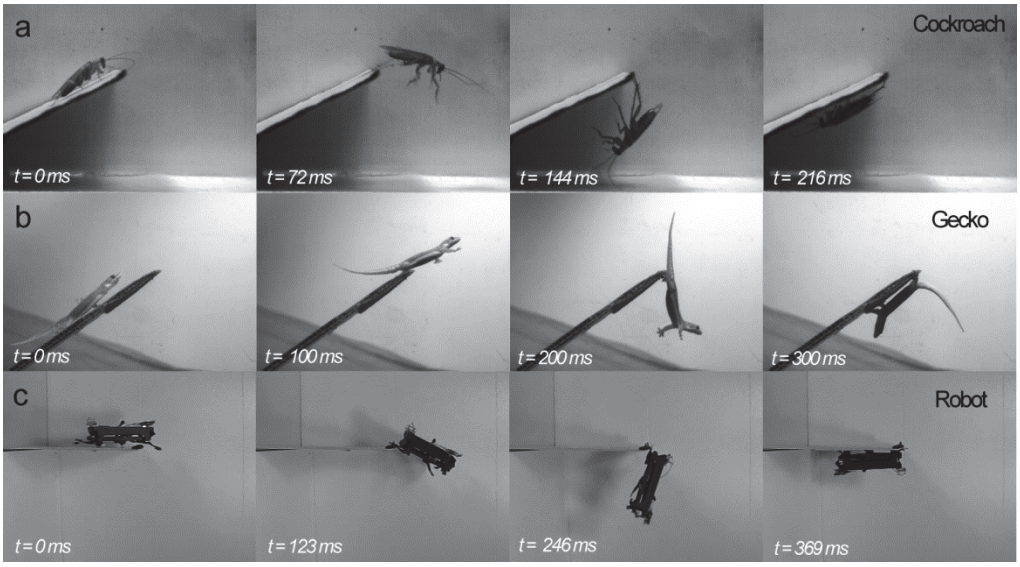
a
Cockroach
t = 0 ms
t = 72 ms
t = 144 ms
t = 216 ms
b
Gecko
t = 0 ms
t = 100 ms
t = 200 ms
t = 300 ms
c
Robot
t = 0 ms
t = 123 ms
t = 246 ms
t = 369 ms

Figure 2. Kinematics of rapid inversion for animals and robot. In the top left panel (a) a representative pendulum-like model of the inversion behavior is shown swinging from rest until it contacts the underside of the ledge. The red circle represents the rostral or head position. In the bottom left panel (b), we plotted position data of the rostral region of the animals and robot with the initial position centered at the origin. In the three panels at the right, head speed data for the cockroach (c), gecko (d) and robot (e) are plotted as a function of scaled time (% cycle) to compare the speed profile across trials and animals. Bold thick lines show the average speed, whereas light thick ones show ± 1 standard deviation. Thin lines in the background show the individual trial data for the animals and robot.

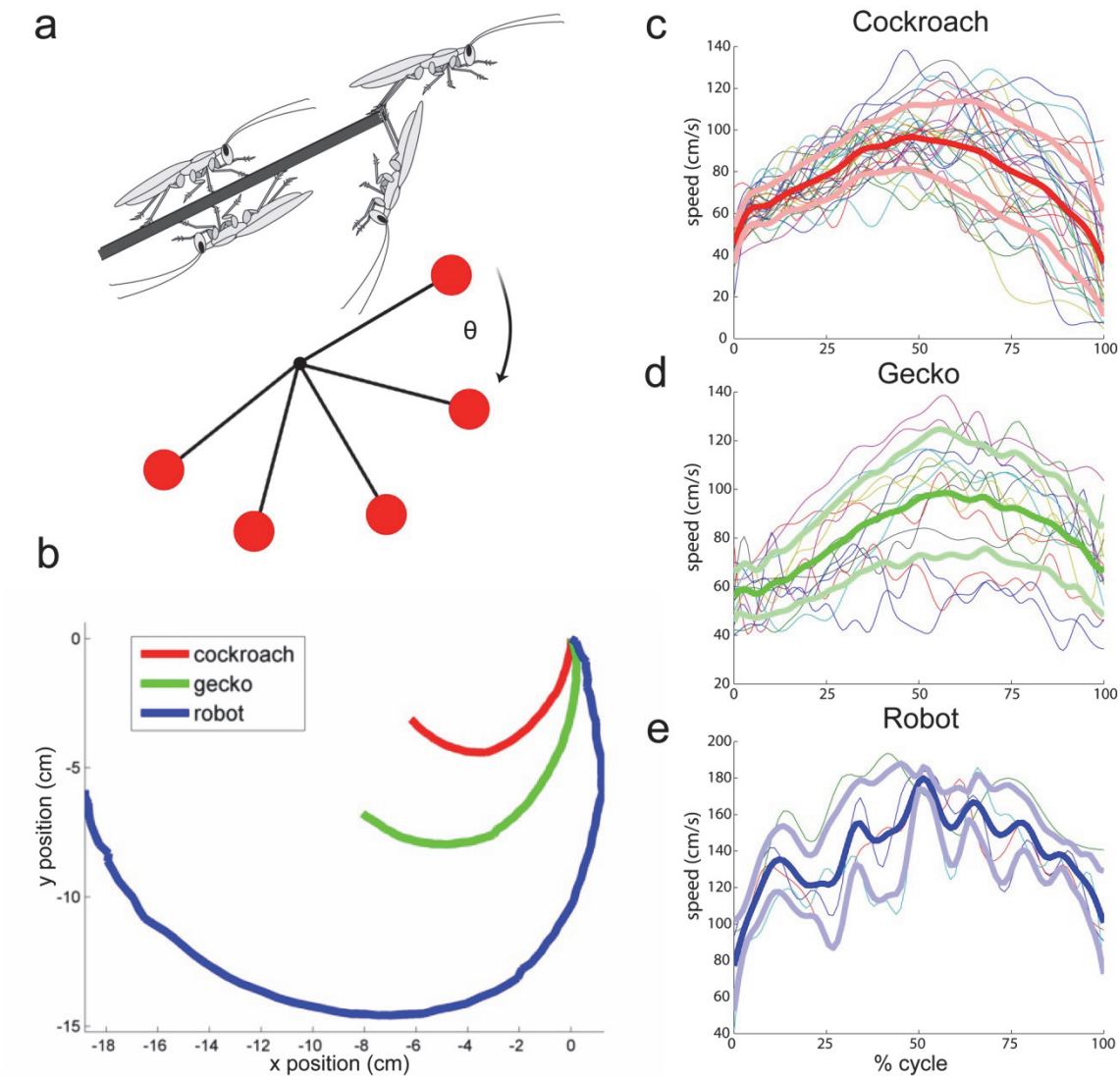
a
θ
b
cockroach
gecko
robot
y position (cm)
x position (cm)
c
Cockroach
speed (cm/s)
d
Gecko
speed (cm/s)
e
Robot
speed (cm/s)
% cycle

Figure 3. Flat-tailed house gecko, *H. platyurus* in its native environment in the rainforests of Singapore. The two panels show a sequence of the inversion behavior from the top (a) and bottom (b) of a fern leaf recorded in the field with high-speed videography. After moving over the robust parts of the fern leaf with a rigid midrib beneath that supported their body weight, the gecko engaged its claws near the tip of the leaf and performed a pendulum-like swing towards the underside.

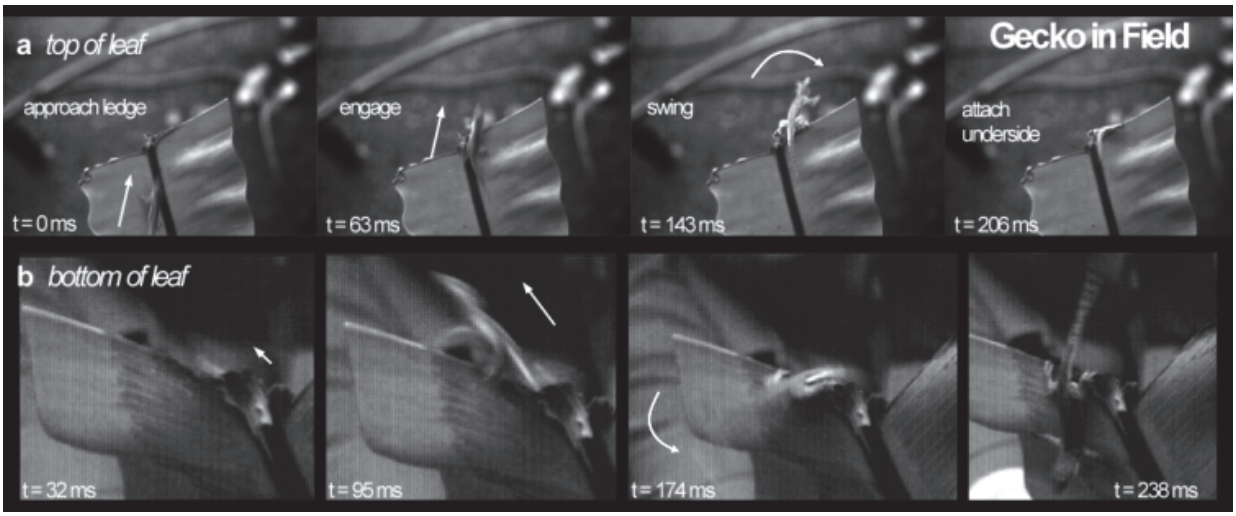
a top of leaf
approach ledge
t = 0 ms
engage
t = 63 ms
swing
t = 143 ms
Gecko in Field
attach
underside
t = 206 ms
b bottom of leaf
t = 32 ms
t = 95 ms
t = 174 ms
t = 238 ms

Figure 4. Comparisons of animal and robot kinematics to a pendulum model. Panel (a) compares a pendulum model without transfer of kinetic energy (KE=0; grey bob) and with complete transfer of kinetic energy (KE>0; magenta bob) to the animal and robot trajectories as a function of time (ms) from representative position data from the COM of the cockroach (red), gecko (green), and robot (blue). The pendulum base joint represents the average position of the feet during the maneuver. The cockroach and gecko started swinging at an angle of approximately 30 degrees from the body long axis relative to the horizontal, whereas the robot initiated swinging near the horizontal relative to the body long axis (0 degrees). Panel (b) shows the change in angle relative to the initial angle at the start of the swing for animals and robot compared to our two models. Panel (c) shows the position of the COM of the animals and robot during the complete rapid inversion maneuver for a representative trial. Arrows indicate the resultant velocity vectors ($m\ s^{-1}$) at intervals of 20ms. The black open circle indicates the region where the speed is slowest. Panel (d) shows the corresponding energy profiles. The grey area represents the period of swinging defined as the point of slowest speed following foot engagement until all legs contacted the underside of the ledge. The dashed curve in magenta shows the total kinetic energy for the pendulum model if transfer were complete.

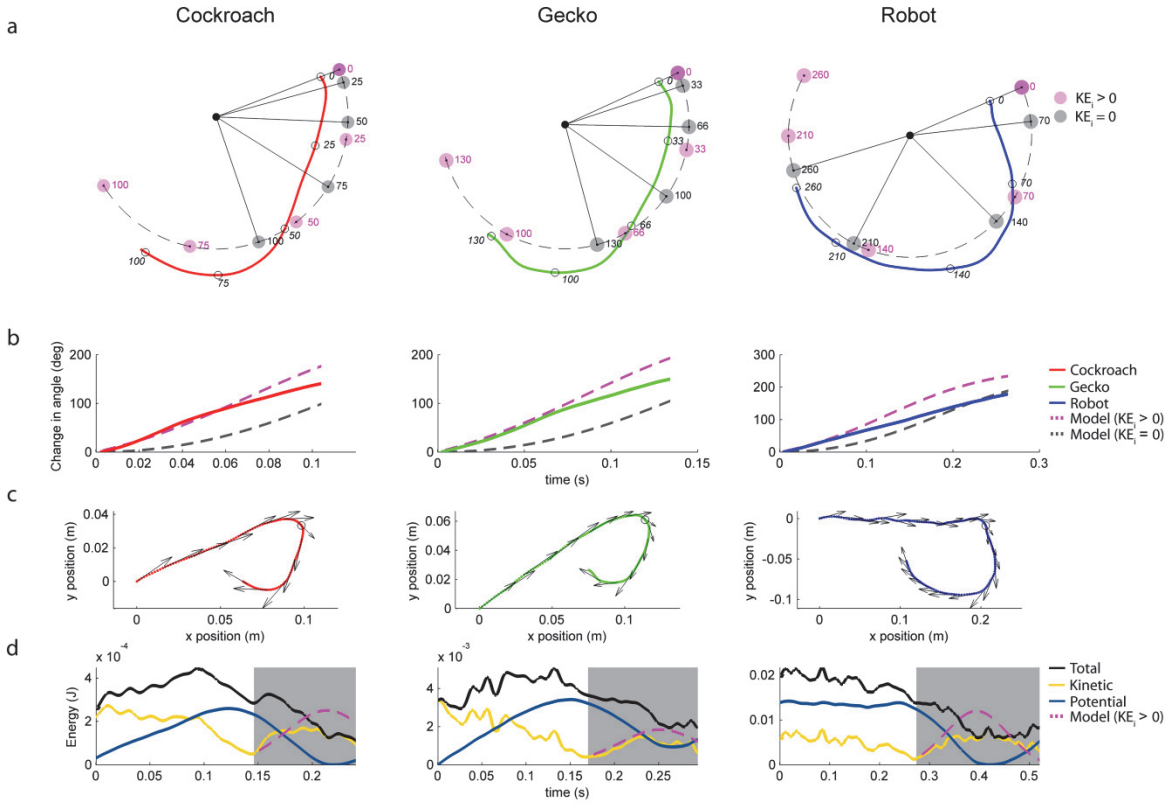
a
Cockroach
Gecko
Robot
KE_i > 0
KE_i = 0
b
Change in angle (deg)
time (s)
Cockroach
Gecko
Robot
Model (KE_i > 0)
Model (KE_i = 0)
c
y position (m)
x position (m)
d
Energy (J)
x 10^-4
x 10^-3
time (s)
Total
Kinetic
Potential
Model (KE_i > 0)

Appendix 1

If we model a cockroach as a rectangular flat plate perpendicular to an air-flow, the drag force is

$$F_d = \frac{1}{2}\rho v^2 C_d A$$

where F_d is the drag force, ρ is the density of the medium, v is the velocity of the object relative to the air flow, A is the cross-sectional area and C_d is the drag coefficient. A cockroach during inversion will experience peak Re numbers of

$$\mathrm{Re} = \frac{Ul}{\upsilon} = \frac{\left(1.10 ms^{-1}\right)\left(0.035 m\right)}{0.000015 m^2 s^{-1}} \approx 3.0 \times 10^3$$

where l is the body length (estimated for *P. americana*), U is the velocity of the air relative to the animal (average peak velocity of 1.10m s^{-1}, see Results) and υ is the kinematic viscosity of the fluid (15 x 10^{-6} for air at 20°C). Since Re < 10^5, we assume that the flow is laminar.

For a flat plate perpendicular to flow in the laminar regime with aspect ratio < 0.1, the drag coefficient is ~ 2 (Munson et al., 2006). We can calculate the peak drag force using estimates of cockroach morphologies as follows and air density at 20°C:

$$F_d = \frac{1}{2}\rho v^2 C_d A = 0.5\left(1.2 kgm^{-3}\right)\left(1.10 ms^{-2}\right)^2 \left(2\right)\left(0.035 m \times .01 m\right) \approx .046 mN$$

which is about 0.6% of body weight for a cockroach of 0.0071kg (average mass, see Results).

For geckos, we can apply the same calculation. We find that geckos experience peak Re numbers of

$$\mathrm{Re} = \frac{Ul}{\upsilon} = \frac{\left(1.10 ms^{-1}\right)\left(0.054 m\right)}{0.000015 m^2 s^{-1}} \approx 4 \times 10^3$$

using morphological data from Jusufi et al. (2010).

Thus, we find that the flow regime is laminar. Again, using the morphologies from Jusufi et al. and assuming that the tail has negligible drag compared to body drag, we can calculate the drag forces using the same the same flat plate model as the cockroach,

$$F_d = \frac{1}{2}\rho v^2 C_d A = 0.5\left(1.2 kgm^{-3}\right)\left(1.10 ms^{-2}\right)^2 \left(2\right)\left(0.054 m \times 0.037 m\right) \approx 2.6 mN$$

which is about 5% of body weight for a gecko with a mass of 0.0526kg (average mass, see Results) similar to that estimated in Jusufi et al. (2010).

References

Munson, B.R., Young, D.F., Okiishi, T.H. (2006). Fundamentals of Fluid Mechanics (Fifth Edition). *John Wiley & Sons.*

Jusufi, A., Kawano, D.T., Libby, T., Full, R.J. (2010) Righting and turning in mid-air using appendage inertia: reptile tails, analytical models and bio-inspired robots. *Bioinspir. Biomim.* 5: 1-12.

Appendix 2

To characterize the transient response of the flagellum following a step input, we used engineering transient-response specifications for under-damped systems (Ogata, 2003). These specifications include the following properties:

- Delay time t_d : Time for the response to reach half of the final, steady state value.
- Rise time t_r : Time for the response to rise from 0 to 100% of the final value.
- Peak time t_p : Time for the response to reach the first peak of the overshoot
- Maximum percent overshoot M_p : Maximum peak value of the response measured relative to the final, steady state value.
- Settling time t_s: Time required for the response to reach and remain within 5% of the final value.

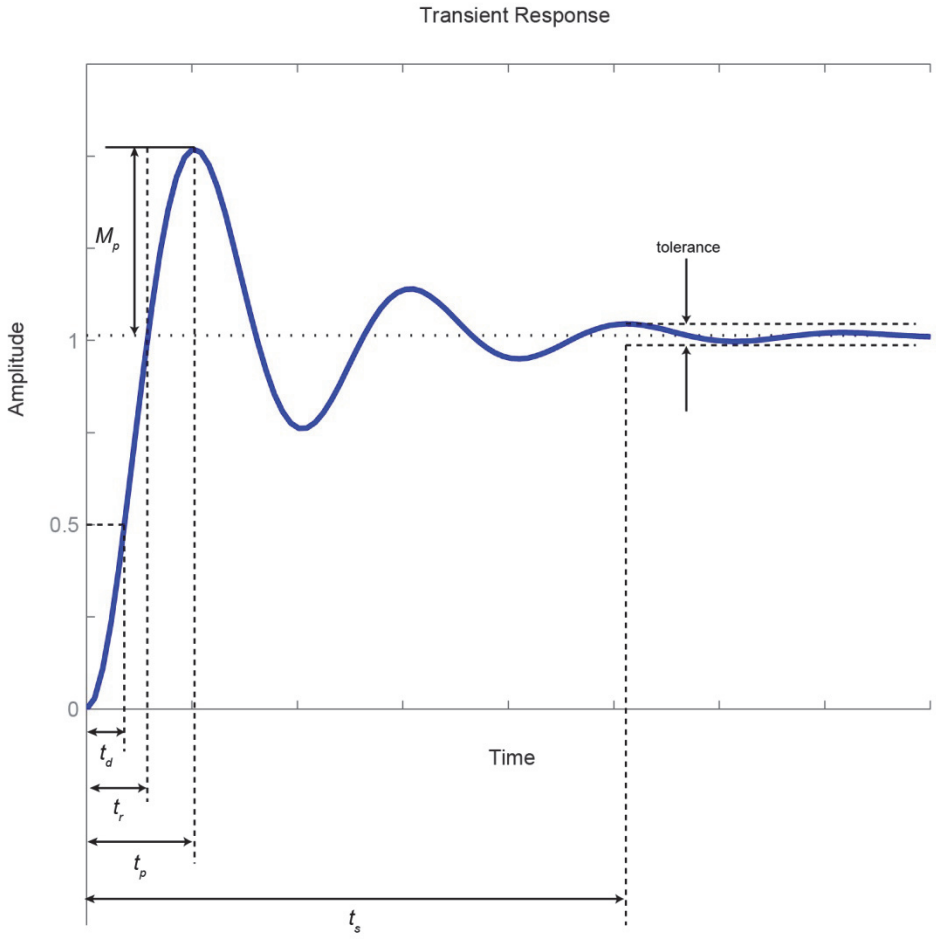

References

Ogata, K. (2003). System dynamics. *Prentice Hall*. 4th edition.